STUDY OF AUTOIONIZATION PROBABILITY FOLLOWING NUCLEAR BETA DECAY

THESIS

presented by

MARIAM MOKHTAR ATEEK

for the degree of

DOCTOR OF PHILOSOPHY

in the

UNIVERSITY OF LONDON

Department of Physics
Bedford College
University of London
London NW1

September 1975

ACKNOWLEDGEMENTS

I should like to express my sincere gratitude to my supervisor, Mr R Thomas, for his patience and help throughout this work.

Thanks to the technicians in the Physics Department at Bedford College for their technical assistance.

I am also indebted to the Computor Unit staff for their help with data analysis.

Ishould like to express my appreciation to Dr J Campbell and Dr J Law for their helpful discussion, and for supplying copies of their notes on the subject.

My continued gratitude goes to my parents for their encouragement during my stay abroad.

I am also grateful to the University of Tripoli for the award of a scholarship.

CONTENTS

ABSTRACT

The purpose of the work was a study of autoionization phenomenon following nuclear β^- -decay.

Three approaches have been adopted in this respect, first, a study of total internal ionization probability and internal ionization probability as a function of β^- -particle energy, using a coincidence technique between emitted electrons (β^- -particles + orbital electrons) and subsequent K X-rays. Two isotopes have been studied using this approach, thallium-204 and promethium-147, where measurements of internal ionization probabilities for K-electrons are presented and results are discussed in terms of available theoretical treatments on total internal ionization.

A second approach was applied in the case of thallium-204 where the internal ionization probability for K-electrons is deduced by comparison of mercury K X-rays resulting from an electron capture process with lead K X-rays due to the studied phenomenon.

The third approach was applied in a measurement on erbium-169 using the straight forward technique of comparing the 118 Kev gamma-ray transition with thulium K X-rays and an upper limit for K-shell

internal ionization probability has been estimated. Difficulties and drawbacks of the experiment have been discussed.

The two solid state detectors used in this work were a lithium drifted silicon detector for electrons and lithium drifted germanium X-ray detector for photons.

Chapter 1

INTRODUCTION

1.1 AUTOIONIZATION PHENOMENA

When a radioactive nucleus disintegrates by emission of an alpha or beta particle, the radio-active disintegration perturbs the electrons of that atom, and may cause electronic excitation to an unoccupied discrete level, or ionization to the continuum. A hole in an inner electronic shell produced in this manner will be filled either by an electron from outer shells and emission of a characteristic X-ray, or by emission of a second electron, which is ejected from the atom, i.e. by an Auger Process, and that two new holes will replace the original one. These new vacancies will then be filled by still more electron transitions from higher shells until the atom, now highly ionized, arrives at a state where no more transitions are possible. This process has sometimes been called a "vacancy cascade".

The ejection of orbital electrons may arise from

(a) the sudden change in nuclear charge and the imperfect overlap of parent and daughter orbital electron wave functions, and

(b) scattering of atomic electrons by the beta particle: a "direct collision". This phenomenon is refered to as autoionization or internal ionization, the term self-ionization is adopted by one of the

authors[1].

Though several phenomena have been under investigation for many years (e.g. internal conversion, Auger effect, external Bremsstrahlung, inner Bremsstrahlung, ...), autoionization came to be investigated seriously for the first time only in recent years.

In addition to beta decay (both β^- and β^+ decay), internal ionization is known to be associated with other decays; such as electron capture decay and alpha decay.[2,3,4,57,58]

The phenomenon has been shown to occur in K-shell internal conversion of nuclear gamma rays,[5] electron impact and photoionization,[6] and more recently in positron annihilation.[7]

It has been of interest to a number of experimental nuclear physicists to throw light on a phenomenon which remained for a long time, merely a theoretical prediction; this led theorists to present new models for the original theory. The problem has been tackled from different points of view, in order to give a good assessment of the agreement between theory and experiment.

Most of the literature published so far, in both theory and experiment, concerned with internal ionization has mainly dealt with internal ionization following nuclear beta decay.

For many reasons, practical and theoretical, it is convenient to study ionization of the K-shell. The K X-ray spectrum following creation of a vacancy in the K-shell is easy to detect; in the sense that, the energies of the emitted quanta fall in a region such that it is possible by means of most available nuclear low-energy gamma ray detectors to obtain both quantitative and qualitative information. Energies and intensities of these X-rays are very well established. Fluorescence yields in K-shell transitions are precisely known too. All these facilitate the interpretation of the spectrum. Theoretically, it is more convenient to perform exact calculations for K-shells (and also for L- and M-shells if Z is large), because in these cases the wave functions of the initial and final states are hydrogen-like.

1.2 THEORY

The theory of autoionization was formulated a third of a century ago, many years before the effect could be observed experimentally. In his pioneer work, Feinberg[8] calculated the effect of beta-decay on

K-electrons. His calculations are based on the consideration that the atomic core suffers two types of perturbation; firstly, due to direct interaction of the β-decay electron with the atomic ones, having a character of a simple collision; secondly, due to a change of central charge within a time interval which is short compared with atomic periods.

Feinberg prescribed his calculations in alternative ways; in two of them, the case of fast β-particles was considered in non-relativistic and relativistic respects. Making use of the fact that the velocity of β- electrons is usually great as compared with velocities of atomic electrons, he assumed that direct collisions could be neglected. If the beta particles are considered to be sufficiently fast (i.e. $E\beta >> I_K$, where $E\beta$ is the kinetic energy of the nuclear beta particle and I_K is the K-shell ionization energy), and the energy transferred by them is sufficiently small (i.e. $\epsilon << E\beta$, where ϵ is the kinetic energy of the ejected electron) it follows that P_K is independent of the β-particle energy. Consequently, the beta particles can be described by wave functions of free motion, neglecting the nuclear field and permitting the neglect of exchange. Considering the ejection of fast electrons where $\epsilon >> I_K$, the Born approximation could be used and the β-particle is described by a spherical wave

outgoing from the nucleus and subject to the disturbance caused by the outer electrons cloud.

Feinberg himself regarded these calculations to be doubtful due to use of unallowed wave functions with the pole in the origin. Using a slightly modified treatment, he called it Fermi method. According to this, the full probability of ionization of the K-shell per one K-electron and per one β-decay is,

$$W_K \simeq 0.32/Z^2 \qquad (1\text{-}1)$$

where Z is the atomic charge.

Taking into account the influence of the presence of other electrons, for the K-electrons only, the screening effect is due to the second K-electron, but the more important factor, the double occupation of the K-level simply doubles the resulting W_K in equation (1-1). Therefore, the probability of ionization of a K-shell having two K-electrons equals $2W_K$ and is denoted by P_K

$$P_K \approx 0.64/Z^2 \qquad (1\text{-}2)$$

In the non-relativistic beta electron case, Feinberg expressed the contribution of the direct collision effect with respect to the shake off process in terms of their squared matrix elements which are denoted by

M_{dc} and M_{sh}, respectively and their ratio is given by

$$\frac{|M_{dc}|^2}{|M_{sh}|^2} = \frac{I_K}{E_\beta} << 1 \qquad (1\text{-}3)$$

Independently Migdal[9] investigated the possibility of having auto-ionization in β-decay in a way which is very much like Feinberg's treatment. Using time dependent perturbation theory, he worked out the probability for the ejection of an atomic electron as a simple overlap integral between the bound initial state and a continuum state for the ejected electron. Migdal's conclusions were in good agreement with Feinberg's, except for the direct collision term which Migdal neglects altogether.

Some years later, Levinger[10] reviewed the Feinberg-Migdal treatment for ionization of K-electrons in beta decay. His result is very close to equation (1-2). Recently, shake off probabilities have been recalculated by Carlson et al.[11], who performed extensive calculations using both non-relativistic Hartree-Fock Slater ($Z > 30$) wave functions, incorporating corrections for screening and relativity, Carlson's calculations differ from earlier results by more than a factor of 2 in heavy elements.

Carlson followed Feiberg in assuming that the shake off mechanism in beta decay occurs in two steps; firstly, the occurance of the nuclear

β-decay, then the orbital electron being suddenly ejected when $E_\beta >> B_K$. Providing this sudden approximation is satisfied, no matter which ever wave functions are used, the internal ionization rate is independent of E_β.

An alternative treatment has been proposed by Stephas and Crasemann,[12,13,14] which is known as the one step model. In this model the decay energy is assumed to be shared in a single step between the β-particle, neutrino and ejected electron, taking the case of β^--decay, as there are two negatons to share phase space, i.e. the internal ionization probability must be a decreasing function of the β^--particle energy according to this model. More recently, support and modification for the one step model came from Law and Campbell[15,16] and independently from Mord.[17,18]

Campbell and Law[19,54] calculated P_K values for a number of isotopes from a model based on vacancy creation mechanisms of shake off and shake up (excitation to unfilled bound states), employing a simple correction for direct collision.

1.3 EXPERIMENT

As was mentioned earlier, the identification of autoionization phenomena

started merely as a thoeretical prediction in the publications of Feinberg, Migdal and Levinger. Some years later, it was of interest for a few experimentalists to perform a number of experiments in order to measure internal ionization probability (P_K) and ($P_{L,M}$) in which various methods were used.

The phenomenon was first observed by Boehm and Wu,[20] in the case of promethium-147 and bismuth-210 (β^--emitter) sources, by detecting X-rays of their daughter nuclei (i.e. X-rays of tin-147 and polonium-210).

Using a NaI scintillation counter as well as proportional counter spectrometers, both K and L radiations were observed. The agreement between Boehm and Wu's original experimental results and the Feinberg-Migdal original theory was satisfactory to some extent, considering the approximate nature of the theoretical calculations and the accuracy with which the experiment was carried out.

A number of other experimental workers[12,21-27] have measured the total P_K per β-decay of this internal ionization process. Using several single β-decay nuclides, they performed experiments where X-rays of the daughter atom are measured in coincidence with beta particles above some threshold energy.

Most of these experimentalists, if not all, tried to interpret their results in terms of the theoretical shake off mechanism calculations due to the fact that it was the only existing theory at that time, though the direct collision was mentioned in Feinberg's original paper, its contribution to the whole process was considered to be negligeably small according to equation (1-3).

An experimental study by Suzor et al.[21,28] claimed that for continious spectra of autoionization electrons emitted simultaneously with β-particles at low energies, there is serious disagreement with shake off theoretical predictions. This disagreement caused Feinberg[1] to reconsider the direct collision as a possible mechanism for autoionization and regard its contribution as being more than it was previously believed to be.

Reproducing equation (1-3)

$$\frac{P_K(dc)}{P_K(so)} \approx \frac{B_K}{E\beta} \qquad (1\text{-}3a)$$

B_K is the K binding energy.

From the above relation (1-3a), $E\beta$ must be replaced by unity for relativistic beta electrons, obviously $P_K(dc) << P_K(so)$, therefore, the condition

for the smallness of the direct collision effect applies only to relativistic beta particles.

Feinberg points out the condition $E_\beta >> B_K$ is not always fulfilled for many isotopes, especially the cases which were studied by Suzor et al. from which the disagreement originated. So it can be clearly seen that the direct collision process is of a considerable importance at low energies. From relation (1-3a) and according to Weiner,[29] (dc) contribution relative to (so) should be much larger for the K-shell than for the outer shells.

Electron-electron coincidence measurement had been performed by Suzor et al.[28,30] The results of these sort of experiments are not very convincing. To date, the internal ionization probability for the K-shell (P_K) has been obtained basically in six types of experiment:

(i) Measurement of daughter atom charge distribution following β^--decay.

(ii) Separate measurements of absolute β^- and X-ray intensities of a source. Normally NaI(Tl) crystals, organic scintillators, or proportional counters are used as detectors, where, in recent

years high energy resolution solid state detectors have been a replacement.

(iii) X-ray spectrum in coincidence with the negaton spectrum (i.e. β^--particles + shake off electrons).

(iv) Comparison of X-ray and γ-ray intensities. This method is restricted to cases where the accompanying γ-ray is of very low energy; so that no K-shell conversion can occur, or it is very weakly converted, this requires accurate knowledge of nuclear constants and branching ratios.

(v) Comparison of K_{α_1} X-ray line in the decay of a parent nucleus and K_{α_1} X-ray line due to K-shell internal ionization in the β^--decay of the daughter nucleus which is again applicable only to a limited number of nuclei.

(vi) Measurement of internal ionization X-rays associated with particular branch of β-decay in coincidence with the prompt γ-rays to the daughter ground state. This method could be considered analogous to method (iv); in sense of the condition that the γ-ray should be weakly converted.

A complete listing of the existing results for K-shell internal ionization probability (P_K) performed by different authors on about nineteen isotopes is given in Table 1.

1.4 THE SCOPE OF THE PRESENT WORK

It has been an aim for this project to present along with other published work a more clear picture about autoionization probability following nuclear β^--decay or more strictly the K-shell autoionization probability.

Due to the fact that only a limited number of results have been published so far for a number of isotopes giving support either to one theory or another, finding new experimental results will be valuable in giving fair support to any of the existing models.

The main part of the present work was devoted to β-energy dependence of autoionization because we felt that not enough work has been done by others in this respect, as this sort of experiment is tedious and lengthy due to the fact of low probability for the event considered.

This study for β^- -energy dependence involved two isotopes Pm-147 and Tl-204 using a coincidence technique, while for the other isotope Er-169; K-shell autoionization probability has been determined applying a different technique where only a straight photon spectrum was detected.

Table 1 Experimental K-Shell auto-ionization probabilities.

Isotope	E_β max. in KeV	daughter nuclei K X-rays in KeV K_{α_2}	K_{α_1}	K_{β_1}	K_{β_2}	Photon detector	Electron detector	$P_K \times 10^4$	Method	Author	Date	Ref.
$_2He^6$	3.508	.0543						1010 ± 20	i	Carlson et al.	1963	31
$_{15}P^{32}$	1710	2.31	2.31	2.46		prop. counter	-	58	ii	G. Renard	1955	32
						prop. counter	G.M.	36	ii	G. Renard	1957	36
						prop. counter	prop. counter	76	iii	Suzor et Charpak	1959	21
$_{16}S^{35}$	167.4	2.62	2.62	2.82		prop. counter	-	27 ± 8	ii	Rubinson et al	1954	33
						prop. counter	prop. counter	20	iii	Charpak et Suzor	1959	22
$_{20}Ca^{45}$	252	4.09	4.09	4.46		Si(li)	-	24.3 ± 3.9	ii	H. Hansen et al	1974	34
$_{28}Ni^{63}$	67	8.03	8.05	8.9		prop. counter	prop. counter	4.0 ± 0.5	iii	Isozumi & Shimizu	1971	26
						prop. counter	prop. counter	4.6 ± 0.6	iii*	Kitahara et al.	1972	27
$_{38}Sr^{89}$	1463	14.88	14.96	16.7	17.0	Si(li)	-	8.6 ± 0.7	ii	Hansen et al.	1974	34
$_{38}Sr^{90}$	546	14.88	14.96	16.7	17.0	Si(li)	-	6.5 ± 0.8	ii	Hansen et al.	1974	34
$_{39}Y^{90}$	2270	15.69	15.78	17.7	18.0	prop. counter	-	4.4	ii	Renard	1957	36
						NaI(Tl)	-	7.0 ± 0.1	ii	Michalowicz & Bouchez	1955	35
						Si(li)	-	7.4 ± 1.5	ii	Hansen et al.	1974	34
$_{38}Sr^{90} + _{39}Y^{90}$	ratio	both Y X-rays and Zr X-rays				prop. counter	-	5.3	ii	Renard	1955	32
						NaI(Tl)	-	12.2 ± 1.4	ii	Michalowicz & Bouchez	1955	35
$_{43}Tc^{99}$	292	19.15	19.28	21.7	22.1	NaI(Tl)	Si(li)	4.8 ± 0.3	iii	Stephas & Crasemann	1967	12
						Si(li)	-	3.89 ± 0.16	ii	Watson et al.	1972	39
						Si(li)	-	3.9 ± 0.3	ii	Hanson et al.	1974	34
$_{49}In^{114}$	1988	25.04	25.27	28.5	29.1	Curved Crystal Spectrometer	-	5.4 ± 0.4	v	Van Eijk et al.	1974	40
$_{59}Pr^{143}$	930	36.85	37.36	42.2	43.3	NaI	magnetic lens Spectrometer	4.25 ± 0.85	ii	Langevin-joliot	1957	37
						NaI	Argonne mag. lens spec.	2.95 ± 0.3	iii	Fishbeck et al.	1971	23
						Curved Crystal spectrometer	-	2.88 ± 0.20	v	Van Eijk & Kooy	1973	41
						Si(li)	-	2.94 ± 0.22	ii	H. Hansen	1974	59

Table 1 (continued)

Isotope	E_β max. in KeV	daughter nuclei K X-rays in KeV K_{α_2}	K_{α_1}	K_{β_1}	K_{β_2}	Photon detector	Electron detector	$P_K \times 10^4$	Method	Author	Date	Ref.
$_{61}Pm^{147}$	224	39.52	40.12	45.4	46.6	NaI	prop. counter	3.85 ± 0.5	ii	Boehm et Wu	1954	20
						NaI	mag. lens spec.	1.30 ± 0.26	ii	Langevin-joliot	1957	37
						NaI(Tl)	Si(li)	0.93 ± 0.14	iii	Stephas et al.	1967	12
						NaI(Tl)	Split outhrocene crystal	0.76 ± 0.1	iii	Isozumi & Shimizi	1971	26
						Ge(li) & Si(li)	-	0.98 ± 0.8	iv	Campbell & Law	1972	19
						Si(li)	-	0.81 ± 0.09	ii	Hansen et al.	1974	34
$_{62}Sm^{151}$	75.9	40.90	41.54	47.0	48.3	Ge(li)		$.041 \pm .006$	iv	Campbell et al.	1971	38
								$.036 \pm .005$		Campbell & Law	1972	19
						Ge(li)	magnetic spect.	$.024 \pm .3$	iii*	Freedman & Beery	1975	55
$_{68}Er^{169}$	340	49.77	50.74	57.5	59.0	Ge(li)	-	1.0 ± 0.2	iv	Campbell et al.	1971	38
						NaI(Tl)	plastic scint. NE102	2.4 ± 0.4	iii	Erman et al.	1968	24
$_{74}W^{185}$	429	59.72	61.14	69.2	71.2	Si(li)		1.0 ± 0.2	ii	Hansen et al.	1974	34
						Ge(li), Si(li)		1.0 ± 0.3	iv	Campbell & Law	1972	19
$_{80}Hg^{203}$	214	70.83	72.87	82.5	84.9	Ge(li)	-	$.15 \pm 0.45$	v	Thibaud et al.	1974	42
						Ge(li)	-	$.11 \pm 0.35$		Bond et al.	1974	47
$_{81}Tl^{204}$	766	72.80	74.97	84.8	87.3	Ge(li)	Si(li)	1.02 ± 0.03	iii	A. Mora	1971	25
						Si(li)		1.0 ± 0.1	ii	Howard et al.	1971	43
						Ge(li)		1.06 ± 0.03	ii	Pathak	1974	44
						Si(li)		1.18 ± 0.06	ii	Martel et al.	1974	45
						Si(li)		1.12 ± 0.09	ii	H. Hansen	1974	59
$_{83}Bi^{210}$	1160	76.86	79.29	89.6	92.4			1.2 ± 0.5	ii	Boehm & Wu	1954	20
								1.3 ± 0.2	ii	Michalowicz et al.	1955	35
						Ge(li)	-	1.23 ± 0.1	iv	Campbell et al	1971	38
						NaI(Tl)	plastic scint. NE102	2.0 ± 0.4	iii	Erman et al.	1968	24
						Ge(li)	-	1.25 ± 0.08	ii	Campbell	1971	46
						Ge(li)	-	1.21 ± 0.05	ii	Pathak	1974	44

* The summing energy spectrum of electrons (β-particles plus emitted K-shell electrons) in coincidence with emitted K X-Rays.

Chapter 2

CURRENT THEORETICAL APPROACHES

2.1 INTRODUCTION

In the process of β-decay, an electron is emitted from the nucleus with a speed which is, in most cases, close to the speed of light. The electron leaves the atom in a time of the order of r/c ((where r is the atomic radius, c is the speed of light)). On the other hand, the periods of electrons in the atoms are of the order of $2\pi r/v$, which is usually at least 100 times greater ((v is the speed of atomic electrons)). This means that for all practical purposes, one can say that the nuclear charge is suddenly increased from z to z + 1 ((in the case of β^--decay)). At the moment that this change has occured, the electronic wave function, $\psi(n,z)$, is that appropriate to a stationary state for an atom of charge z. In the new atom of charge z + 1, this wave function no longer corresponds to a stationary state; but must be expanded in terms of the stationary state wave functions $\psi_f(n', z+1)$ for the new charge z + 1. This means that there will be a certain probability that the atom will be left in an excited state of the new atom as a result of the suddenness of the process of β-decay. This excitation can be detected by the subsequent emission of radiation, which is usually in the X-ray region.

In fact, there is a whole spectrum of electron energies emitted in β-decay. A small fraction of the electrons are emitted at very low

velocities. Those electrons with velocities well below those of the mean atomic electronic velocities will tend to produce adiabatic perturbations of the atomic electrons, and those will not leave the atom excited. There are few of these low-velocity electrons.

One established fact is that the rearrangement of the orbital electrons occurs as an integral part of the decay process and not as a subsequent step. A striking demonstration of this fact is based on the effect upon the β spectrum; the change in total binding energy increases with atomic number and reaches approximately 18 KeV for z = 90 (ref 74), so in the case of β^- -decay, the atomic binding energy increases. According to conservation laws, this increase should appear in the kinetic energy of the emitted particles.

If this energy transfer took place after the nuclear decay, there will be no beta particles with energy less than the total increase in binding energy. However, it was found experimentally by Freedman et al.[75], that the β^- -spectrum extends well below the total increase in binding energy. This shows that the whole atom undergoes the transition in a single step, where energy is shared between the atomic electrons and the nucleus.

It is already established that two separate mechanisms can, in principle, account for internal ionization during nuclear β-decay; there are: (a) shake off mechanism due to sudden change in nuclear charge and imperfect orbital-electron wave function overlap, and (b) direct collision mechanism where atomic electrons are scattered by the β-particles.

In this chapter, the theory of internal ionization and its current approaches is reviewed. We will concern ourselves with the probability of the K-shell ionization in nuclear β^--decay.

Before going into details of the theory of internal ionization, it will be of help to the reader to give a brief account of some of the basic assumptions used by different authors in their calculations.

2.2 SUDDEN APPROXIMATION

In many cases, one has a large disturbance, which is, however, turned on very rapidly, in comparison with the period involved in a transition; e.g. when a nucleus of atomic number z decays by emission of a beta-particle, which has a velocity very much larger than that associated with the orbital electrons, the orbital electrons suddenly find

themselves in the field of a nucleus of charge $z + 1$. Suppose there is an instantaneous change in the Hamiltonian of an atom from H_0 ((the initial state)) to H_1 ((the final state)), the time-dependent wave function describing the electron in that atom is made up of the overlap integral of wave functions for the initial state i and wave functions for the various possible final stationary states f. Denoting the corresponding atomic wave functions ψ_i and ψ_f, the probability P_{i-f} can be calculated using the sudden approximation method yielding the following overlap integral:

$$P_{i-f} = |\int \psi_f^* \cdot \psi_i \ \tau|^2 \qquad (2\text{-}1)$$

If ϵ_0 and ϵ_1 are the atomic energy levels, and the transformation of the Hamiltonian takes the time τ, the criteria for the sudden approximation can be expressed as:

$$\tau = \frac{\hbar}{\epsilon_1 - \epsilon_0} \qquad (2\text{-}2)$$

In his work in 1941, Feinberg[8] considered the change in nuclear charge to be sudden. Using time-dependent perturbation theory ((sudden approximation)), he wrote the transition probability for the atom as a whole.

The transition probability for beta decay not accompanied by internal ionization can be written as:

$$dW(W) = 2\pi |\langle \psi_\beta(W_\beta)\psi_f(N)|H_\beta|\psi_\nu(W_\nu)\psi_i(N)\rangle|^2 \rho(\beta,\bar{\nu})$$

$$= 2\pi |M_N|^2 S_\beta(W_\beta, W_{\bar{\nu}})\rho(\beta,\bar{\nu}) \qquad (2\text{-}3)$$

Where $\psi_f(N)$ and $\psi_i(N)$ are the final and initial nuclear wave functions, H_β is the beta decay Hamiltonian, $\rho(\beta,\bar{\nu})$ is the two-particle density-of-states factor, $S_\beta(W\beta, W_{\bar{\nu}})$ is shape factor in which energy-dependent part of the matrix element has been included and $|M_N|$ is the nuclear matrix element.

The probability of ejecting one electron from the K-shell is given by:

$$dW_k(W_e, W_\beta) = 2\pi |\langle \psi_e(W_\beta)\psi_f(N)|H_\beta|\psi_\nu(W_\nu)\psi_i(N)\rangle|^2$$

$$\times \quad |M(W_e)|^2 \Xi \rho(\beta,e,\bar{\nu}) \qquad (2\text{-}4)$$

Where $|M(W_e)|^2$ is the square of the overlap integral between the atomic electron states and Ξ is antisymmetrization correction factor.

Feinberg restricted his discussion to allowed beta decay (this allowed him to neglect the anti-symmetrization correction factor Ξ). He eliminated the energy-dependent shape factors, and made the approximation that the three-particle density-of-states factor $\rho(\beta,e,\bar{\nu})$ is approximately equal to the two-particle density-of-states factor $\rho(\beta,\bar{\nu})$. Dividing equation (2-4) by equation (2-3); Feinberg obtained the following expression for the probability of ejecting an atomic electron

with energy W_e per beta decay:

$$\frac{dW_k(W_e, W_\beta)}{dW(W_\beta)} = \frac{(W_k - W_e - W)^2}{(W_o - W_\beta)^2} |M(W_e)|^2 \qquad (2\text{-}5)$$

Feinberg made further simplification by making the assumption that the total decay energy W_o is much larger than the K-shell binding energy E_k and the neutrino carries out most of this decay energy, i.e. $W >> (E_k + E_e)$, and equation (2-5) simply becomes:

$$P_k(W_e) = 2dW_k(W_e, W_\beta)/dW_\beta(W_\beta)$$
$$= 2|M(W_e)|^2 \qquad (2\text{-}6)$$

the factor 2, here, comes from the fact that two electrons are accommodated in the K-shell.

2.3 SELF-CONSISTENT-FIELD

The hydrogen atom in wave mechanics represents a simple mathematical problem which could be given an exact solution, but any atom with more than one electron is so difficult to find an exact solution for it. Approximate solution and rather elaborate one of Schrödinger's equation is applied for helium, which is a two-electron atom.

Approximation for solving problem of atoms having more than two

electrons could be achieved by making an assumption that each electron moves in a central, or spherically symmetrical, force field, produced by the nucleus and the other electrons. This method is referred to sometimes as central field model, there are three ingredients going into this method, one of these follows from wave mechanics, which is merely an approximate method of solving Schrödinger's equation for many-body problem of Z electrons moving about a nucleus of charge Z units, the other two are extensions of the wave-mechanical principles introduced into atomic structure in 1925; these are the postulates of, the electron spin and Pauli's exclusion principle.

Feinberg[8], derived the nonrelativistic hydrogenic matrix element, $|M(We)|^2$, using what he called Schrödinger approximation method. He started his calculation by assuming Born approximation not only for β-particle, but for the second electron in the final state as well, restricting his discussion to the ionization of K-shell for simplification reasons , as this shell contains two electrons, approximation for outer shells becomes very complicated.

Feinberg wrote the following wave functions as a starting point.

$$\psi(W, Z) = \pi B^{3/2} e^{-Br} \qquad (2\text{-}7)$$

$$\psi(P,z+1) = 2B'^{\frac{1}{2}}(1-e^{-2\pi\gamma})(4\pi)^{-3/2}(Pr)^{-1} \times \oint (Z+\tfrac{1}{2})^{\gamma-1}(Z-\tfrac{1}{2})^{-\gamma-1}e^{i2Prz}dz \qquad (2\text{-}7a)$$

Where $B = \alpha z$, $B' = \alpha(Z+1)$, $\gamma = B'/iP$, and

$\alpha = 1/137$; the fine-structure constant.

The integral over r is evaluated, then the contour integral is carried out; which encloses the points $Z = \pm 1$ and the result is given as:

$$|M(We)|^2 = \frac{2^6 B^5 B'}{Z^2(P^2+B^2)^4} \quad \frac{\exp[-4\gamma \tan^{-1}(P/B)]}{1-\exp(-2\pi\gamma)} \qquad (2\text{-}8)$$

However, these simple hydrogenic wave functions are known to be inaccurate for outer atomic shells, so advantage has been taken from what is called Self-Consistent-Field wave functions. This self consistent field is defined as the instantaneous action of all the electrons of an atom on one of their number, in order to perform the SCF ((Self-Consistent-Field)) calculation, it is necessary to take wave functions which belong to the proper irreducible representations of the eigen states of the final-state Hamiltonian to satisfy the Pauli principle.

Green[76] made calculations for Krypton (Kr) using interpolated solutions from SCF calculations for rubidium (Rb^+). A number of cases relating to electron shake off following β^- decay have been reported[11], in which use has been made of SCF wave functions.

SCF wave functions are known as Hartree-Fock wave functions which are the same as Hartree functions where the latter do not include the symmetrization factor. The Hartree-Fock functions result in a rather accurate calculation for the ground state of almost all light atoms. For heavier atoms relativistic Hartree-Fock-Slater wave functions are applied.[11]

With the use of high-speed computers, it is possible to obtain good SCF wave functions for all the elements.

Shake-off probability for the K-shell as a function of nuclear charge Z is shown in Fig. 2.1.

2.4 TWO STEP MODEL

In the simple electron wave function overlap theory, sudden change in the coulomb potential is provided, if the kinetic energy of the β-particle is much greater than the K-electron binding energy, i.e. if

$$E_\beta >> B_K \qquad (2\text{-}9)$$

Starting from this point, the two step approach states that: the shake-off can only occur when a β particle has initial energy in excess of B_K ((the binding energy)).

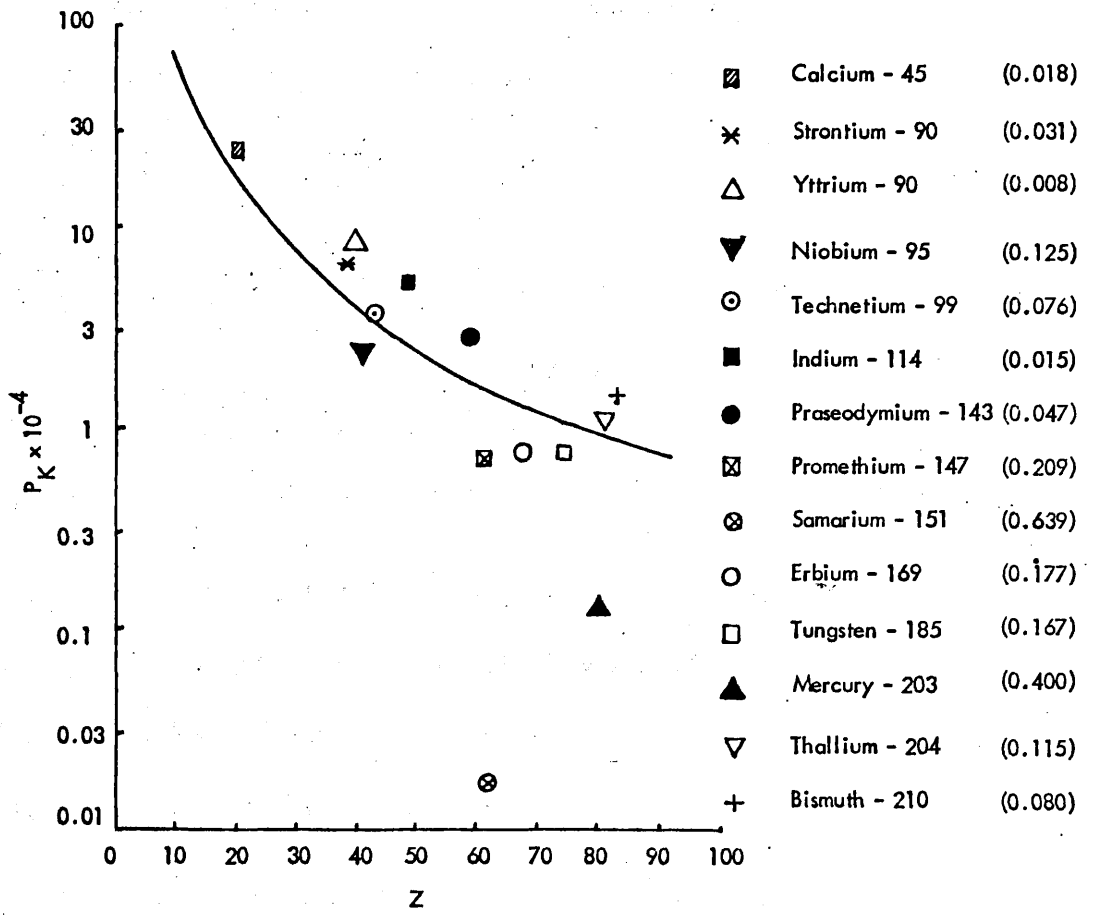

Fig 2-1. Shake off probability, per β decay, of the K shell as a function of atomic charge Z. Theoretical values are obtained from ref. (54). The values between brackets represent B_k/E_o. The solid curve represents the prediction of the simple wave function overlap theory (Eq. 1-2): $P_k = 0.64/Z^2$.

Carlson et al.,[11] viewed internal ionization process occurring in two distinct steps, first the β decay occurs; in which the β-particle obtains the normal energy E_β and then shake-off takes place for which the energy is derived from E_β. Shake-off is thus forbidden for $E_\beta < B_K$ and should have constant probability as a function of E_β provided $E_\beta \gg B_K$.

Carlson and his colleagues followed the original approximation made by Feinberg that E_β, $E_{\bar{\nu}} >> E_e$, using equation (2-1), they wrote the probability of excitation to the coninuum and to unoccupied states as:

$$\bar{P}_K = 1 - P_{KS} - P_F \qquad (2\text{-}10)$$

Where P_{KS} = the probability that a K electron will stay in the same orbital. The probability that at least one of the two electrons in the K-shell will leave due to shake off is $(1 - P_{KS})$.

$$P_{KS} = 1 \int < \psi_f(z+1) \, 1 \, \psi_i(Z) > 1^2 \qquad (2\text{-}11)$$

If the electron does not stay in the same orbital, it may go either to the continuum or to a discrete state, however some of these levels are filled already and transitions to such orbitals are not physically possible according to the Pauli exclusion principle and since nothing in the calculation of $(1 - P_{KS})$ has excluded the possibility for transitions to orbitals that are already filled, the incorporation of factor P_F in equation 2-10 is a necessity, where P_F = sum of probabilities for

excitation to occupied shells (L, M, -----).

Carlson et al[11], evaluated shake-off probabilities for all shells of 15 elements, they based their calculations on equation (2-10)using non-relavistic Hartree Fock wave functions for $Z < 30$ and relativistic Hartree-Fock-Slater wave functions for $Z > 30$.

It is obvious, from this model, that internal ionization probability is strictly defined as the number of K-vacancies created per β-particle having $E_\beta > B_K$ and denoted by the symbol $\bar{P}_K$ in order to eliminate confusion with P_K evaluated in other models and to be consistent with other authors nomination.[24]

To test this model, Erman et al.[24] performed an X-ray electron coincidence experiment on Er^{169} and Bi^{210}, their results seem to be in rather good agreement with the two step theory.

2.5 ONE STEP MODEL

As internal ionization accompanying β-decay is the process in which two electrons and an antineutrino are emitted from a β-active atom simultaneously, leaving a vacancy in the atomic cloud. An alternative one step theory has been proposed by Creasemann and Stephas,[13] in which they assumed that the decay energy is shared

among β^-, antineutrino, and ejected electron, since β^- and e share phase space; shake off probability must be a decreasing function of E_β in this model. Also, shake off may take place for any β-particle energy from zero to the maximum allowed by energy conservation, i.e. up to $E_o - B_K$ and the symbol P_K is used to denote the number of K-vacancies created per decay.

In accordance with this model, it is compulsory to include atomic electron wave-functions, in addition to nuclear β^- and antineutrino wave functions in the matrix elements that determine the transition probability, so the probability that an orbital electron, initially in state $\psi_i(z,n)$, goes to a state $\psi_f(z',n')$ due to the change in nuclear charge during β^- decay is:

$$dW_k(W_e,W_\beta) = 2\pi \left| \langle \psi_f(\beta,z',n')\, \psi_f(N) | H_\beta | \psi_\nu \psi_i(N) \psi_i(z,n) \rangle \right|^2 \times \rho(\beta,\bar{\nu},e) \qquad (2\text{-}12)$$

Where $\psi_i(N)$ and $\psi_f(N)$ are the initial and final nuclear wave functions, $\psi_f(\beta,z',n')$ is the antisymmetric final state wave function for the β-particle and the ejected orbital electron, $\psi_{\bar{\nu}}$ is the antineutrino wave function, H_β is the weak interaction Hamiltonian, and $\rho(\beta,\bar{\nu},e)$ is the density of final states for the three components nuclear β^- particle, orbital electron, and antineutrino. The units used such that $\hbar = c = m = 1$.

For allowed transitions, the nuclear, β^-, and antineutrino contributions to the matrix element are independent of energy and equation (2-12) can be written in the form of equation (2-4). We get the resulting $P_K(We)$ analogous to equation (2-6).

$$P_K(We) = 2\,|\langle \psi_f(z',n')\,|\,\psi_i(z,n)\rangle|^2 \qquad (2\text{-}13)$$

Stephas and Crasemann calculated the wave function overlap probability of the above expression for a K electron in the field of the parent nuclear charge z and a continuum electron in the field of the daughter nuclear charge z', using relativistic hydrogenic wave functions.

For β-energy dependence of internal ionization probability, K-shell ionization probability per decay, as a function of β energy is given by:

$$P_k(W_\beta) = [\,2\pi (W_o - W_\beta)^2\, S_\beta(W_\beta, W_o - W_\beta)\,]^{-1} \cong$$

$$\times \int_1^{W_k - W_\beta} dW\, (W_k - W_\beta - W)^2 PW|M|^2 \times S(W_\beta, W_k - W_\beta - W) \qquad (2\text{-}14)$$

S is the shape factor.

The overlap integral M is given by:

$$|M|^2 = Ae^{-B(W-1)} + FW^{-2(1+\gamma)} \qquad (2\text{-}14a)$$

Where A, B and F are fitting parameters:

$\gamma^2 = 1 - \zeta^2$, the energy-normalized final state wave function.

$\zeta = \alpha z$, where α is the fine structure constant, z is the nuclear charge.

Comparison of electron shake-off as a function of β-energy for different theoretical treatments is shown in Fig. 2.2.

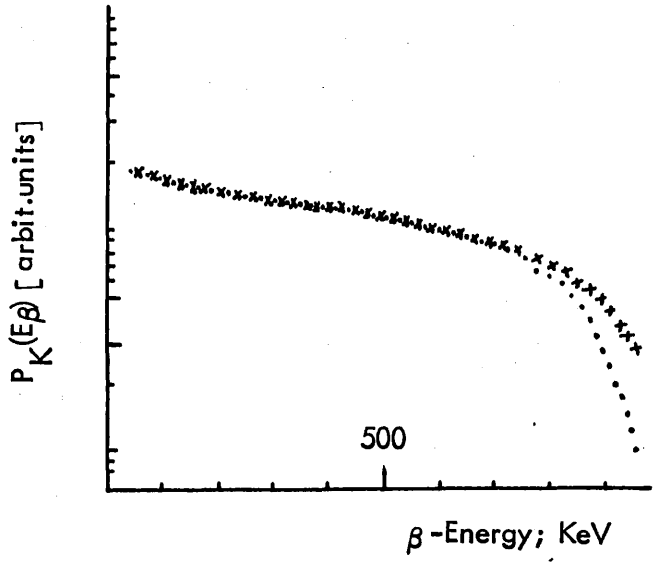

Fig 2.2 Electron shake-off as a function of β-energy for two different theoretical treatments. The curve with crosses represents the two-step model, and the dotted curve represents the one-step model with shape factor $S(\beta, \bar{\nu}, e) = S(\beta, \bar{\nu})$. The two-electron problem is not considered, here, in both treatments.
[adapted from ref. 24]

2.6 RECENT THEORETICAL TREATMENTS

Campbell et al.[38] described a method for measuring P_K, by selecting a number of isotopes which undergo beta decay only to levels of the daughter nucleus whose excitation energy is less than the K-electron binding energy. In such cases the subsequent transitions in the daughter nucleus cannot be internally converted in the K-shell and all K vacancies created may be ascribed to the internal ionization process. However, they claimed that this will bring the experiment into more agreement with theory as what is a so called two electron problem is avoided while in performing experiments where K X-rays are detected in coincidence with β^- particles, the electron observed in coincidence could be either the β^- particle or the ejected orbital electron.

The treatment of Law and Campbell[15,78] is a modified approach for the one step model where explicit account is taken of the indistinguishability of the two coninuum negatons.

Mord[17] calculated, P_K K-shell internal ionization probability for 14 isotopes according to the one step theory. He re-evaluated the relativistic hydrogenic atomic matrix element and rather an exact form has been obtained instead of the approximate one evaluated by Stephas and Crasemann.

Presently there are three groups who associate themselves with theoretical aspects of autoionization phenomena; Law and Campbell[53], Isozumi et al.[52], and Freedman[77].

Theoretical work is mainly devoted for shake off process as being the major contributor to autoionization probability. A rather good step forward in the theory has been made recently by Law and Campbell[54], where the roles of different mechanisms (shake off, shake up, and direct collision) are discussed. Theoretical calculations for shake off and shake up autoionization probabilities for K-electrons are presented. Their prediction for direct collision contribution does not differ from previous estimates.

So far it seems that the agreement between theory and experiment is quite good for allowed decays as no shape factor is needed in this case, whereas agreement for first forbidden decays with essentially allowed shapes is satisfactory.

Chapter 3

EXPERIMENTAL TECHNIQUES

3.1 DETECTION SYSTEM

In the present work, the K-shell internal-ionization probability P_K was determined by the use of two methods:

(a) The detection of the K X-rays of the daughter nuclei in coincidence with electrons emitted from the source (β^- particles + shake off electrons).

(b) The detection of the K X-rays of the daughter nuclei.

This implies that for method (a), two detectors are required, one as an X-ray detector and the other as an electron detector. This method has been successfully used to study the spectrum of emitted X-rays.[12,23,24,25]

Restricting the experiment to ionization of the K-shell greatly simplifies the interpretation of the results, since wave functions available for calculations are much more accurate for the K-shell than for the outer shells. Experimentally, K X-rays are less troublesome to detect and to carry out subsequent area calculations as the shape of the peak is well defined at these energies.

The development of semiconductor detectors has improved considerably in recent years and widely spread for use in gamma-ray and electron spectroscopy. They are well known for their high energy resolution which permits the relative determination of the energy of a gamma-ray with very

high precision. Using semiconductor detectors in autoionization experiments should result in more accurate results being obtained. As part of this work, a comparison (theoretical and experimental) was made between the relative advantages of scintillation and semiconductor detectors. A thin NaI(Tl) X-ray crystal was used as a photon detector and a plastic scintillator as an electron detector, trying different timing systems; a fair comparison of NaI (Tl) X-ray spectrometer with Ge(li) X-ray detector for the present work had been carried out. It was concluded that the advantages of solid state detectors outnumbers the drawbacks. The detection system finally achieved a reliable performance.

In the present experiment, photons were detected by a lithuim-drifted germanuim detector having a small volume which was ideal for the detection of photons in the X-ray region. It gave resolution of 250 ev at 14 KeV (Co -57 gamma-ray line). A very important aspect of a high resolution Ge(li) detector in the present work is its ability to distinguish between K X-rays of the daughter atom arising from auto-ionization and K X-rays of the parent arising from normal ionization of the source material by β^- particles.

For most of previous works, NaI (Tl) detectors had been in use and due

to their insufficient energy resolution for this sort of experiment, P_K values, possibly, would have great uncertainty. Attempts to allow for this defect by measuring P_K as a function of source thickness is regarded as tedious and impractical.

Since the photon detector used is small in volume, it has a low efficiency for high energy gamma rays which means that the background due to Compton scattering is low.

The electrons were detected by a lithium-drifted silicon detector which gave a resolution of 17 KeV at 625 KeV K-conversion line of Cs-137.

The advantages and the drawbacks of semiconductor electron detectors, have been discussed by Bertolini and Rota.[48]

The set up of the two detectors and the associated electronics for the coincidence experiment are shown in Fig. 3.1.

3.2 Ge (li) X-RAY DETECTOR

The lithium-drifted germanium detector used in the present work was a special purpose spectrometer manufactured by Nuclear Enterprises

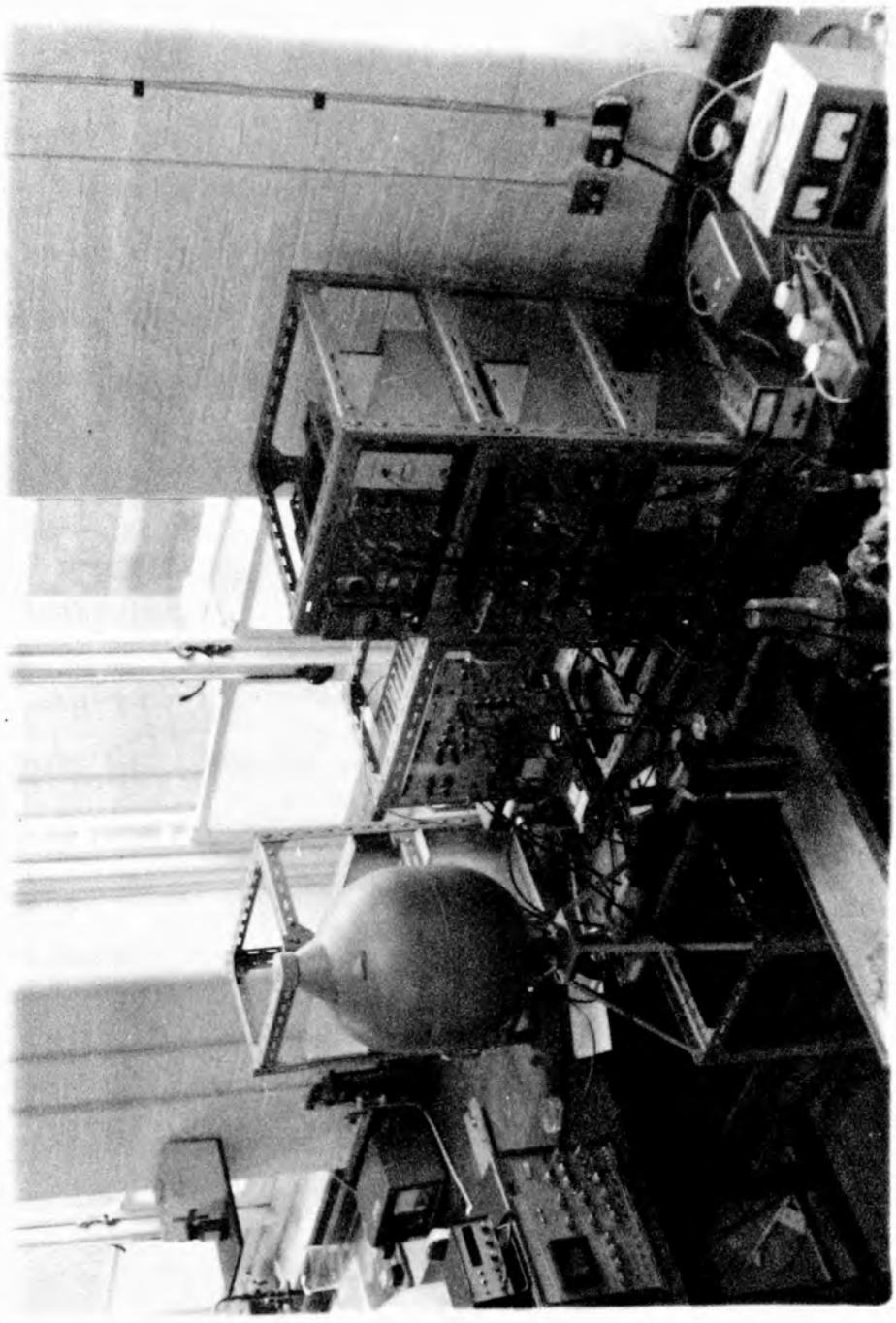

Fig 3.1 View of the experimental arrangement.

Limited (Edinburgh, U.K.). The actual detector is 75 mm^3 in volume supplied in a cryostat fitted with a very low noise, cooled preamplifier and liquid nitrogen dewar. The cryostat is horizontal dripfeed type, the detector is furnished with 0.008 in. thick beryllium window for minimum absorption in low energy photon spectroscopy. Vacuum was maintained at better than 10^{-6} torr. by a 1 litre/second ion getter pump.

3.3 CALIBRATION OF THE X-RAY DETECTOR

An accurate knowledge of the detection efficiency of Ge(li) detectors is often required for quantative work. In contrast to scintillation detectors, each particular semiconductor detector is unique in its detailed efficiency response due to the impossibility of precise control on the fabrication of these devices.

In principle, the efficiency of a detector can be determined in two ways, firstly by calculations based on geometrical data and photon matter interaction coefficients, secondly using reference sources emitting a known number of γ-photons. Both methods are in use, but the second, which is more accurate and therefore used more frequently was applied in this experiment.

The detector used had previously been calibrated by Thomas[49], but, since it is generally agreed that the efficiency of these detectors should be redetermined periodically, the detector was calibrated twice during this course of work to ensure consistency in the calibration data for sets of experiments performed at different times.

The Ge(li) X-ray spectrometer consisted of the following components: N.E. Ge(li) Crystal, detector Cryostat, a FET NE preamplifier, an ortec 440A active filter amplifier and 512 channels (memory) analyzer.

The radioactive sources used for this calibration were Cd^{109}, Co^{57}, Cs^{137}, Am^{241}, Eu^{152} and Ra^{226}. The first four sources were prepared by evaporating a few drops of the solutions on aluminium planchets covered with paper labels, while the Eu^{152} source was mounted inside 2.5 mm thick perspex container and the Ra^{226} source obtained from The Radiochemical Centre (Amersham) was mounted in a platinum container with 0.5 mm wall thickness and housed into identical container as Eu^{152}. It was very convenient that these perspex containers acted as beta absorbers as well. To carry out the experiment under the same conditions and to avoid attenuation factor calculation which might lead to inaccuracy in the final results for the efficiency, a perspex plate of the same thickness was placed in front of the detector for the rest of the sources.

Mass absorption coefficient for different photon energies in beryllium (detector window) and platinum were obtained from ref. 79 and the necessary corrections were made. The relevant data on photon energies and their relative intensities for calibration sources were obtained from refs. 80, 81, 82, 83, 84.

The duration of a measurement on any source depended on the source strength and the intensities of the transitions of interest, with a compromise made in time so that electronic drifts in the system did not cause severe problems. Measurement times ranged from one day to two days. Data from the analyzer were read out by a paper tape punch and a tele-typewriter. The information obtained on the paper tape served as input data for a computer program called SAMPO (see section 3.7), developed for an accurate determination of energies and intensities of the spectral peaks. Briefly, Sampo searches the spectrum for distinct peaks, or closely situated groups of peaks, based on a modified smoothed second difference inspection of the spectrum. When such a peak is located, a polynomial function is fitted to the background in the vicinity of the peak, after which it is subtracted from the total peak area while a gaussian function is fitted to the peak situated on this background.

The area under an integrated photo peak gives the number of γ-rays Nm

of a particular energy measured by the system during the live time, t, of the measurement. The registered number of γ-rays per unit time $Nm/_t$ is compared with the total number of γ-rays/sec, Ne/t, of that energy which were emitted by the radioactive source. If A_o denotes the calibrated activity of the source in emission particles per unit time as determined at the time the source was calibrated, then the number of photons emitted per second by the source at the time of the measurement is given by

$$Ne/t = A_o \, I \exp(-0.693 \, T/T_{\frac{1}{2}}) \tag{3-1}$$

Where I is the relative intensity, or photons per decay, of the particular photon emission of energy E, T is the time interval between the calibration of the source and the measurement and $T_{\frac{1}{2}}$ is the half life of the source.

The detection efficiency ϵ is defined as:

$$\epsilon = \frac{Nm/t}{Ne/t} \tag{3-2}$$

$$\epsilon = (Nm/A_o I) \exp(0.693 \, T/T_{\frac{1}{2}}) \tag{3-3}$$

In the first set of calibrations carried out, use was made of Ra^{226} source to determine the absolute efficiency of the detector as this was essential for the present work. [At 2 cm source-detector distance and 186.8

KeV energy, the absolute efficiency was $(2.97 \pm 0.15) \times 10^{-5}$].
The Ra^{226} was accurately calibrated within 4% uncertainty by The Radiochemical Centre. Corrections for photon intensities emerging from the source through the container were made. Photon attenuation factors in perspex, $(C_5H_8O_2)$ methyl metha crylate, were determined, making use of the following expression:

$$(\mu/\rho)_{cpd} = (\mu/\rho)_A \, p\frac{A}{M} + (\mu/\rho)_B \, q\frac{B}{M} + (\mu/\rho)_C \, n\frac{C}{M} \qquad (3\text{-}4)$$

Where (μ/ρ) is mass absorption coefficient in cm^2/gm, M is the molecular weight of compound $A_pB_qC_n$. The relative data were obtained from ref. 79.

The solid angle, Ω, subtended between the detector and the source was calculated from the relation:

$$\Omega = 2\pi[1 - (1/((\frac{r}{d})^2 + 1)^{\frac{1}{2}}] \qquad (3\text{-}5)$$

Where r is the radius of the detector sensitive area, and d is the source detector distance.

Using SAMPO, a relative efficiency curve was generated for each calibration source, finally they were normalized and fitted into one

Table 3.1. Ge(li) Photon Spectrometer relative efficiency at 2 cm source-detector distance.

Source	Energy (KeV)	Relative Efficiency	Source	Energy (KeV)	Relative Efficiency
Am^{241}	13.9	2.63 ± 0.31	Eu^{152}	121.9	0.999 ± 0.057
Co^{57}	14.408	3.22 ± 0.40	Co^{57}	122.061	0.964 ± 0.096
Am^{241}	17.8	3.37 ± 0.45	Co^{57}	136.33	0.729 ± 0.063
Am^{241}	20.8	3.57 ± 0.42	Ra^{226}	186.8	0.373 ± 0.013
Cd^{109}	22.1	3.67 ± 0.33	Ra^{226}	242.0	0.118 ± 0.004
Am^{241}	26.348	4.98 ± 0.35	Eu^{152}	244.75	0.114 ± 0.0068
Cs^{137}	32.1	5.82 ± 0.6	Ra^{226}	295.2	0.0796 ± 0.0057
Cs^{137}	36.5	7.43 ± 0.7	Eu^{152}	295.8	0.0779 ± 0.0039
Eu^{152}	39.5	7.93 ± 0.39	Eu^{152}	344.4	0.0587 ± 0.003
Eu^{152}	45.2	8.45 ± 0.84	Ra^{226}	352.0	0.0543 ± 0.0024
Am^{241}	59.543	4.79 ± 0.33	Eu^{152}	411.3	0.0345 ± 0.0013
Cd^{109}	87.7	2.49 ± 0.22	Eu^{152}	444.2	0.02057 ± 0.002

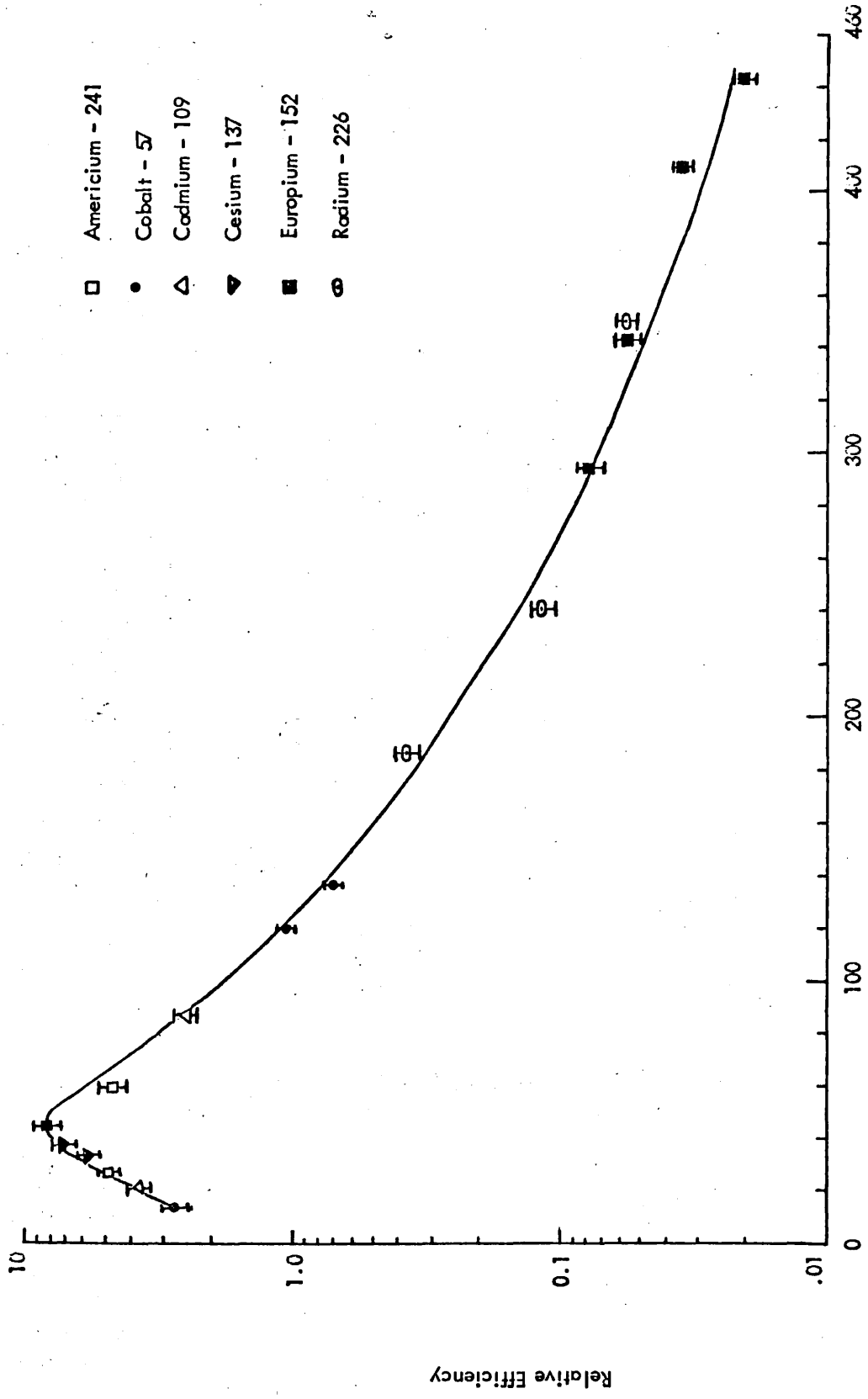

Fig 3.2 Photo peak relative efficiency for Ge(li) X-ray detector at 2 cm

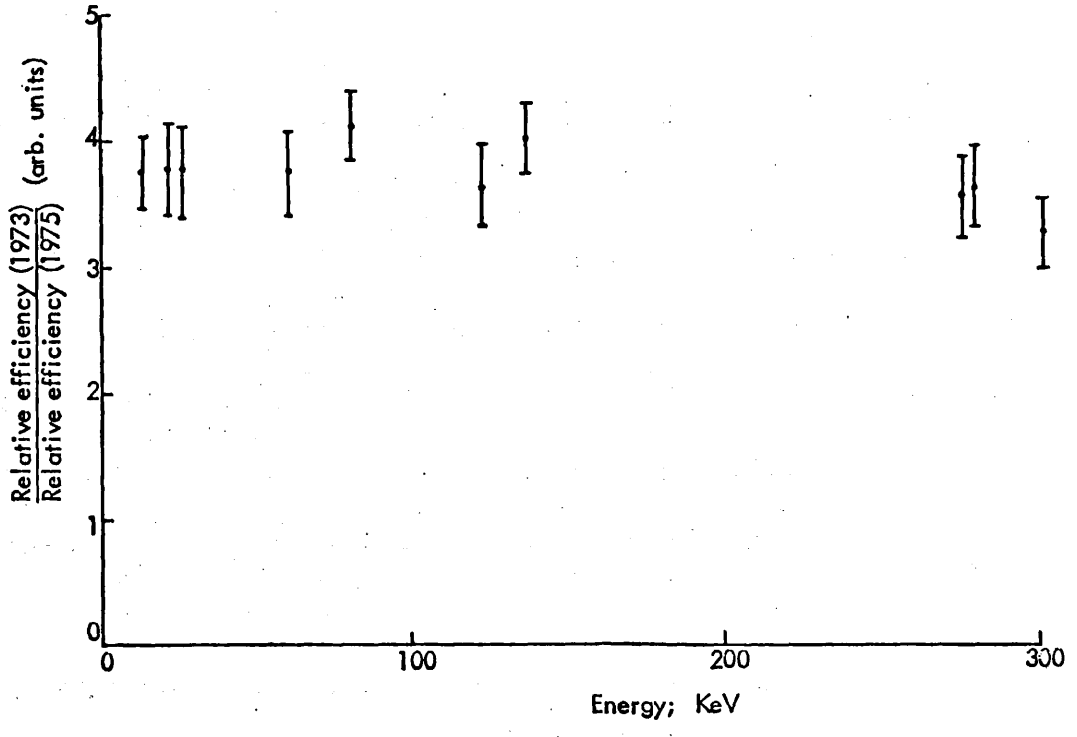

Fig 3.3 Variation of Ge(li) X-ray detector efficiency with time.

curve which is shown in Fig. 3.2.

The energy range covered was 13.9 Kev (Am-241) to 444.2 KeV (Eu-152). Energies and the corresponding efficiencies are shown in Table 3.1.

As mentioned previously, the detector was calibrated twice. Different sets of sources were used the second time; the sources were Co^{57}, Ba^{133}, Cs^{137}, Hg^{203} and Am^{241} obtained from The Radiochemical Centre (Amersham). They were accurately calibrated within given uncertainty. Relevant information was obtained from ref. 85. Efficiency results proved to be consistent with the previous measurements and comparison between relative efficiencies obtained in both cases is shown in Fig. 3.3.

Energy calibration was performed as well where a polynomial fit of different degrees applied to the data showed a good linearity.

3.4 Si(li) ELECTRON DETECTOR

The lithium-drifted silicon detector used to detect electrons was purchased from Nuclear Enterprises Limited (Edinburgh, U.K.). The detector dimensions are 200 mm^2 x 3 mm having a resolution of 17 KeV full width at half maximum for the 625 KeV conversion electron line from

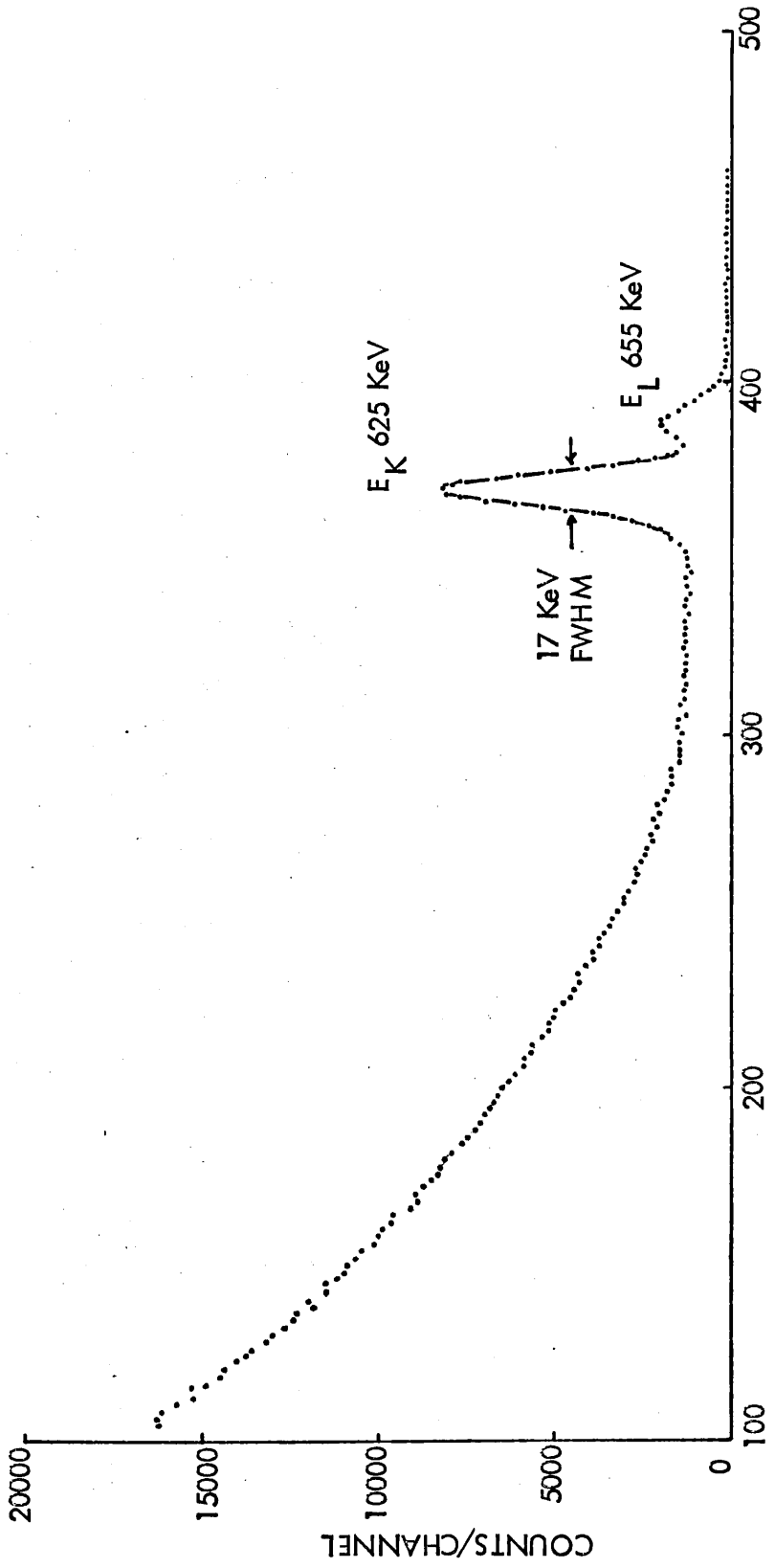

Fig 3.4 Cs^{137} Electron Spectrum taken with a 200 mm^2 x 3 mm Si(li) detector, biased at 300 V, at room temperature.

the decay of Cs^{137} (a spectrum is shown in Fig. 3.4). The surface of the detector is coated with a thin layer of gold.

A special cryostat was designed and constructed (see appendix C) to house the detector that is directly coupled to a vacuum chamber housing the electron source as well. A rotary/diffusion oil pump (Edwards High Vacuum) constantly evacuated the chamber during the measurements. Vacuum was maintained at $\lesssim 10^{-6}$ torr. Bias to the detector was supplied by NE 5321 power unit. Since the bias should be kept switched off during pump-down, as the detector may suffer damage due to corona discharge, a special vacuum monitor (see Appendix B) was constructed to detect change in pressure so that, in case of vacuum failure, e.g. due to leakage, the power supply was automatically switched off.

3.5 CALIBRATION OF THE ELECTRON DETECTOR

Silicon detectors can be profitably used as an electron counter due to their high efficiency (electrons with energies up to 2 MeV can easily be stopped inside available detectors). The total absorption peak efficiency is about 0.7 times the geometrical efficiency, so it is comparatively easy to calibrate these detectors.

Since Si(li) detectors have been in use only in recent years, very little

has been reported on efficiency curves for Si(li) diodes used as electron detectors and not much work has been published to date to discuss which method could be considered more reliable in efficiency calculations. One way has been described by Easterday et al.[50] to calibrate an apparatus for measuring internal conversion coefficients and which could be applied to the present work. Their method utilizes nuclear transitions having known conversion coefficients. The simultaneous detection of electrons and gamma quanta by a Si(li) detector and a Ge(li) detector of known gamma efficiency permits determination of the efficiency function. This method was not applied in the present work, as it was suspected that a large error in the efficiency function determination might be enhanced due to uncertainty in the photon detector efficiency.

A straightforward way has been established to suit this work in calibrating the Si(li) detector. Fig. 3.5 shows a block diagram of the experimental configuration used.

The distance between the source and the front end of the detector was 4 cm which was the same separation that would be used in the actual coincidence experiment.

Two accurately calibrated Pm^{147} and Tl^{204} beta sources obtained from

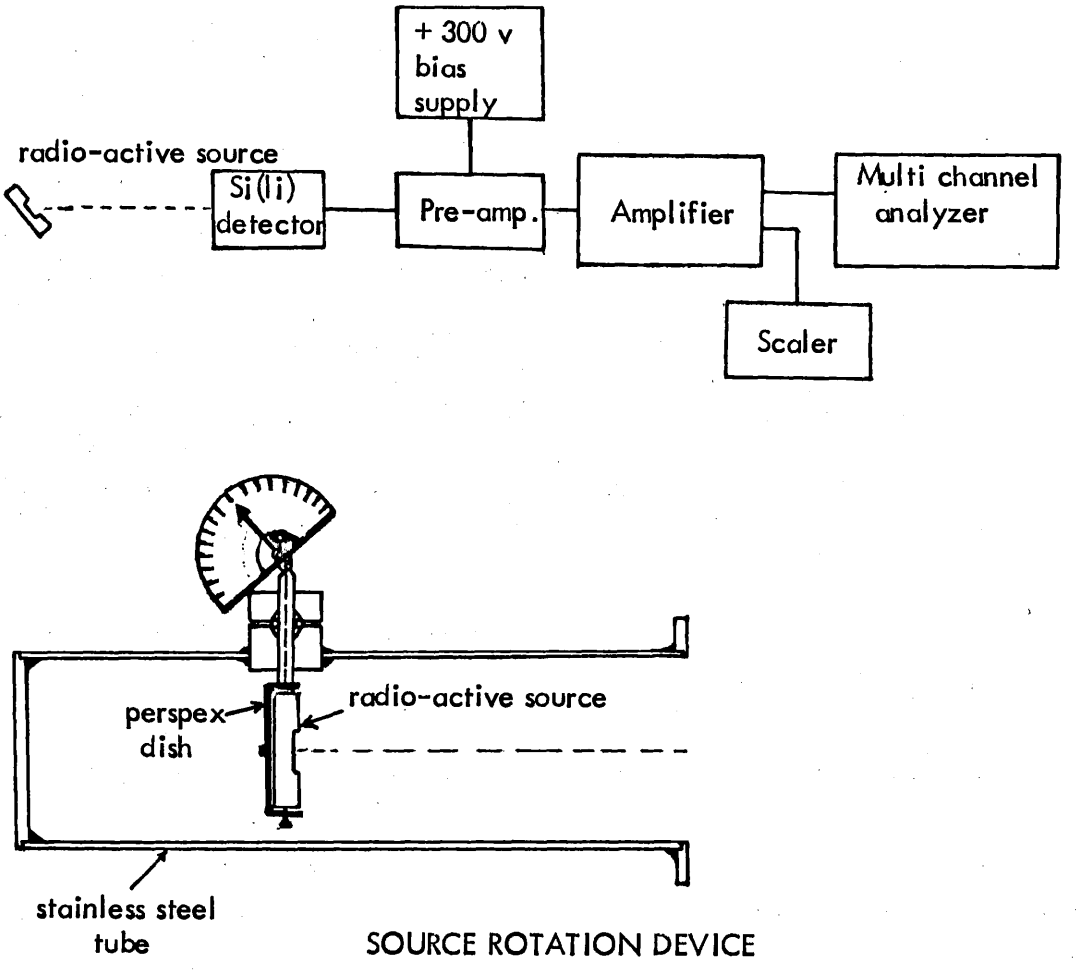

Fig. 3.5 Experimental arrangement for the electron detector efficiency measurement.

The Radiochemical Centre had been used in the calibration. The advantage of using these two sources for calibration was that they were the same sources to be studied later.

The sources were finite, each having diameter of 1 cm, covered with nominal thickness of 4 mg/cm^2 and 20 mg/cm^2 of silver for Pm^{147} and Tl^{204} respectively. The rate at which beta particles were emerging from the front of the source and overall uncertainty were given. Corrections had been made to allow for the decay of the sources.

Special care was taken in performing this measurement, in order to avoid any serious error from being propagated to the final results of the calibration. When the chamber was constructed, a device was incorporated to rotate the source at different angles with respect to the detector to determine any change in the counting rate. It was found that beta particles emerging from the front of the source have a "cos-squared" distribution.

For an uniform source, emitting electrons isotropically, at the rate N_o per second, the counting rate should be:

$$N = N_o \, \Omega / 4\pi \qquad (3\text{-}6)$$

where Ω is the solid angle subtended by the detector given to the order of $(r/d)^2$, by

$$\Omega = 2\pi\left(1 - \cos\theta\left[1 + \frac{3r^2}{2d^2}\left(\frac{\sin 2\theta}{4}\right)^2\right]\right) \qquad (3\text{-}7)$$

where r = finite source radius,

d = distance between source and end of the detector,

and θ is the angle subtended by the detector from the centroid of the source. In calculating the efficiency, it was taken into account that the source calibration carried out by the manufacturer was under conditions of 2π geometry. The final absolute efficiency results showed a slightly lower value for Pm^{147} which was expected as most of beta particles emitted by this source are considerably of lower energies than in the case of Tl^{204}.

Energy calibration of the Si(li) detector was performed using a number of isotopes purchased from Radiochemical Centre (Amersham), these were Cs^{137}, Cd^{109}, Bi^{207}, and Ce^{141}, they were in a form of a solution, sources were prepared by evaporating droplets of these solutions on a thin foil of aluminized VAPCOLEX previously treated with insulin to improve the adherence and uniformity of the sources, all the sources were used inside vacuum. Relevant information on these isotopes was obtained from ref. 80. An energy calibration curve was generated using SAMPO program.

The detector had been examined for any appreciable sensitivity to

photon detection from the sources used; no photon lines had been observed in the spectra.

3.6 THE ELECTRONIC SYSTEM AND ITS ADJUSTMENT FOR COINCIDENCE MEASUREMENTS

The coincidence system used in this work was essentially of the type shown in Fig. 3.6, and specific units are listed in Table 3.2.

The output of the silicon detector was fed, through a short low-capacitance coaxial cable, to a low-noise Tennelec Tc 164 preamplifier (An Ortec 109A preamplifier was used subsequently for Pm^{147} measurements). A linear amplifier of the type NE 4603 was used for the electron detector and an Ortec 440A selectable active filter amplifer for the X-ray detector. Crossover timing was used where the bipolar outputs from the main amplifiers were fed to timing single channel analyzers with built-in variable delays and operated in differential mode for the electron channel and in integral mode for X-ray channel. The unipolar output from the main amplifier for X-rays was fed to the multichannel analyzer through the delay amplifier.

The coincidence unit was operated with a 75 n sec resolving time. A

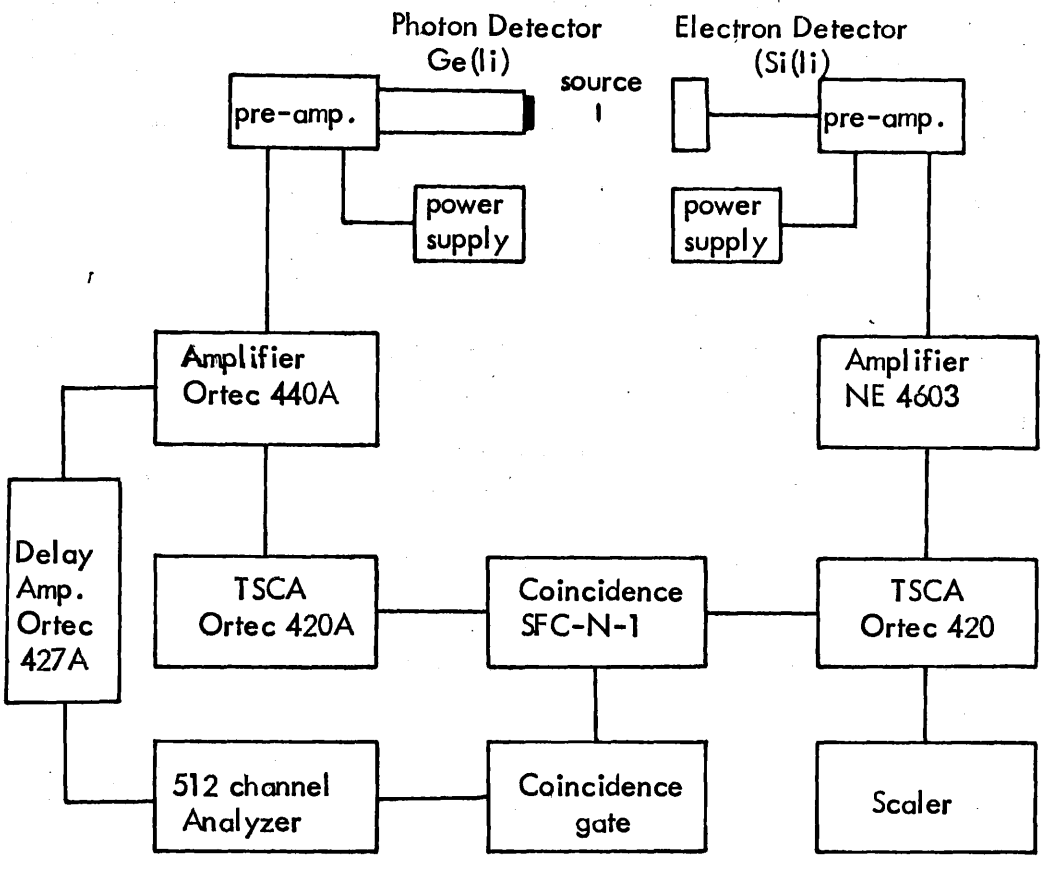

Fig 3.6 Block diagram of electronics for autoionization measurements.

Table 3.2. List of Electronics

Components	X-ray Channel	Electron Channel
Detector	Lithium Drifted Germanium X-ray spectrometer GDX 25-3A	Lithium Drifted Silicon Model NE 200-3A
Power supply	Detector voltage NE 4605	Detector bias supply type NE 5321
Pre-amplifier	Nuclear Enterprises pre. amp. type NE 5287A	Tennelec Tc 164, Ortec 109A
Amplifier	Ortec 440A selectable active filter amplifier	NE 4603 main amplifier
TSCA	Ortec 420A	Ortec 420
Delay Amplifier	Ortec 427A	
Coincidence Unit	Fast slow coincidence model	SFC-N-1
Gate Generator	(Locally constructed)	
Scaler		Harwell fast scaler
Analyzer	512 channels analyzer Northern Econ I Series	

typical delay curve obtained is shown in Fig 3.7.

The total number of β-particles in the energy window was recorded with a high counting rate scaler.

Use was made of triple slow coincidence unit constructed (see Appendix A) to act as a gate pulse generator, so coincident pulses were fed to this gate generator. The generated pulses opened the gate of the multi-channel pulse-height analyzer to record the X-ray spectrum.

Since the stability of the whole system was crucial to the success of the experiment, before long run measurements were started, the drift of the system was examined carefully using Bi^{207} and Cs^{137} sources (in each experiment, either of the two sources was used to suit the criteria of the isotopes to be studied), where the lead K X-rays were detected in coincidence with the 976 KeV electrons, and the 32 KeV Ba K X-rays were observed in coincidence with the 625 KeV K-conversion electrons. The fluctuation in stability of the whole system was found to be less than 1% within a week in both cases.

As nothing has been done in the system to correct automatically for the chance coincidences, corrections were made which followed the expression:

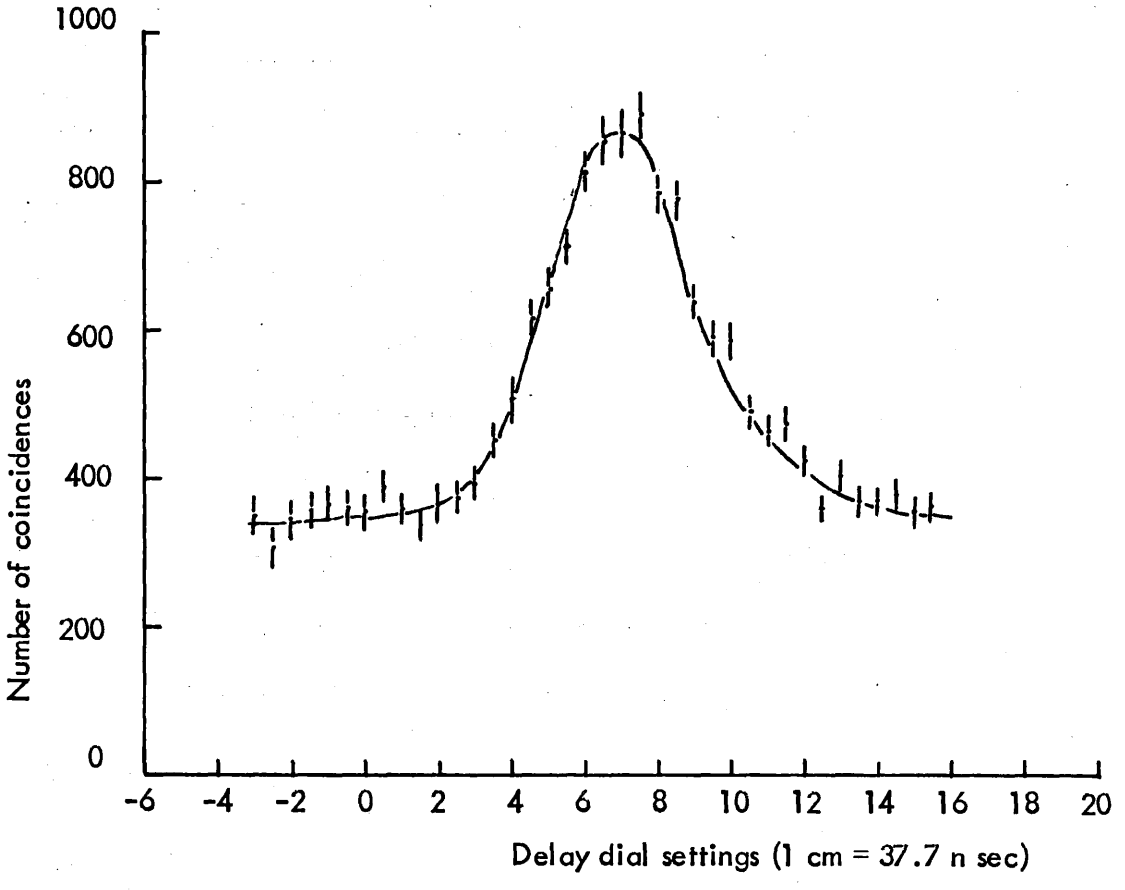

Fig 3.7 Time resolution curve for Cs^{137} e_k - X coincidences recorded by Si(li) electron detector and Ge(li) X-ray detector, using crossover timing.

$$N_c = 2\tau N_x N_e / t \qquad (3\text{-}8)$$

N_c = The chance coincidence counts

N_x = The number of particles detected by the X-ray detector.

N_e = The number detected by the electron detector.

2τ = The resolving time of the coincidence unit.

t = The run time.

on average the chance coincidence accounted for less than 10% of the total coincidences as weak sources were used.

One advantage of the coincidence system selected for the present work is the reliability of the different components used and the simplicity of the system if compared with more complicated systems where more electronic units are incorporated.

3.7 IMPLEMENTATION OF SAMPO FOR DATA ANALYSIS

A few years ago Routti and Prussin[51] introduced a semiconductor spectral analysis code called SAMPO. This program has been used extensively at this and other laboratories to analyze gamma-spectral data, it is regarded as a reliable and consistent procedure for analysis of a wide variety of semi-conductor detector spectra.

In the present work, SAMPO was a very convenient program because of its multifunctional nature. The code can be used to locate the exact positions for peaks in the spectra, perform line shapes, fit single and even very close-lying multiples with these shapes. The peak-shape energy and efficiency calibration can also be performed within the code.

The program was used for both spectra from the Ge(li) X-ray and the Si(li) electron detector (for conversion electron spectra).

Energy calibrations for both detectors were performed where a polynomial least squares fit was applied to a number of energy calibration points by minimizing the expression:

$$X^2 = \sum_{i=1}^{n} \frac{1}{D_i} \left[E_i - \sum_{j=1}^{m} P_j C_i^{J-1} \right]^2 \qquad (3\text{-}9)$$

where C_i, E_i, and D_i are the channel numbers. By knowing the parameter P_j, the resulting curve is used for subsequent energy determinations.

The efficiency data for the Ge(li) detector were fitted in a curve where a function of the following form had been used for the fitting.

$$E_{ff} = C_1 (E^{C_2} + C_3 e^{C_4 E}) \qquad (3\text{-}10)$$

where C_1, C_2, C_3 and C_4 are parameters to be determined and E is energy in KeV.

The real advantage of using SAMPO in the present work was its ability for fitting closely situated peaks of the X-rays (resulting from the auto-ionization). The fittings obtained for these peaks are considered to be very satisfactory.

Chapter 4

K-SHELL INTERNAL IONIZATION ACCOMPANYING THALLIUM-204 DECAY

4.1 INTRODUCTION

The present work on Tl^{204}, was aimed at finding the K-shell internal ionization probability as a function of β energy. To date, no work has been done regarding this aspect, except for the study made by Mord.[25]

In principle, two approaches could be applied; first performing electron-electron coincidence measurement in order to distinguish orbital electrons ejected in the event considered from those emitted in ordinary beta decay process. Feinberg[1] states that atomic electrons are usually ejected with kinetic energy equal to or less than their binding energy, and hence detection of electrons with quite low energies becomes necessary. This is rather difficult to achieve practically. Another difficulty of this approach is the interpretation of the electron-electron coincidence results as there is no way of telling from which atomic shell a given electron originated.

The approach which had been applied in the present experiment for its practical convenience is to measure the K X-rays of the daughter atom which quickly follow the creation of K-shell vacancies by internal ionization, in coincidence with the emitted electrons (beta particles or atomic electrons).

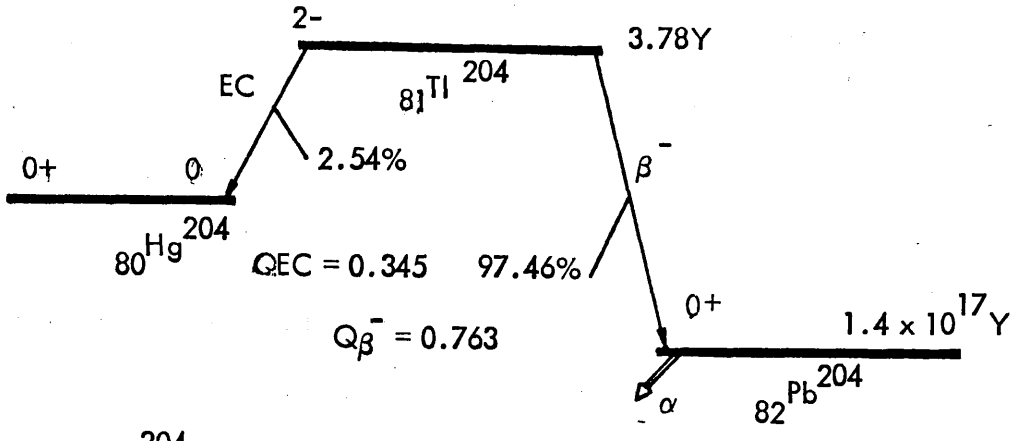

Fig. 4.1 Tl^{204} decay scheme. The branching intensities have been taken from ref. 86.

The choice of Tl^{204} introduced no complications, as it is particularly suitable. As shown in fig. 4.1, Tl^{204} can decay by two alternative mechanisms: 97.46% of the decay goes via β^- decay to Pb^{204} and 2.54% by electron capture to Hg^{204}. Transitions to excited levels of either Pb^{204} or Hg^{204} do not exist. Recently Bond and Lancman[87] observed no gamma rays in the Tl^{204} spectrum with energies in the range of 100 - 700 KeV. This results in a simpler photon spectrum and the absence of X-rays following internal conversion. So any Lead K X-rays observed will be produced by internal ionization and Mercury K X-rays are produced in the electron capture process.

Due to the isotope's high atomic number, Z = 82, the K X-rays are easily detected. The Si(li) detector of 3 mm depth is able to stop all of the energetic electrons (the decay energy of Tl^{204} is 763 KeV). The isotope half-life (3.78 years) is long enough to perform lengthy experimental runs without complication.

Another approach has been adopted for the study on Tl^{204}, where the K-shell autoionization probability was determined from the intensities ratio of Mercury and Lead K X-rays. This did not involve any special technical considerations. The necessary data were obtained from the Tl^{204} straight photon spectra in the Ge(li) X-ray detector which was ideal for this experiment with its good resolution. The data were analyzed later using SAMPO.

4.2 PREVIOUS INVESTIGATIONS

Howard et al.[43] performed their experiment in which they used a lithium drifted silicon detector as an X-ray detector to detect the photon spectrum from a Tl^{204} source, in measurement of the relative intensities of the Mercury and Lead K X-rays with the knowledge of the branching ratio of electron capture to β^- emission, they were able to calculate electron shake off probability obtaining a value of $(0.99 \pm 0.07)10^{-4}$ per β^-, the

calculations were based on Carlson's values for shake off probability. Their measured $Hg/_{Pb}$ K X-rays intensity ratio was larger by a factor of two than the predicted ratio based on Carlson's calculations ($P_K = 2.06 \times 10^{-4}$).

Mord[25], made a study of Tl^{204} which is similar to the present work. He used the coincidence technique, by detecting the electrons in a Si(li) detector and the K X-rays in aGe(li) detector. He measured K-shell internal ionization probability as a function of energy and his experimental data compared with theoretical predictions are shown in Fig. 4.2.

Pathak[44], using a Ge(li) spectrometer, measured the K-shell auto-ionization probability following Tl^{204} decay. A value of $(1.06 \pm 0.03)10^{-4}$ was obtained. His calculations were based on the same principles used by Howard et al.[43], by comparing the intensities of the Mercury K X-rays resulting from the electron capture process and the Lead K X-rays resulting from the auto-ionization mechanism. Their final results were very close though they used different branching ratios which undoubtedly should give rise to serious discrepancies.

Later Ljubičić et al.[45] carried out a rather similar study on Tl^{204} to other authors'[43]. Using a Si(li) detector, their measured P_K $(1.18 \pm 0.06)10^{-4}$ is in agreement with the previous results.

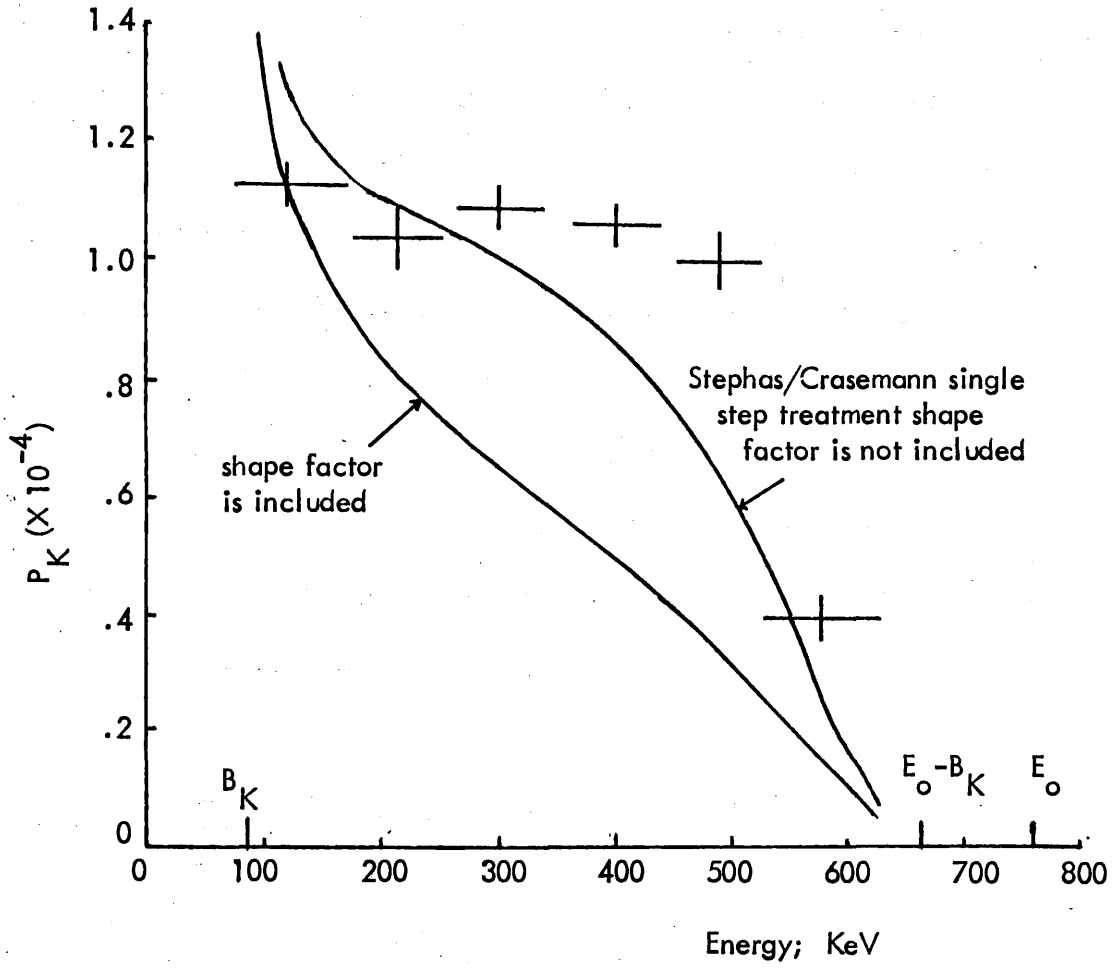

Fig 4.2 Mord's experimental data compared with theoretical predictions. Vertical bars represent one standard deviation. Horizontal bars indicate widths of electron energy intervals.
(adapted from ref. 25)

Though it is argued that in performing experiments where only photon spectra are detected, the two-electron problem is avoided which arises from indistinguishability of an orbital electron and β^- particle involved in coincidence experiments, obviously these straight forward techniques are easier to perform but are not of application in finding $P_K(E\beta)$, and consequently not able to offer precise assessment for the different existing models where the $P_K(E\beta)$ shape is their basic argument. From this point, use of the coincidence technique becomes vital, the experiments are lengthy and elaborate, and could be applied only to a few isotopes due to many practical problems.

4.3 SOURCE PREPARATION

The Tl^{204} source was purchased from The Radiochemical Centre (Amersham, England) in the form of $^{204}TlNO_3$ solution in HNO_3. A number of sources were prepared with activities ranging from 10 μCi to 30 μCi by evaporating the desired quantity of the solution on 0.0001 in aluminized VAPCOLEX plastic film (George M. Whiley Ltd). As thin sources were needed, the foil was previously treated with insulin, (5 per cent in water) solution was pipetted on to the spot desired for the source. The insulin was dried, and a drop of the isotope solution was transferred with a syringe. The use of insulin improved the adherence

and uniformity of the source thickness as noted by Yaffe[88]. In addition, the insulin controlled the location and size of the spot of dried radioactive sample. Fig. 4.3 shows a schematic diagram of the source mounting.

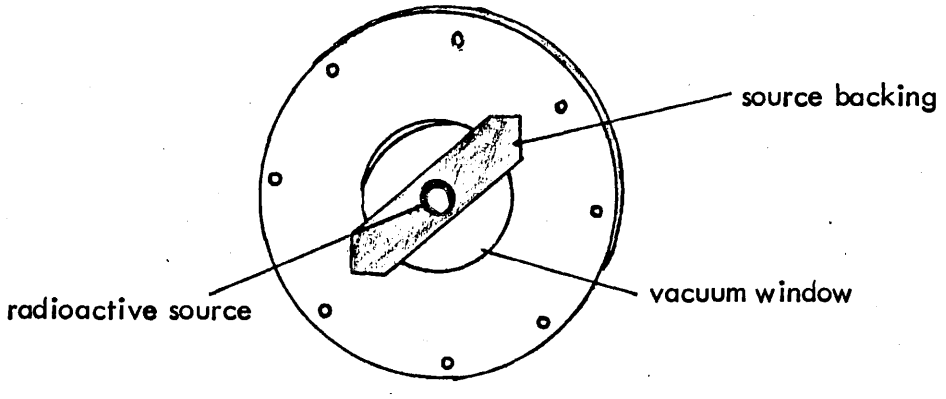

Fig 4.3 Source Mounting Schematic Diagram

4.4. PRESENT WORK

The coincidence system was operated as described in Chapter 3. The solid angles subtended by the two detectors were made as large as practical in order to maximize the coincidence counting rate. A 3mm perspex absorber was placed between the two detectors to stop electrons reaching the Ge(li) X-ray detector which would result in more complicated spectral background. A bismuth-207 source was used to set up the system for the coincidence measurements.

The choice of bismuth-207 was due to the fact that the source emits Lead K X-rays which are the same K X-rays expected from K-shell autoionization in the β^- decay of Tl^{204}. The coincidence resolving time was 75 n sec; checks made before and after the course of the experiment showed 2τ was constant within the statistical uncertainty of the measurements.

For $\bar{P}_K$ the total K-shell autoionization probability determination, the Lead K X-rays in coincidence with emitted electrons having initial energy greater than the K-shell binding energy were recorded in the multi-channel analyzer and the β-particles were registered using a fast scaler.

For the energy dependence measurement, the energy region of the

spectrum was divided into seven segments by adjusting the window of the single channel analyzer in the β-particle channel. Taking into consideration the gradual decrease in number of β-particles at higher energies, window settings for these electrons were made wider. The lower energy setting that we could manage to separate noise associated with electronics, from the true beta spectra, was $\sim$80 KeV which is just lower than the Tl K-shell binding energy. This limitation of window setting was in part imposed on the system for a number of problems associated with low energy electron detection due to scattering and window thickness.

Any sort of shielding - especially Lead - around the detectors had been avoided, since this might result in undesired Lead fluorescent X-rays which would enhance to that due to the studied phenomena.

The stability of the system was examined from time to time and, after each run, data of coincident spectra beside the straight spectra of both detectors were recorded. Window settings were checked before and after each run.

Each individual run took a period of seven days, except for the total range electron spectrum coincidence where each run lasted for three to

four days. Finally, ten runs were analyzed from a total of twelve runs.

In the case of the straight photon spectrum, a period of two to three days was taken for each measurement.

A total period of seven months was spent for data collection on Tl^{204}.

4.5 DATA ANALYSIS AND DISCUSSION

The obtained coincidence spectra for Tl^{204} were analyzed and the scanned peaks were fitted into a gaussian function using shape calibration data generated by SAMPO from the Bi^{207} photon spectrum.

The X-ray attenuation coefficients for perspex, which was used as electron absorber, were taken into account earlier in the detector efficiency determination.

The probability per β^- decay of forming a hole in the K-shell is given by:

$$P_K(E_\beta) = (N_K \epsilon_e)/(N_e \omega_K \epsilon_x) \qquad (4\text{-}1)$$

Where N_K is the number of coincident K X-rays in the photon spectrum.

ϵ_e is the electron detector detection efficiency.

ϵ_x is the X-ray detector detection efficiency.

N_e is the number of electrons (β-particles + orbital electrons) in the electron-channel window.

ω_K is the fluorescence yield of the daughter nuclei Lead).

The electron detection efficiency ϵ_e was of the order $(7.72 \pm 0.79)10^{-3}$ while the X-ray detector efficiency ϵ_x (including solid angle) for Lead K X-rays were given as follows:

X-ray Line	Detection Efficiency
PbK_{α_2}	$(26.5 \pm 2.4)10^{-5}$
PbK_{α_1}	$(25.2 \pm 2.5)10^{-5}$
PbK_{β_1}	$(17.9 \pm 1.8)10^{-5}$
PbK_{β_2}	$(16.6 \pm 1.7)10^{-5}$

The ω_K fluorescence yield had been taken as 0.968 from ref. 89.

In some of the runs where reliable fitting for PbK_β peak areas was not achieved, N_{K_α} was introduced instead of N_K in equation 4-1, where N_{K_α} is the number of K_α X-rays coincidences and a figure F is incorporated in the denominator of the equation where F is the ratio of K_α X-rays to the total K X-rays, 0.782 (taken from ref. 90).

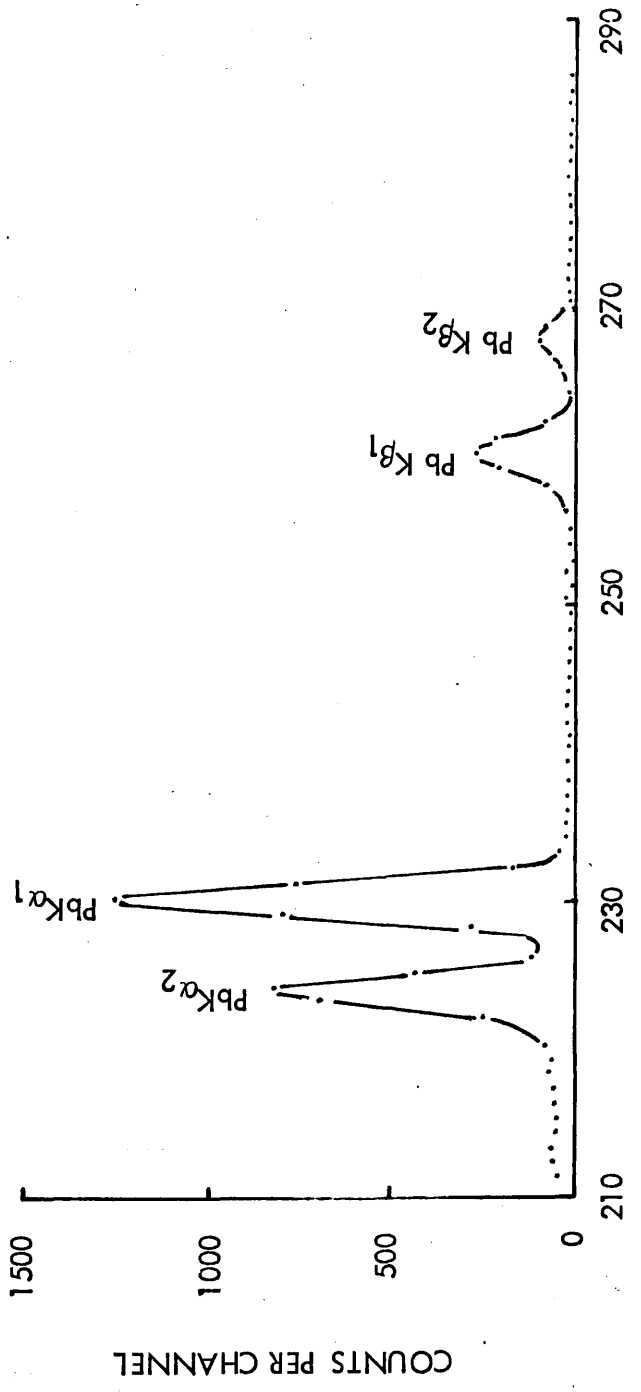

Fig. 4.4. Photons of Tl^{204} observed in coincidence with β^- particles (electrons)

The coincidence spectrum obtained for electrons of 220.5 KeV to 270 KeV energy is shown in Fig 4.4.

The $P_K(E_\beta)$ values derived from the present measurements are shown in Table 4.1. Furthermore, these $P_K(E_\beta)$ values are plotted in Fig 4.5. where the horizontal bars represent the energy settings in the electron channel and the vertical bars represent errors due to those of a statistical nature and uncertainties for the differenent components in equation 4.1.

The measured $\bar{P}_K$ (total K-shell internal ionization probability for $E_\beta > B_K$) is also shown in Fig 4.5.

Table 4.1 Measured energy-dependent K-shell autoionization probability $P_K(E_\beta)$ in the β^- decay of Tl^{204}.

Lower settting for energy window E KeV	Upper setting for energy window (E +ΔE) KeV	$P_K(E_\beta)10^{-4}$
80	140.3	1.079 ± 0.08
150	190	1.095 ± 0.09
220.5	270	1.084 ± 0.087
280.1	330.4	1.09 ± 0.07
350	450.5	1.09 ± 0.09
450	530	0.93 ± 0.06
540.5	625	0.61 ± 0.13

Total probability $\bar{P}_K = (1.15 \pm 0.08)10^{-4}$

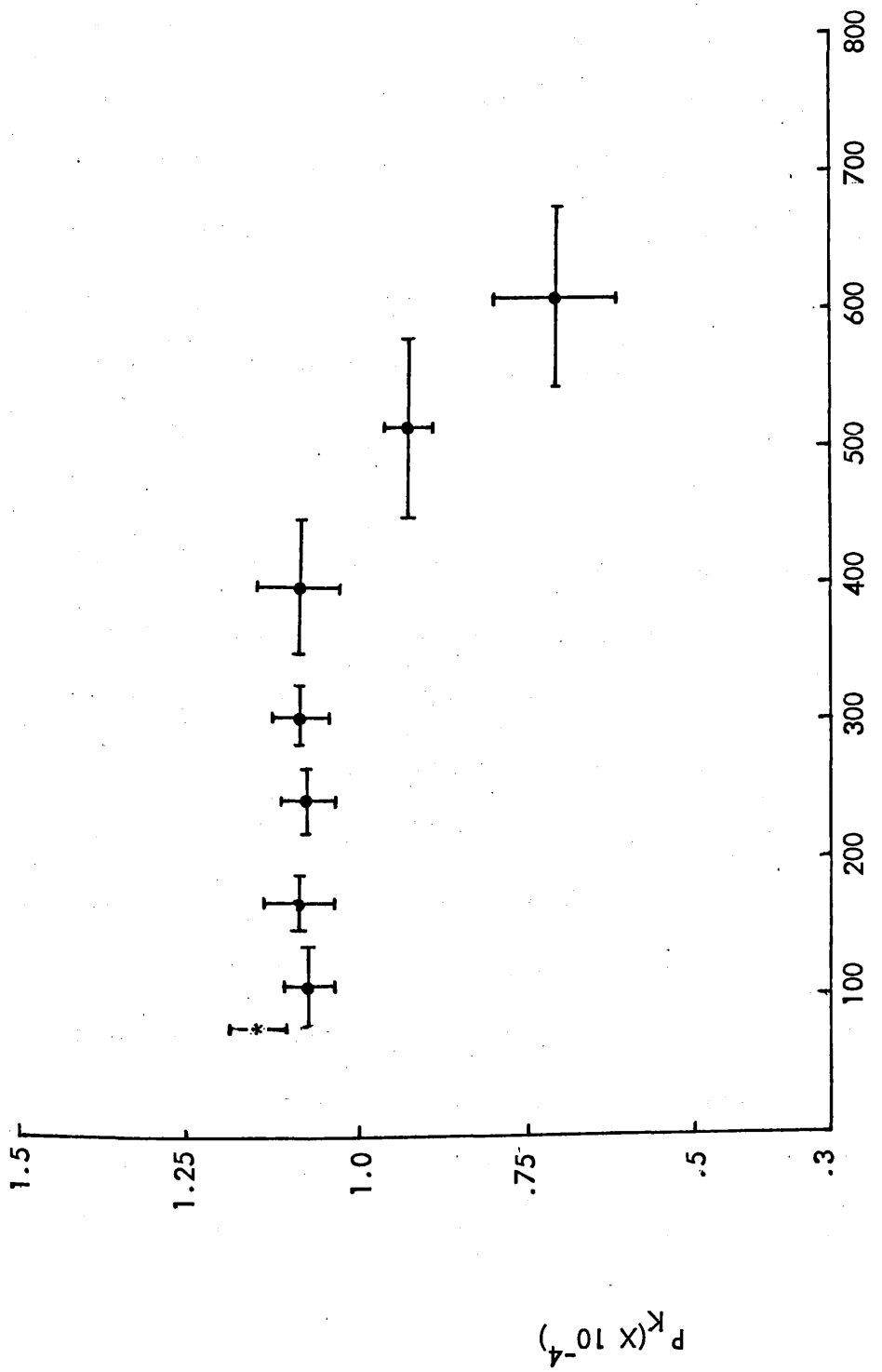

Fig. 4.5 Measured energy-dependent K-shell internal ionization probability $P_K(E_\beta)$ for Tl^{204} horizontal bars indicate widths of electron energy intervals, vertical bars represent errors.

*measured total ionization probability $\bar{P}_K$.

Mord's measurement[25] regarding β-energy dependence of internal ionization in the decay of Tl^{204} predicted that the Stephas/Crasemann theory in its unmodified form (i.e. the factor arising from antisymmetrization of the final state wave function is ignored) comes to close agreement with the experimental results in shape but with a discrepancy of roughly a factor of 4 in magnitude. His results were in a very poor agreement with Stephas Crasemann theory both in shape and magnitude. Mord made an allowance for an error of a factor of 2 due to the use of non-relativistic wave functions and ended up with an unexplained discrepancy of a factor of 2.

Our results of β-energy dependent $P_K(E_\beta)$ are in close agreement with Mord's results in magnitude but we do not feel strongly about the results being in good agreement with the one step treatment given by Stephas and Crasemann neither in magnitude nor in shape. Mord's results did not offer a fair explanation for his support for this theory, as all his measured $P_K(E_\beta)$ values were well above the magnitude of (1×10^{-4}) except for the last setting of the energy window which gave a lower magnitude. In fact, our results show greater energy dependence than that of the Mord measurement. However, we do not reject the theory but we believe that this kind of technique is not going to get the experimental results in any closer agreement with the theory as it is now; so more elaborate theoretical

work has to be done to overcome the existing discrepancies and to bring the experimental data in line with the calculated values.

Our total $\bar{P}_K$ probability $(1.15 \pm 0.08)10^{-4}$ is in good agreement with Law and Campbell's[16,54] calculated value (1.27×10^{-4}) for P_K (So + Su + Dc); where the three mechanisms are included; shake off, shake up and direct collision.

The other approach applied in the present work to determine K-shell autoionization probability P_K in the β^- decay of Tl^{204}, was that of comparing Lead K_{α_1} X-rays with Mercury K_{α_1} X-rays in the photon straight spectrum as P_K is given by.

$$P_K = \frac{N_{Pb}}{N_{Hg}} \frac{\epsilon_k}{\beta} \frac{\omega_{Hg}}{\omega_{Pb}} \frac{D_{Hg}}{D_{Pb}} \frac{P_{Hg}}{P_{Pb}} \qquad (4\text{-}2)$$

Where N_{Pb} and N_{Hg} are the areas under K_{α_1} X-ray fitted peaks of Lead and Mercury; $\frac{\epsilon_K}{\beta}$ is the K-shell electron capture to β^--decay branching ratio; ω_{Hg} and ω_{Pb} are the fluorescent yields of Mercury and Lead; D_{Hg} and D_{Pb} are the relative detection efficiencies for Mercury and Lead; P_{Hg} and P_{Pb} are the ratios of the K_{α_1} X-rays to the total K X-rays for Mercury and Lead.

The values of ϵ_{K/β^-}, $\frac{\omega_{Hg}}{\omega_{Pb}}$, and $\frac{P_{Hg}}{P_{Pb}}$ were obtained from refs. 86, 89

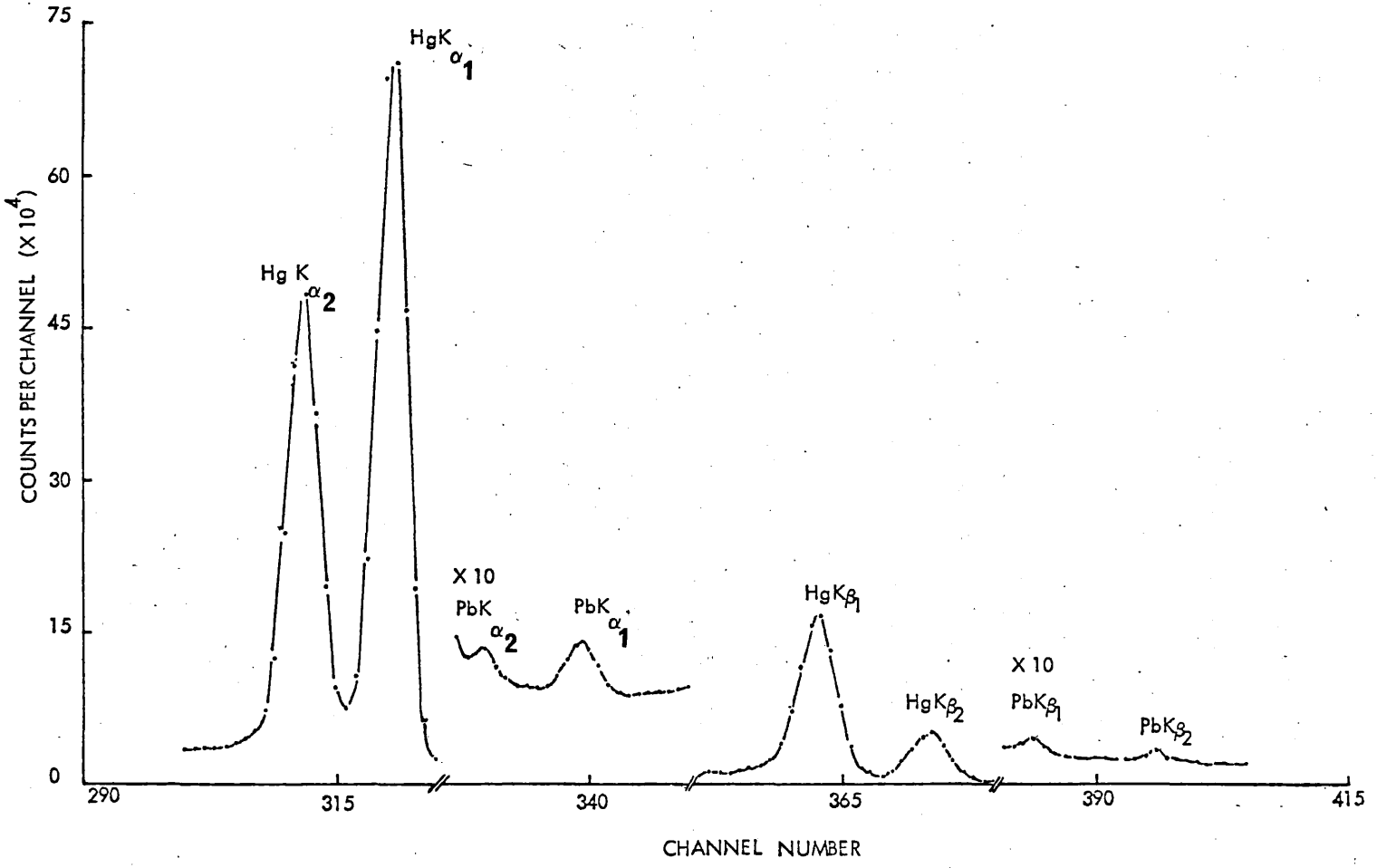

Fig 4.6 Tl^{204} K X-ray spectrum taken with the Ge(li) detector

and 91 respectively. The spectrum is shown in Fig 4.6 and the average value of $\frac{N_{Pb}}{N_{Hg}}$ was found to be $(7.81 \pm 0.19)10^{-3}$, our measurement resulted in a P_K value of $(1.37 \pm 0.07)10^{-4}$. This value is in good agreement with the calculations of Law and Campbell.[15,54,78]

In comparison with P_K values measured at other laboratories mentioned previously in section 4.2, using the same technique, our experimental result for P_K is in agreement with other measurements except for those of Howard et al.[43] As these authors obtained a lower value than the present work, this could be attributed to the low K-shell electron capture to β-decay branching ratio they had assumed in their calculations. Neither our result nor other results are in agreement with Mord's[17] predictions for P_K in the β^- decay of Tl^{204}.

Chapter 5

K-SHELL INTERNAL IONIZATION ACCOMPANYING PROMETHIUM-147 DECAY

5.1 INTRODUCTION

The present work carried out on Pm^{147}, in principle, is identical to that on Tl^{204} (chapter 4).

There has been a great deal of work on Pm^{147}. It was the isotope with which Boehm and Wu[20] started the experimental study of autoionization phenomena. It has been an isotope of interest for the present work for practical reasons rather similar to the ones mentioned in the previous chapter for Tl^{204}; also the study of autoionization as a function of β-energy for Pm^{147} has not been given much attention by other workers, except for the study made by Stephas et Creasemann[12], and Isozumi et Shimizu.[26]

Apart from the reasons above, it was of importance for the present work to compare measurements on different isotopes as this would result in a better judgment of the existing theories on the subject. Theoretically Pm^{147} represents lower medium mass nuclei (Z = 61) while Tl^{204} represents upper medium mass nuclei (Z = 81). Although both isotopes are first forbidden β decays; the degree of forbiddenness differs in some respects because Pm^{147} is considered to be a first forbidden non-unique decay and Tl^{204} is a first forbidden unique decay. The decay energy

of Pm^{147} (224 KeV) is much lower than that of Tl^{204} (763 KeV). All these factors together might permit one to assess with a reasonable degree of confidence clues to the conflict present between different models favoured by different research groups.

Promethium-147 decays according to the scheme shown in Fig 5.1. A correction must be made for the minute contribution to the observed X-ray peak, which is caused by K-internal conversion from the 122 KeV first excited state of samarium-147 to its ground state.

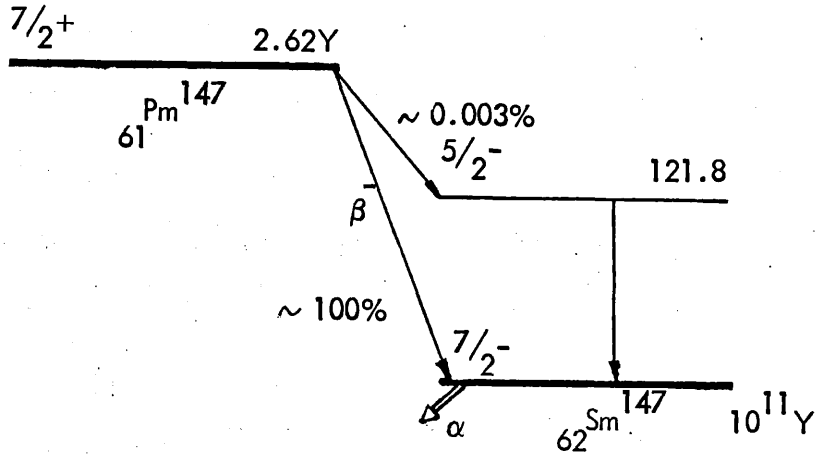

Fig 5.1. Decay sheme of promethium-147.

5.2 PREVIOUS INVESTIGATIONS

Reviewing the early measurements, Boehm et Wu[20] presented their original experimental evidence for internal ionization by recording Sm K X-rays from a Pm-147 source; the X-rays were detected in a NaI crystal while the β^--particles were recorded in a proportional counter.

Independently Langevin Joliot[37] used a similar technique where a magnetic lens spectrometer was used for the β^--particles. The results of these two early measurements have been regarded by a number of authors as being inaccurate. Nevertheless, these experiments served as an introduction to the field. It was Stephas and Crasemann[12] who tried to measure the K-ionization probability as a function of β-energy. Their experiment resulted in a strong energy dependence in the case of ^{147}Pm, which gave support for the single step model. Isozumi and Shimizu[26] detected Sm K X-rays in a NaI(Tl) scintillation counter in coincidence with emitted electrons for various segments of the β spectra of Pm-147 using 4π detection geometry for these electrons. The source was mounted in the electron detector (a split anthracene crystal). The energy dependent ionization probability $P_K(E_\beta)$ was measured as a function of E_β. The energy dependence and the simultaneously measured total ionization probabilities were claimed to

be in fairly good agreement with theoretical values calculated by the theory based on a relativistic one step treatment of electron shake off. Their conclusion was that electron shake off is the predominant mechanism even for electrons (β particles plus K-electrons) emitted with very low energies.

For most β-emitters, the X-rays of the daughter atom that signify autoionization ($\sim 10^{-4}$ per β decay) are swamped by those arising from K-internal conversion transitions that de-excite the daughter nucleus. Only in special cases can the intensity of K X-rays signifying autoionization be measured accurately, where the transition in the daughter nucleus has insufficient energy to convert in the K-shell. The photon spectrum then contains K X-rays whose intensity is proportional to the occurrence of autoionization N_x together with the γ-ray whose intensity is proportional, via accurately known decay scheme parameters, to the overall decay rate N_e. The defined $\frac{N_x}{N_e}$ ratio is then obtained from a single spectrum with the knowledge of relative detector efficiency. This method has been extended by Campbell and Law[19] to cases where one γ transition in the daughter is very weakly converted. They applied this approach to the case of Pm-147, and used an Ortec Ge(li) X-ray spectrometer of energy resolution approximately 200 eV (FWHM) at 6.4 KeV to record the photon spectra from a Pm-147 source.

Table 5.1 Total K-shell autoionization probability $\bar{P}_K$ in the decay of Pm-147

$P_K \times 10^4$ Experiment	Author	$P_K \times 10^4$ Theory	Author
3.85 ± 0.5	Boehm et al.	.517	Mord
		.354	Mord
1.30 ± 0.26	Longevin Joliot	.941	Mord
		.663	Isozumi et Shimizu
0.93 ± 0.14	Stephas and Crasemann	2.88	SCF Calc. by Carlson
		.515	SCF Calc. corrected
0.76 ± 1.1	Isozumi et Shimizu		
0.98 ± 0.08	Campbell and Law		
0.81 ± 0.09	Hansen et al.		
0.43 ± 0.17	Present work		

Their measured P_K was $(0.98 \pm 0.08) \times 10^{-4}$ compared with a magnitude of 0.91×10^{-4} for P_K calculated by the same authors from a model based on vacancy creation mechanisms of shake off and shake up and employing a simple correction for direct collisions.

In recent measurements on K-shell internal ionization probability in Pm-147 by Hansen and Parthasaradhi[34] using a high energy resolution Si(li) X-ray detector, the number of emitted K X-rays was measured in comparison to the absolute β^- decay rate resulting in a P_K value of $(0.81 \pm 0.09) \times 10^{-4}$. Table 5.1 gives a comparison between measured P_K values for Pm-147 obtained by different authors including the present work and recent theoretical calculations of P_K.

5.3 SOURCE PREPARATION

The source material was obtained from Radiochemical Centre (Amersham, England) in the form of $^{147}PmCl_3$ in HCl. A series of sources were prepared by evaporating droplets of the solution on 0.008 mm platinum foil backing (Good Fellow Metals Limited, Surrey, England).

Colloidal Silica treatment was applied, as proposed by Merritt et al.[95] who introduced a small amount of Silica sol. to act as nucleation centres

during the drying process. They used a $1:10^4$ aqueous dilution of Ludox SM (Dupont) and in a study of beta efficiencies as a function of the amount of "Ludox", they showed that about 10 to 20 μl of the diluted Sol (about 0.2 to 0.4 μg residual silica) was optimum for most source preparations. Although high ionic concentrations should be avoided to prevent gelation of the silica, Ludox has been successfully used with solution as acidic as 0.5 N. Ludox SM30 (Dupont) has been used in the present source preparation. The particles of this Ludox are dispersed in alkalic medium of sodium hydroxide. The particle size of order 7 - 8 nanometer is the smallest particle size among other grades of Ludox.

A 5 μl disposable pipette was used to transfer $\sim$ 15 μl of freshly prepared $1:10^4$ aqueous dilution of Ludox SM30, to the centre of the platinum foil source backing and droplets of the radioactive material were delivered into the solution and dried under an infrared lamp to yield a roughly circular deposit of about 0.75 cm^2. Platinum foils of thicknesses .001 mm and 0.008 mm were tried; the thin foil being supported by acrylic resin. Different source strengths were prepared. The final choice for the source to be used depended on how good was the shape of the β-spectrum (with a minimum amount of distortion) in addition to a reasonable strength of the source to fulfill the requirements of the experiment. A source of strength

$\sim$ 27 μCi mounted on 0.008 mm Pt backing foil was finally used.

In the course of the earlier source preparation, it was found that the hydrochloric acid was reacting with the aluminium from aluminized VAPCOLEX and then attacking the acrylic resin itself. This was one of the reasons for using the platinum backing though it has a higher atomic number. The arrangement of the source holder and the vacuum window was in the same manner as for Tl-204 experiment. One feature of the use of the platinum backing is that there arise fluorescent Platinum X-rays due to β^--particles from the source. However, this did not contribute a serious problem in the actual measurements as platinum X-rays are well separated in energy from Sm K X-rays.

5.4 PRESENT WORK

In the present work, the β-ray emitter pm-147 was chosen, because the relatively large value of B_K/E_o is advantageous for observing the phenomenon in the low-energy region of the β-spectra (E_o = 224 KeV and B_K = 47 KeV). The nuclide has been shown to decay to the ground state of Sm-147 through β^- decay but with a very weak β^- branch to the 122 KeV first excited level of Sm-147. The branching ratio of this weak β^- decay, determined by Mowatt and Merritt[93] as 2.7 X 10^{-5} has

to be taken into account in the present work.

The experimental arrangement was the same one used for the Tl^{204} measurement except for the preamplifier in the electron channel where an ORTEC 109A charge sensitive preamplifier replaced the Tennelec TC164 preamplifier. This resulted in less noise and a timing improvement.

The coincidence circuit connecting both detector channels including the amplifiers and timing single channel analyzers was operated with a time resolution $2\tau = 70$ n sec.

In the present experiment, the ratio of the random to true coincidences was found to be negligibly small as calculated from the recorded spectrum which will contain true coincidence counts plus $N_x N_e 2\tau t^{-1}$ chance coincidence counts, where N_x is the number of particles detected by the X-ray detector, N_e is the number detected by the electron detector, 2τ is the timing resolution and t is the run time. This has been confirmed by inserting a delay in one of the channels and recording chance coincidences in the multichannel analyzer; there was no significant number of counts in the channels corresponding to Ba K X-rays in the case of Cs-137, or to Sm K X-rays in the case of Pm-147. The fluctuation in both cases lies within the statistical errors.

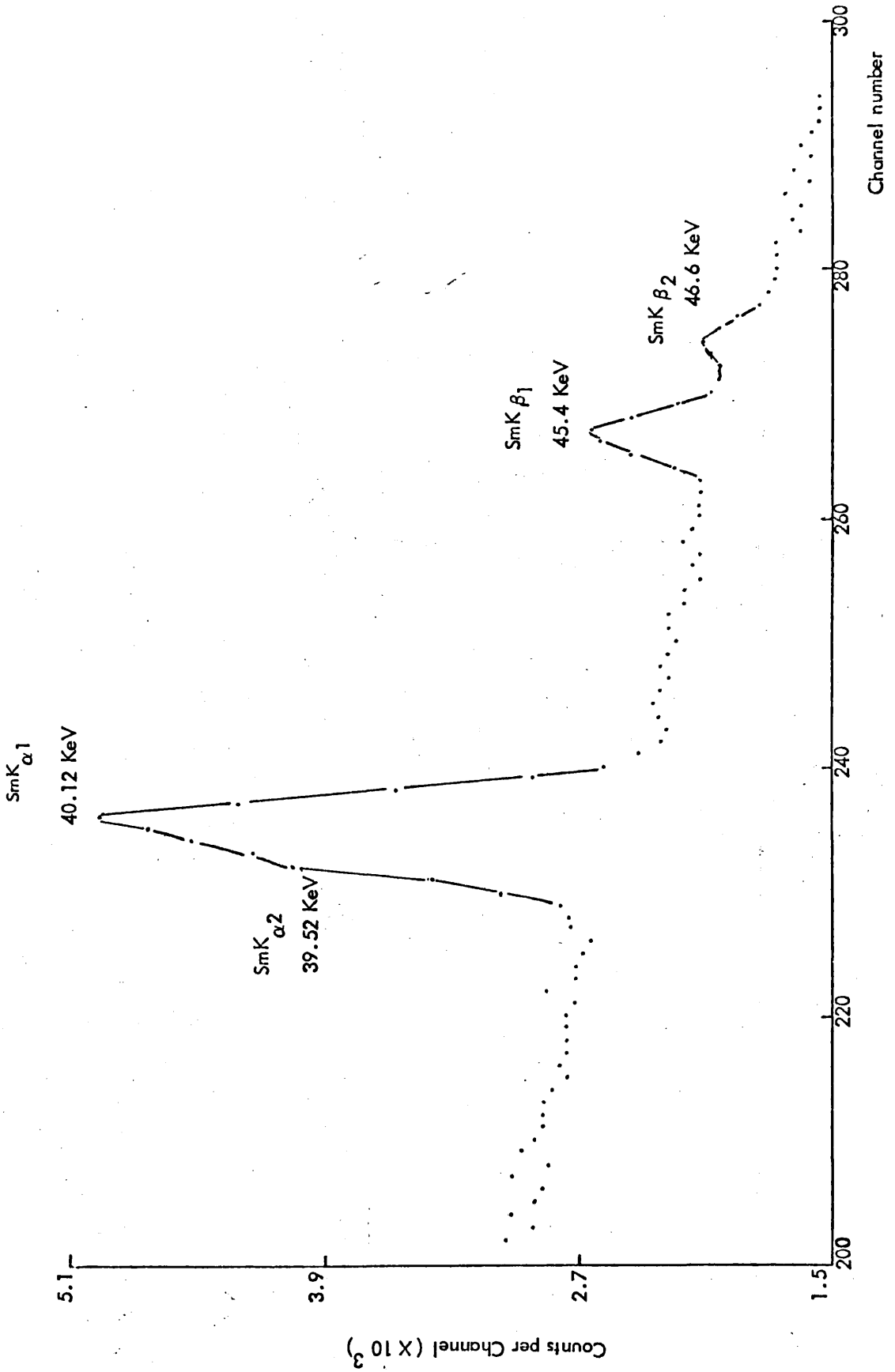

Fig 5.2 Pm-147 straight photon spectrum

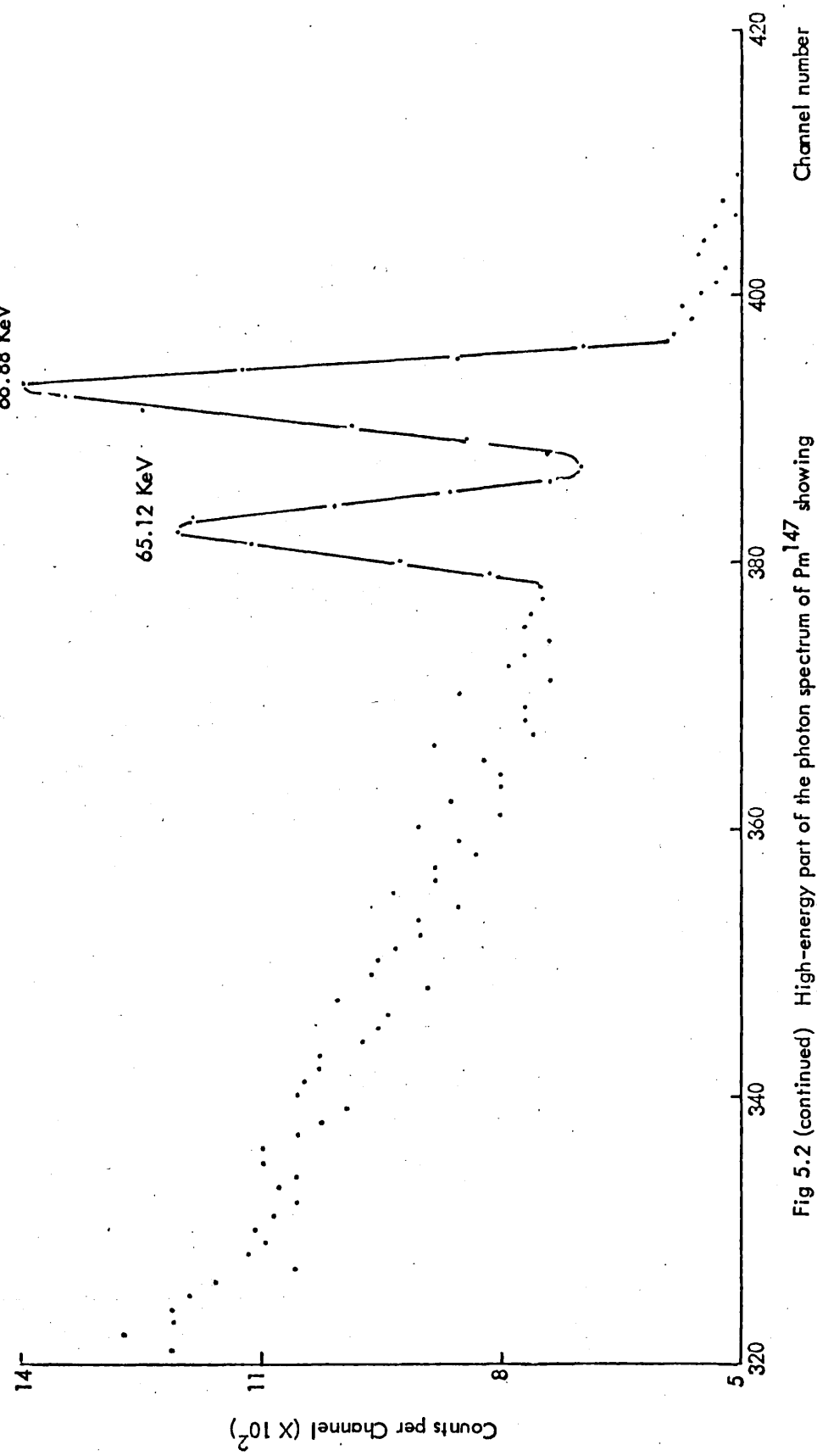

Fig 5.2 (continued) High-energy part of the photon spectrum of Pm^{147} showing platinum fluorescent X-rays

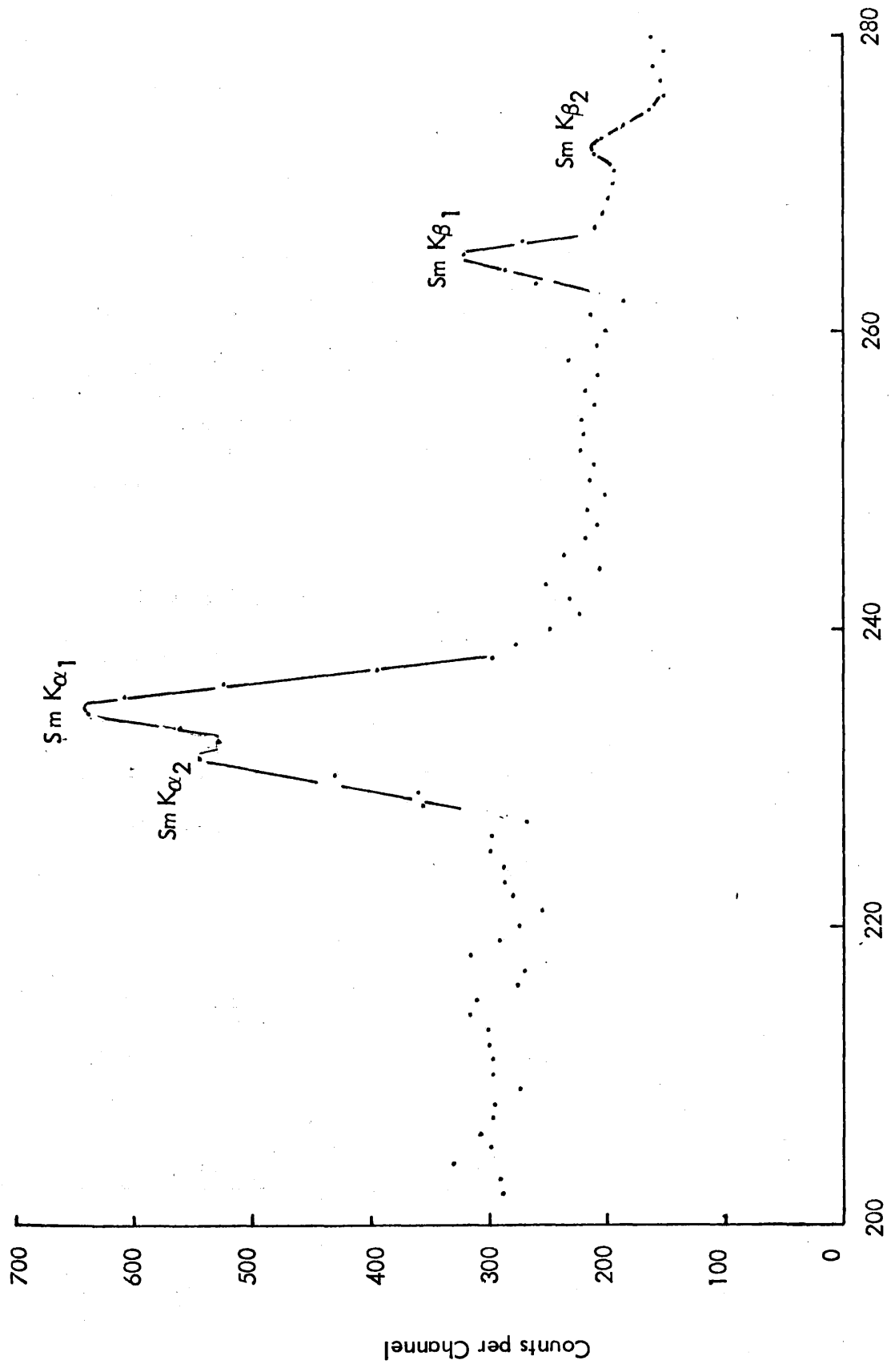

Fig 5.3 Photons of Pm^{147} observed in coincidence with β^- particles

The energy region of the β-ray spectrum was divided into six segments. Each segment was selected by adjusting the window of the single channel analyzer in the β-particle channel and the window was made wider for β-particles with higher energies taking into consideration the gradual decrease in number of β-particles in the higher energy region of the spectrum. The window was set to cover electron energies from $\sim$ 45 KeV to the maximum β-ray energy, 224 KeV. The lower limit of the window setting was necessary to eliminate noise from the electronics.

From time to time checks on the performance of the whole measuring system were made (counting rates of both X-ray and electron channel).

Typical straight photon spectra and the coincident spectrum observed in coincidence with pulses from the electron channel are shown in Figs. 5.2 and 5.3.

Details of data analysis and correction procedure are discussed in the following section.

5.5 DATA ANALYSIS AND DISCUSSION

In accordance with Tl-204 calculations, $P_K(E_\beta)$ for Pm-147 have been

calculated using the expression:

$$P_K(E_\beta) = (N_{K\alpha_1} \epsilon_e)/(N_e \omega_k \epsilon_x P) \quad (5.1)$$

Where $N_{K\alpha_1}$ is the number of coincident Sm K_{α_1} X-rays.

ϵ_e is the electron detector efficiency $(7.7 \pm 0.8)10^{-3}$

ϵ_x is the X-ray detector efficiency $(4.92 \pm 0.25)10^{-4}$ for 40 KeV Sm K_α X-ray.

N_e is the number of electrons (β^- -particles + orbital electrons) in the electron channel.

P is the ratio of the K_{α_1} X-rays to the total K X-rays.

A value of 0.511 was adopted from ref. 92.

ω_K is the fluorescence yield ($\omega_K = 0.928$ from ref. 89)

Since Pm-147 decays according to the scheme shown in fig 5.1 and to evaluate the contribution only from the process studied here, a correction was made for the contribution to the observed X-ray peak, which is caused by K internal conversion from the 122 KeV first excited level of Sm-147 to its ground state.

The correction factor of the order $\frac{f\alpha_k}{\omega_k}$ was deducted from each individual measurement, where f is the branching ratio of the 122 KeV excited level. A value of $(2.7 \pm 0.2)\ 10^{-5}$ has been adopted here, based on other measurements[93]; α_K is the K-shell internal conversion coefficient (a value

of 0.701 has been taken from ref. 94).

An upper limit of 25% of the observed K X-rays were due to the internal conversion contribution.

The energy dependent K-shell autoionization probability values in the decay of Pm-147 are given in table 5.2.

The total K-shell autoionization probability, $\bar{P}_K$ measurement was based on the definition for $\bar{P}_K \cdot E_\beta > B_K$.

The results are plotted out in fig 5.4. Horizontal bars indicate the electron channel window selected in each coincidence measurement. Vertical bars represent statistical errors due to those of counting statistics, uncertainty in the shape function fitting of the photon spectrum and uncertainties in efficiencies of the detectors and other factors in equation (5.1).

Our measurement for $P_K(E_\beta)$ in the β^- decay of Pm^{147} showed rather close agreement with the nonrelativistic antisymmetrized one step theoretical treatment of Stephas and Crasemann[12], but there is a discrepancy of roughly a factor of 2 between their experimental results

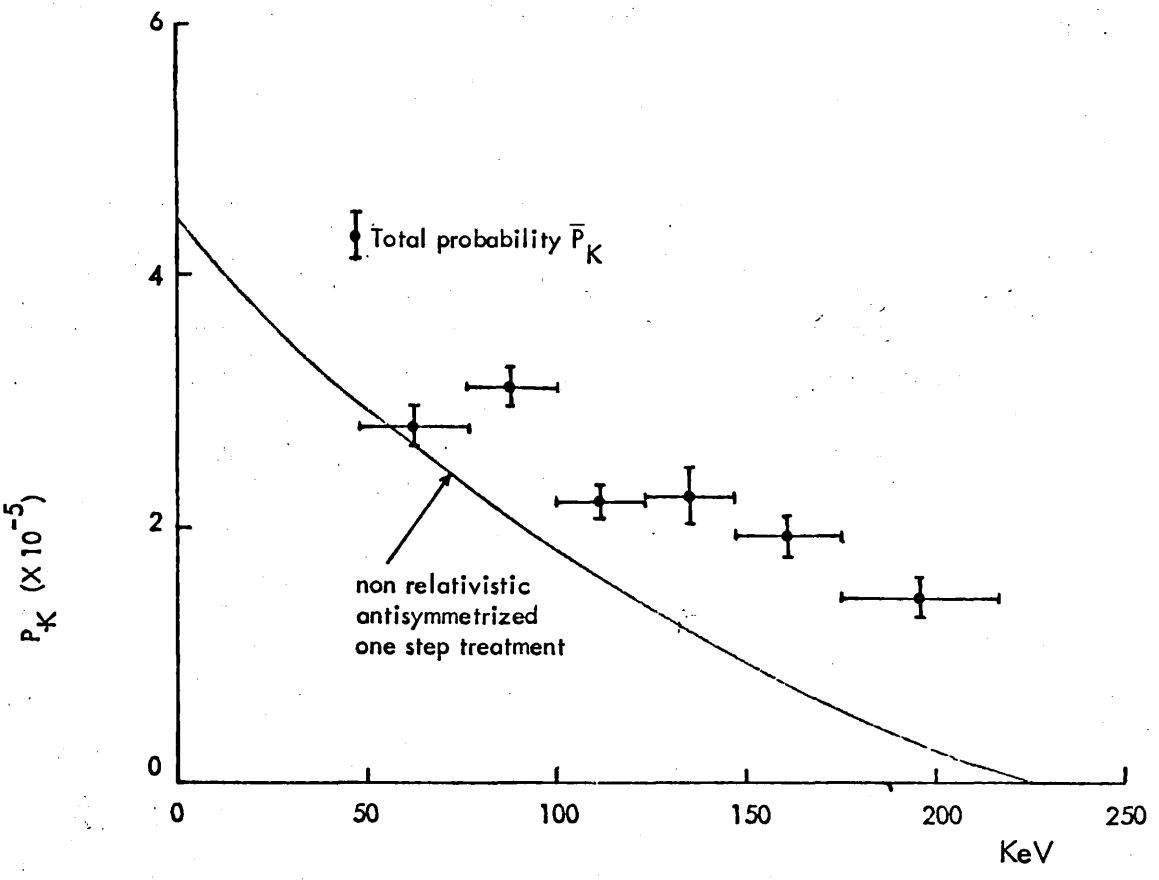

Fig. 5.4 Measured energy-dependent K-shell auto-ionization probability $P_K(E_\beta)$ for Pm-147. Horizontal bars indicate the electron-channel window in coincidence measurements and vertical bars represent statistical errors. The solid curve represents the theoretical curve based on the one step electron shake off treatment.

Table 5.2 Energy-dependent K-shell autoionization probability $P_K(E_\beta)$ in the β^--decay of Pm-147.

Lower setting for energy window E KeV	Upper setting for energy window (E +ΔE) KeV	$P_K(E_\beta) \times 10^{-5}$
48.3	76.6	2.83 ± 0.14
76.6	99.9	3.11 ± 0.13
99.9	121.6	2.21 ± 0.10
121.6	144.1	2.25 ± 0.23
144.1	170.8	1.98 ± 0.16
170.8	217.5	1.48 ± 0.12

Total K-shell autoionization probability $\bar{P}_K = (4.31 \pm 0.17)10^{-5}$

and our data. The present work is in disagreement with the results of Isozumi and Shimizu[26] regarding the shape of the measured energy dependence of P_K. Their measured $P_K(E_\beta)$ values are nearly constant in the higher energy region but decrease below $2B_K$ until they reach zero value at B_K. Our results decrease smoothly in the higher energy region but have no tendency to decrease in the lower energy region. However, in principle, one would not expect the P_K value to decrease at low energies if it is agreed that the direct collision mechanism can be ignored

even though the ejected orbital electrons are of low energy.

Our total $\bar{P}_K$ probability value $(4.31 \pm 0.17)10^{-5}$ showed a lower magnitude than other results and closer agreement to Isozumi and Shimizu (see table 5.1).

Law and Campbell[54] calculated $\bar{P}_K$ for Pm^{147} to be (0.89×10^{-4}) which is greater than our results by roughly a factor of 2. Using SCF calculations, the $\bar{P}_K$ is given a value of (5.15×10^{-5}); (see ref 26) which is in better agreement with our experimental measurements.

Comparing our experimental results for both Tl^{204} and Pm^{147} and how well they fit with the single step treatment, it seems there are discrepancies in the two cases regarding the magnitude but not as such in the shape of the obtained energy-dependent P_K values.

Since the Pm^{147} decay is considered to be first forbidden and Tl^{204} to be first forbidden unique type, it is expected that the Tl^{204} will have a higher P_K value. Furthermore, comparing B_K/E_o ratios in both cases; 0.115 for Tl^{204} and 0.209 for Pm^{147} gives P_K an even higher value for Tl^{204}. This is in disagreement with Mord's[17] calculations where he predicted higher P_K value for pm^{147} and in the case when he assumed the

Tl^{204} decay to be of allowed type, his calculated $_3P_K$ (see ref. 17) is greater for Pm^{147}.

Chapter 6

K-SHELL INTERNAL IONIZATION ACCOMPANYING ERBIUM-169 DECAY

6.1 INTRODUCTION

The common feature of all internal ionization experiments is the measurement of X-rays emitted following the filling of a K-shell vacancy produced in the internal ionization process. These X-rays are then compared with the total or differential β^--decay rate. As there are very few β^- emitters which do not have subsequent γ transitions that yield K holes via internal conversion; Campbell and Law[38] introduced a method of making use of the relative K X-ray and γ-ray intensities measured with a Ge(li) spectrometer. This procedure is restricted to cases where the accompanying γ-ray is of very low energy so that no K-shell conversion can occur, or the γ-ray is weakly converted. The knowledge of the nuclear constants and the branching ratios with great accuracy is essential for the success of this method.

This approach has been adopted in the present work and an independent measurement of P_K, the K-shell autoionization probability in the decay of Er-169 was made in order to supplement the limited data available for this isotope.

Erbium-169 represents medium heavy mass nuclei (Z = 68) and decays (see fig. 6.1) via three β^- branches, two to excited states at 118.2 and

8.6 KeV; the third one to the ground state of Tm-169. Since the K and L binding energies of Tm are larger than 8.4 KeV, then the 8.4 KeV transition from the first excited state only creates holes in the M and higher shells via internal conversion and the only expected contribution to Tm K X-rays through internal conversion comes from the 109.7 and 118.2 KeV transitions.

The experiment was straightforward in principle and the Ge(li) X-ray spectrometer was ideal for this type of work.

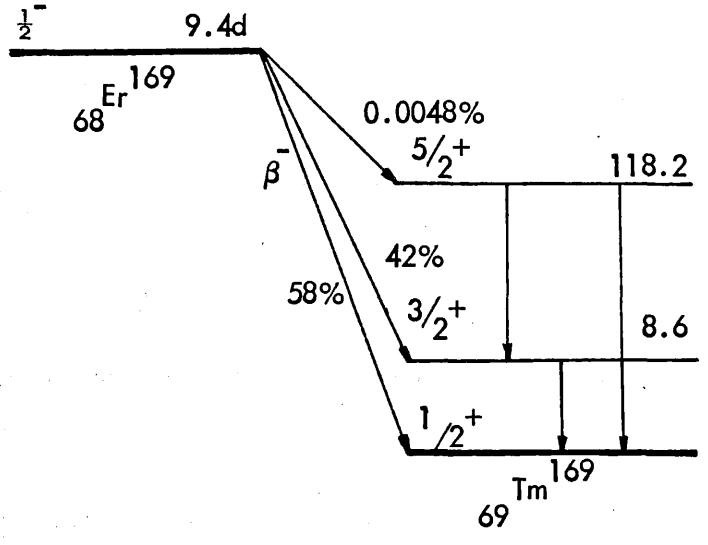

Fig 6.1 Decay scheme of Er-169 (ref. 96)

6.2 PREVIOUS INVESTIGATIONS

Very few measurements have been made on Er-169 to date. Erman et al.[24] measured the K-vacancy creation probability as a function of electron energy in the decay of Er-169. Where the subsequent K X-rays were recorded in coincidence with various segments of the β^- spectra. The experiment was aiming to distinguish between the shake off and direct collision contributions to the autoionization phenomenon in nuclear β^- decay. Their basic assumptions to identify these two mechanisms were:

$$\text{Shake off } P_K(E_\beta) = \text{Const.}$$

$$\text{direct collision } P_K(E_\beta) \simeq \frac{1}{v^2}$$

As E_β is the initial energy of the β^- particle, and v the corresponding velocity.

Their conclusions were analogous to previous results with respect to the minor contribution of the direct collision process. Moreover, they interpretted shake off results in terms of the two step theory. The measurement was carried out before the decay scheme of Sharma et al.[96] was suggested which means that K-shell internal conversion via 109.7 and 118.2 KeV transitions was not considered due to the absence of these

transitions in the early decay scheme. Furthermore, a value of $(2.4 \pm 0.4)10^{-4}$ was measured by these authors for $\bar{P}_K$, the total K-shell autoionization probability for Er-169.

Campbell et al.[38] claimed a P_K value of $(1.0 \pm 0.2)10^{-4}$. Their work on Er-169 was mainly an interpretation of the results of Sharma et al.[96] for the suggested decay scheme, noting that the Tm X-ray intensity in the spectrum measured by Sharma et al. was considerably in excess of that expected from K internal conversion of the 109.7 and 118.2 KeV transitions. The intensities of Tm K X-rays and of the gamma ray at 109.7 and 118.2 KeV energy were calculated from the spectrum, and with the knowledge of the K conversion coefficients they deduced that 20.7% of the observed K X-rays arose from internal conversion of these transitions. From the remaining K X-ray intensity and the β^- branching ratio to the 118.2 KeV level, they were able to determine a P_K value.

6.3 SOURCE PREPARATION

The source preparation contributed considerable difficulties. Erbium is one of the lanthanides; which are very difficult to separate chemically, so it was a problem to obtain an Er-169 source in a sufficiently pure form. The source was prepared in three different forms, as special considerations

were given to the source production to avoid unwanted impurities.

The three forms were:

(i) Erbium metal

Erbium foil (99.9% purity) was obtained from Koch-Light Laboratories (Colnbrook, Bucks, England). The foil was 0.25 mm thick. Samples of erbium metal (each is 100 mg in weight), were irradiated at the University of London reactor. The active sources were then just placed on thin aluminium discs and covered with paper labels. Initial source activity was about 97 μCi.

(ii) Erbium oxide (Er_2O_3)

The activities were produced in the University of London reactor with a flux of 10^{12} n/cm^{2}sec by irradiating Er_2O_3(99.9% purity) obtained from BDH Chemicals Ltd. (Poole, England). The irradiated samples were of $\sim$100 μCi strength. Since it is extremely difficult to dissolve the oxide powder; the source was used in its powder form which was sandwiched and compressed between two plastic containers with specific dimensions to ensure thickness uniformity; ultimately, this facilitated calculations for intensity attenuation in the source backing and within the source itself. Furthermore, the plasticcontainer acted as a β^- absorber in front of the Ge(li) X-ray detector.

(iii) Erbium Chloride ($^{169}ErCl_3$)

As a result of the drawbacks and impurities in both the metal and the oxide,

which will be discussed later, Erbium-169 was obtained as chloride in 0.1 N HCl solution with specific activity 30.6 μCi/mg from The Radiochemical Centre (Amersham, England), and thin sources were prepared by evaporating droplets of radioactive solution on aluminium planchets previously treated with insulin to ensure source uniformity. Thin perspex discs were also used instead of the aluminium planchet. The activity of the sources ranged between 30 to 67 μCi.

According to the information obtained from the producer; the initial activities were produced in the reactor by irradiating the erbium oxide for 7 days. The final activities were then produced by separating the mass number 169 from the rest of the activities; therefore, the only possible contaminent of importance should be Yb-169 as it is formed from a very high neutron capture cross-section (11000 b). As the photon spectrum showed a considerable amount of impurities in the sample; a request was made to the producer to ask if any spectrographic analysis had been done. A number of suspected impurities were listed including Er^{171}, Lu^{177}, Yb^{169}, Yb^{175}, Er^{172} and Tm^{172}; where the first two were of negligible activity, while stating an upper limit for the presence of the last three contaminants to be less than 0.2% (figures as obtained from the producer).

6.4 PRESENT WORK

The photon spectra from previously mentioned Er-169 sources were recorded in a Ge(li) X-ray detector (see chapter 3 for detector specifications and efficiency calibration). The detector was employed in conjunction with an ORTEC 440A selectable filter amplifier and Northern Econ I series pulse height analyzer (512 channels memory). For erbium-169 chloride source measurements, the 440A amplifier was replaced by an ORTEC spectroscopy amplifier and the photon spectrum was recorded simultaneously into two analyzers, the 512 channels instrument and one of 4096 channels (Northern NS 630 series), the latter was operated with a conversion gain of 2048. The energy calibration was done from time to time using standard sources of Am^{241}, Ba^{133}, Co^{57} and Cs^{137} obtained from The Radiochemical Centre. The resolution of the detector was quite consistent with previous results.

In each experiment a considerable number of runs were taken, each run for about 24 hours, while the run time for the last measurements using the Er-169 chloride was extended for two days.

In the oxide experiment, the main troublesome factors were the fluorescent erbium X-rays which could not be avoided due to the

thickness of the source. Since erbium L X-rays lie in the region 6.9 to 8.2 KeV; the 8.4 KeV gamma from Er^{169} was inseparable from those X-rays as the resolution of the detector was not sufficiently high. One apparent solution to the problem was to know the exact relative intensities of the L to the K shell X-rays. Since not enough relevant information was found in literature; an independent measurement of the $L/_K$ ratio was made using an unirradiated sample of Er_2O_3 with a few drops of Pm-147 ($\sim$ 50 μCi) added to the top of the sample to act as an electron source, producing erbium X-rays which are exclusively fluorescent ones. Promethium-147 was chosen for this purpose due to its reasonable half-life (not being short) and its decay energy which is not very different from that of erbium-169.

The whole data collection for the Er-169 measurements took a period of six months. The photon spectra belonging to different source forms are shown and results are discussed in the following section.

6.5 DATA ANALYSIS AND DISCUSSION

From each independent measurement, the photon spectra obtained were analyzed using SAMPO, the energies of the peaks, the relative intensities and decay rates were determined and conclusions were drawn

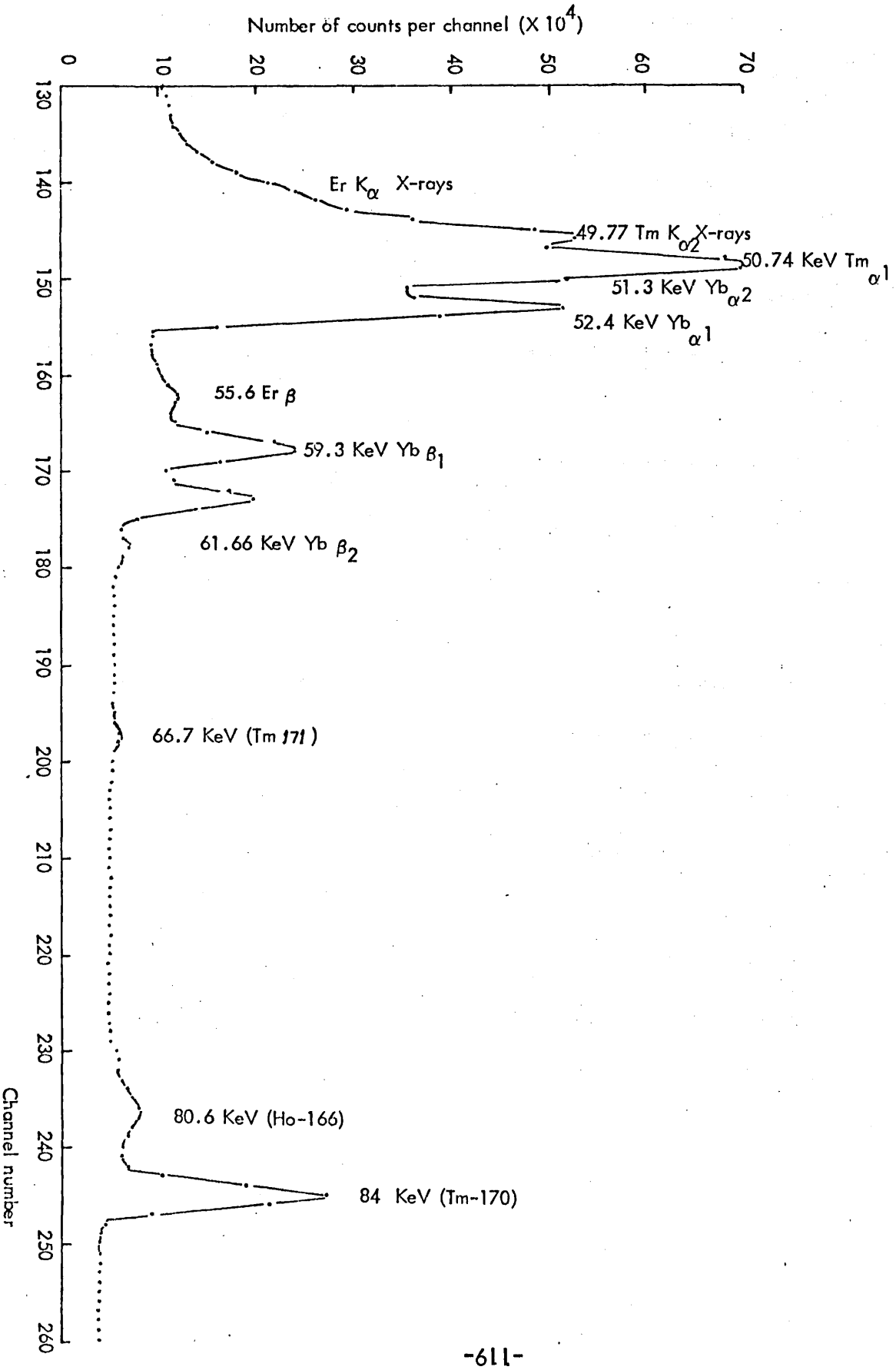

Fig 6.2 Photon spectrum of Er-169 showing the impurities radiations (Erbium metal)

out on the basis of this analysis.

Comments on spectra obtained with different source forms are outlined and P_K K-shell autoionization in the β^- decay of erbium-169 was estimated from the last measurements on $Er^{169}Cl_3$.

Though the active sources were all in principle produced in (n,γ) reaction; the contribution of impurities differed in each case due to the purity of the Er sample before irradiation and for $Er^{169}Cl_3$, it was the purification procedure and irradiation period which accounted for improvement in the results.

In the case of the erbium metal, the spectrum (see fig 6.2) shows that the main contaminants were identified as Er^{172}, Tm^{170}, Tm^{172} and Tm^{171}.

The Er^{172} impurity gave rise to Tm X-rays which unfortunately are the same X-rays of interest as those produced in the decay of Er^{169}. The other three impurities produced Yb X-rays. These isotopes are of comparatively long half lives; Tm^{170} (134d), Tm^{171}(1.92y) and Tm^{172} (63.6 h) with respect to Er^{169} (9.6 d). Consequently, their presence caused rather serious problems because of the Yb L X-rays masked the 8.4 KeV gamma ray line expected from Er^{169}. Unfortunately, in this

measurement we were not able to detect the 109.7 and 118.2 gamma ray lines, and the results were regarded as invalid for P_K calculations.

Fig. 6.3.1 shows the spectrum obtained with the erbium source in its powdered (oxide) form, whilst Fig. 6.3.2 shows the relevant region of the spectrum after most of short lived isotopes impurities had decayed.

The analysis of the results showed that the 111.7, 116.6, 124.0 KeV gamma ray lines are due to the main impurity Er^{171} (7.52 h) which is formed in the (n,γ) reaction on Er^{170} having a thermal neutron cross section (σ) of 9 barns which is nearly 4 times greater than that of Er^{168}. The spectrum showed the 80.6 KeV line which had been identified to be due to Ho^{166} (26.9 h); the only possibility for formation of this isotope is the impurity Ho present in the erbium oxide powder. Ho^{165} has an abundance of 100% and σ_c = 64 barns to Ho^{166}; $\sigma_c \approx 1$ b to Ho^{166m}. Ho X-rays were believed to be due to Er^{165} (10.34 h) and in part due to Er^{160} (29.4 h) and Er^{161} (3.1 h) which might result from some knock-on protons on Er. The Holmium impurity caused presence of Er X-rays also.

Er^{172} (49.5 h) contributed some of the Tm X-rays and its daughter Tm^{172} (63.6 h) radiations resulted in the presence of Yb X-rays.

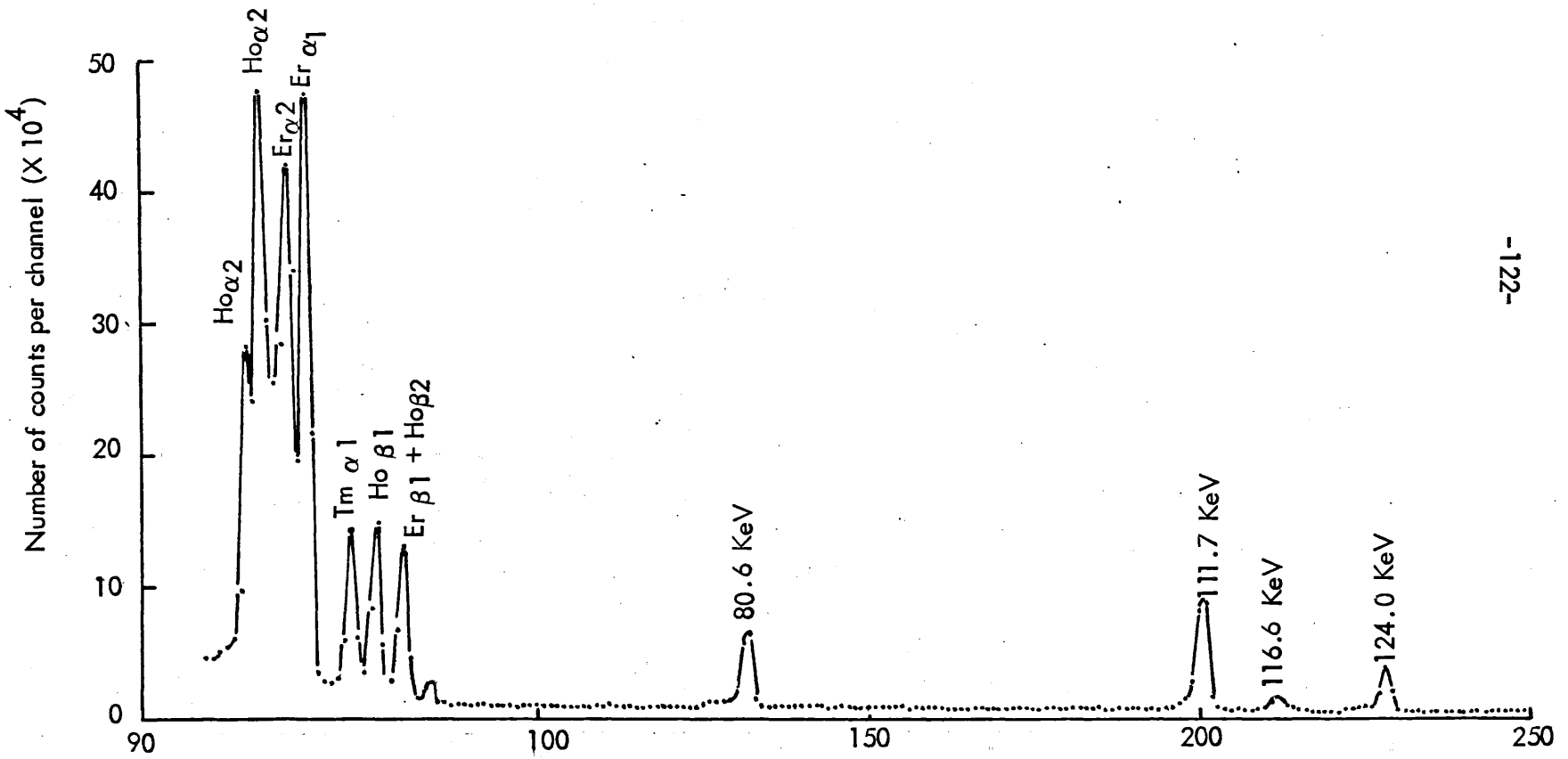

Fig 6.3.1 Photon spectrum of Er-169 plus impurities radiations (the source in powdered oxide form)

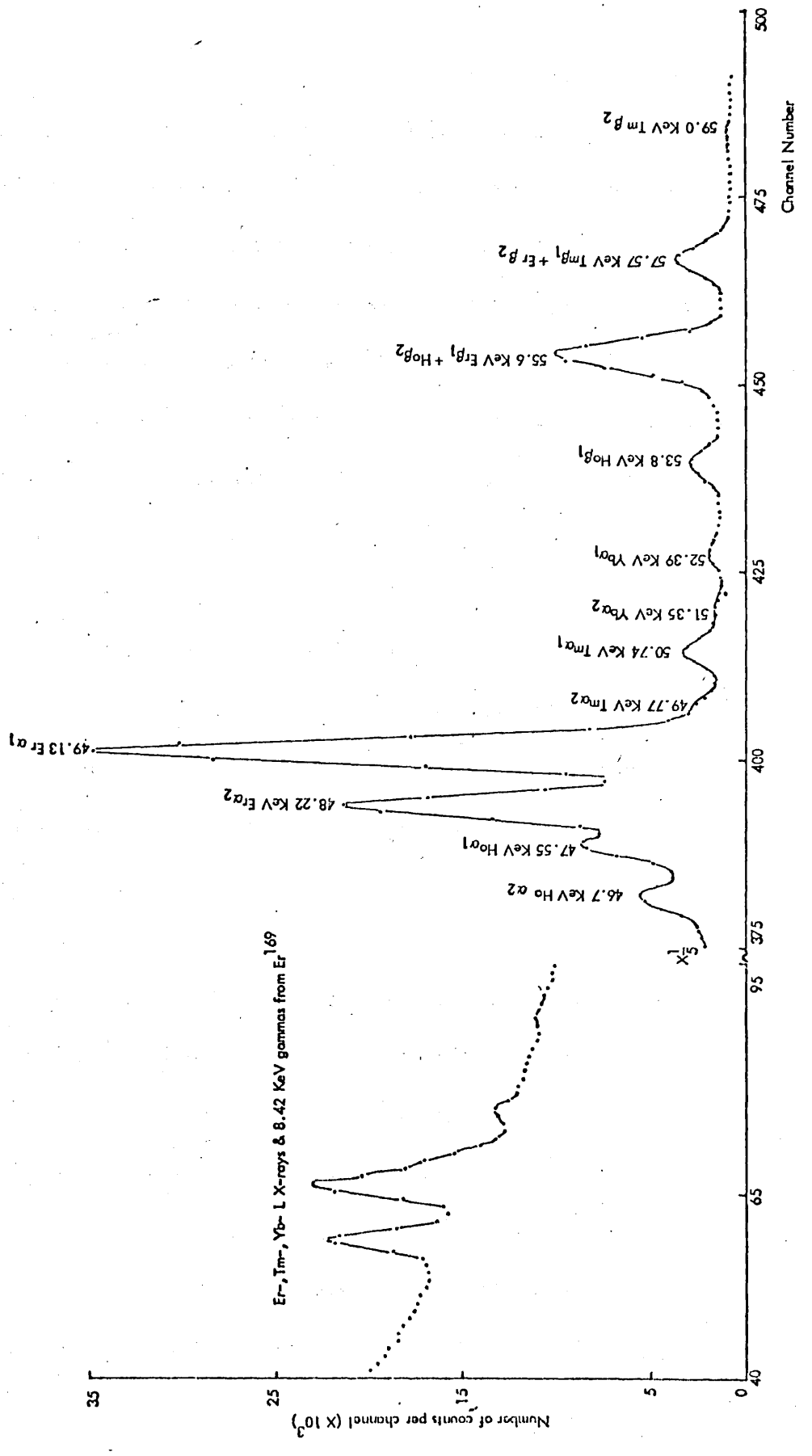

Fig 6.3.2 The relevant region of the photon spectrum of Er-169

The measurement was based at the beginning on the comparison of the 8.4 KeV gamma ray transition with the Tm K X-ray resulting from autoionization in the β^--decay of Er^{169}. This gamma ray line was inseperable from the fluorescent Er L X-rays and other X-rays in the region and, as mentioned, previously (see section 6.3 ii) an independent measurement had been made in order to evaluate the relative intensities of Er X-rays but this did not work out as expected because of the presence of other Er and Tm X-rays present in the region suspected to be due to impurities.

Tm K X-rays, 10 days after the irradiation date, were mainly believed to be due to Er^{169} but the essential part of the measurement remained unsolved; that is the absence of a clearly defined gamma ray line (a measure of the β^- intensity of the source) to compare these X-rays with for P_K determination.

It is obvious from fig. 6.3.2 that the Tm K X-rays are of low intensity as a result of Er^{169} weak activity which could be improved by irradiation for longer periods but this would result in higher activities of long lived impurities as well, unless some sort of purification procedure was adopted.

From our previous discussion, one can conclude that we were not able to determine an accurate P_K value from the sources so far used. This led

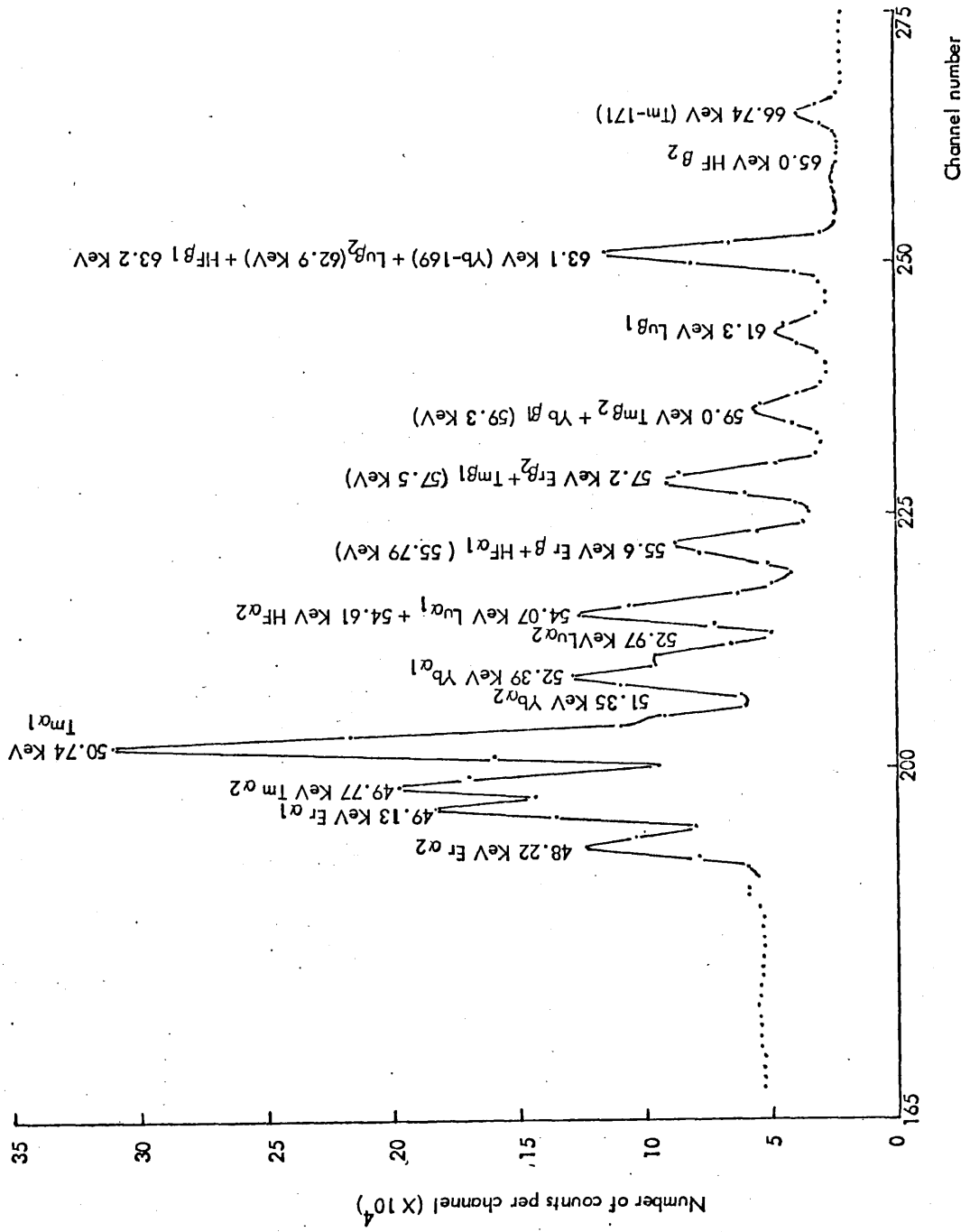

Fig 6.4.1 The photon spectrum of Er-169

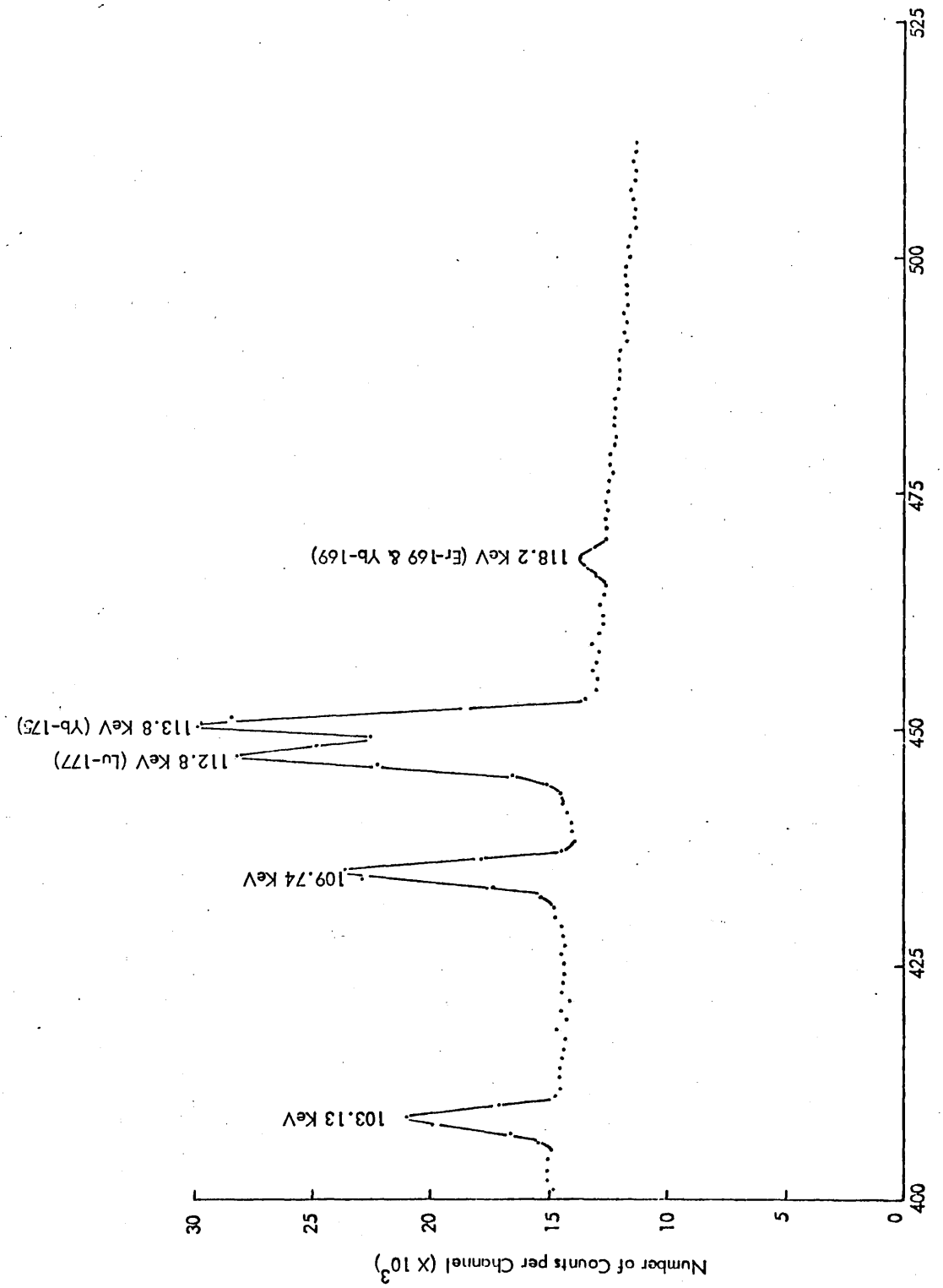

Fig 6.4.2 High-energy part of the photon spectrum of Er-169

Table 6.1 Photon energies emitted by Er-169 and other impurities in the source. (The lengths of the lines indicate the approximate relative intensities.)

Photon energies in KeV	Type of radiation	Studied isotope	Impurities							
		Er-169	Ho-166	Er-172	Tm-170	Tm-171	Tm-172	Yb-175	Yb-169	Lu-177
48.22	$Er_{\alpha 2}$		—							
49.13	$Er_{\alpha 1}$		—							
49.77	$Tm_{\alpha 2}$	—		—					—	
50.74	$Tm_{\alpha 1}$	—		—					—	
51.33	$Yb_{\alpha 2}$				—	—	—			
52.39	$Yb_{\alpha 1}$				—	—	—			
52.97	$Lu_{\alpha 2}$							—		
54.07	$Lu_{\alpha 1}$							—		
54.61	Hf $\alpha 2$									—
55.6	Er $\beta 1$		—							
55.79	Hf $\alpha 1$									—
57.2	Er $\beta 2$		—							
51.5	Tm $\beta 1$	—		—					—	
59.0	Tm $\beta 2$	—		—					—	
59.3	Yb $\beta 1$				—	—	—			

Table 6.1 (continued)

Photon energies in KeV	Type of radiation	Studied Isotope	Impurities							
		Er-169	Ho-166	Er-172	Tm-170	Tm-171	Tm-172	Yb-175	Yb-169	Lu-177
61.0	$Yb\beta_2$				—	—	—			
61.3	$Lu\beta_1$							—		
62.9	$Lu\beta_2$							—		
63.1	γ-line								—	
63.2	Hf β_1									—
65.0	Hf β_2									—
67	γ-line					—				
79.0	γ-line						—			
80.6	γ-line		—							
84.0	γ-line				—					
93.6	γ-line								—	
109.74	γ-line	—							—	
112.8	γ-line									—
113.8	γ-line							—		
118.2	γ-line	—							—	

us to look for a more highly purified Er^{169} source. As mentioned in section (6.3.iii), a source of Er^{169} chloride was obtained and since it was extremely difficult to obtain a very clearly defined spectral shape for the 8.4 KeV gamma ray line without other radiations being added to it; the Er^{169} Cl_3 measurement was based on the knowledge of the β^- intensity of Er^{169} from the 118.2 KeV gamma ray transition and then comparing this with Tm K X-rays to determine P_K.

The impurities are mentioned in section (6.3.iii). A very thorough analysis had been followed all through this measurement trying to obtain an estimate for P_K with reasonable accuracy.

Figs. 6.4.1 and 6.4.2 show the relevant region of the observed spectra. From these figures, it is obvious that the nature of the spectrum was rather complicated as a result of the impurities. In addition to the impurities previously listed by The Radiochemical Centre (Er^{171}, Er^{172}, Tm^{172}, Yb^{169}, Yb^{175}, and Lu^{177}) and which were confirmed to be present in the spectral analysis (except for Er^{171} and Er^{172} which had decayed already at the time of the measurement) a number of other impurities were shown to be present in addition; these were identified as Ho^{166}, Tm^{170} and Tm^{171} from the photon spectrum, taking into account the photon energies and half-lives. Table 6.1 shows photon energies

resulting from these impurities.

In order to carry out the calculation, a number of steps were outlined. The first of these was to know the amount contributed to the photon spectra from each impurity and how much it is relevant to the lines of interest; secondly, a calculation of the absolute photon peak areas belonging to the Er^{169} decay. The contribution from Er^{171} (7.52 h) and Er^{172} (49.5 h), if there is any, is very minute as there was a considerable period of time between irradiation and the measurement date; especially Er^{171} which was of shorter half-life (the 112 and 124 KeV gamma ray lines were not observed). Furthermore, an upper limit of 2% for the Er^{172} impurity was estimated and the necessary corrections were made because Tm K X-rays might arise from this isotope.

Tm^{170} (134 d), Tm^{171} (1.92 y), Tm^{172} (63.6 h), Yb^{175} (101 h), Lu^{177} (6.74 d) and Ho^{166} (27.0 h) impurities did not present a significant problem as the first three resulted in Yb X-rays and 80, 84, and 67 KeV gamma ray lines only; whilst Ho^{166} present Er X-rays and an 81 KeV gamma ray line. The only relevant contribution from the above mentioned impurities were Yb^{175} and Lu^{177} as these resulted in Lu X-rays and Hf X-rays which enhance the 63.1 KeV gamma ray line from Yb^{169} as this line is of moderate importance to the present calculation, as discussed below.

So the important major impurity was Yb^{169} (31.8 d). This would result

in Tm K X-rays and 63.1, 109.7 and 118.2 KeV gamma rays which are the same photon spectral lines expected from Er^{169} except for that at 63.1 KeV. The 63.1 KeV gamma peak was used as a reference peak to calculate contributions to the 109.7 and 118.2 KeV gamma peaks from Yb^{169}. Before this had been carried out, the 63.1 KeV gamma peak was corrected for contributions from the 62.9 KeV Lu $K_{\beta 2}$ X-ray (Yb^{175}) and the 63.2 KeV Hf $K_{\beta 1}$ X-ray (Lu^{177}). The amounts of these X-rays were calculated from the 113.81 KeV γ-ray peak (Yb^{175}) and 112.97 KeV peak (Lu^{177}) with the knowledge of K-shell internal conversion coefficients, K X-rays relative intensities (relevant data were obtained from ref. 80) and the relative efficiency for the Ge(li) X-ray detector.

The contributions of Yb^{169} to the 109.7 KeV, 118.2 KeV, and Tm K X-ray peaks were calculated from the obtained value for the 63.1 KeV gamma ray line.

Now the corrected areas of Tm K X-rays (strictly speaking, they were Tm K_{α} X-rays as more accurate fitted areas were obtained) and 109.7 and 118.2 KeV are exclusively attributed to the Er^{169} decay.

The other major correction was the contribution of K-shell internal conversion of the 109.7 and 118.2 KeV transitions in the decay of Er^{169}

to the Tm K X-rays. The values used for K-conversion coefficients were those given in ref. 90. The obtained Tm K_α X-ray value was finally corrected for contributions from Er^{172}. As mentioned at the beginning of the discussion, an upper limit of 2% had been estimated for the amount of Er^{172} present in the sample and knowing roughly the strength of the source, the intensity of the Tm K X-rays arising from Er^{172} were calculated using the K-conversion coefficients (ref. 80) and $K\beta/K_\alpha$ ratio (ref. 90).

The final corrected value of Tm K_α X-rays and the 118.2 KeV γ-ray areas were introduced in the following expression for P_K determination:

$$P_K = \frac{K_\alpha X}{\gamma} \quad \frac{\epsilon_\gamma}{\epsilon_{K_\alpha}} \quad \frac{(1+P)}{\omega_K(1+\alpha)(1+S)} \qquad (6\text{-}1)$$

Where K_α is the Tm K_α X-ray peak area

γ, is the 118.2 KeV γ-ray peak area.

ϵ_γ and ϵ_{K_α} are the relative detection efficiencies for 118.2 KeV gamma and Tm K_α X-rays.

ω_K is the fluorescence yield of the Tm nuclei (0.948 ± 0.02; ref. 89).

P, is $K\beta/K_\alpha$ ratio (0.264; ref 90).

S, is the branching ratio of the ground state to the excited state (a value is taken from ref. 96)

α, the total conversion coefficient (this was calculated from the known multipolarity for the 118.2 KeV transition and a magnitude

of 1.79 was assigned for α).

Errors, including those of peaks fitting and uncertainty in values empolyed at different parts of these lengthy calculations, were taken into consideration. The final given P_K value $(0.77 \pm 0.15)10^{-4}$ is accurately estimated within the indicated uncertainty. This P_K is obtained by averaging two P_K values; $(0.75 \pm 0.16)10^{-4}$ and $(0.79 \pm 0.14)10^{-4}$ calculated independently from two experimental runs considerably apart in time to ensure consistency in the results. The different peak areas of interest were believed to be fitted with great accuracy. The errors in the final value of P_K are not a standard deviation, since not only statistical errors are incorporated but systematic errors are also present. Consequently, the indicated error for the mean P_K was the average of the errors in the individual P_K values.

One mysterious peak was present in the spectra which could not be attributed to any of the impurities: this was a line at 103.13 KeV. Since a beta absorber was used in front of the photon detector, there was no chance of the peak being a conversion electron line. The peak was decaying roughly with 46 hours half-life. The only impurity having close half-life to this is Er^{172} (49 h) but there is nothing mentioned in the decay scheme of such transition and there should be no gamma ray of this energy except for Tm^{162} (77 m), Ho^{161} (2.5 h) and Lu^{167} (55 m), these

being short-lived isotopes. Also, their possible presence in the source had been excluded . There was not enough time in the present work to carry out further investigation about the origin of this gamma ray line, so it remained unexplained. However, it did not account for any error in the P_K calculations.

Our measured P_K $(0.77 \pm 0.15)10^{-4}$ is in good agreement within the indicated errors with the calculations of Law and Campbell[54] for P_K (so + su) 0.84×10^{-4}; (P_K for shake off and shake up mechanisms).

The P_K measured in the present work is lower than that obtained by Erman et al.[24], their result is considered to be of less accuracy as a consequence of the technique they had employed which is not suitable for Er^{169} measurement. Since this isotope is of comparatively short half-life, a coincidence experiment will give poor results and their use of NaI (Tl) for photon detection would introduce even more uncertainty to the results.

Comparing P_K measured in this laboratory with the P_K of $(1.0 \pm 0.2)10^{-4}$ measured by Campbell et al.[38], values are in reasonable agreement within the indicated uncertainties in both measurements.

Chapter 7

GENERAL DISCUSSION

From the present experimental work on $P_K(E_\beta)$ differential K-shell internal ionization probabilities in the β^- decays of Tl^{204} and Pm^{147}, one can conclude that there are still considerable discrepancies between experimental data and the calculated values.

The total $\bar{P}_K$ probabilities appear to be in better agreement with theory than the differential values.

We might agree with Law and Campbell[54] that β-energy dependence approach is not in a position to distinguish between different theoretical models, due to discrepancies within each individual model itself. However, we do not agree with Law and Campbell that the approach is no longer useful or even relevant; but we believe that it will be useful when there is a better theoretical interpretation for the experimental data obtained to date using the coincidence technique for differential P_K.

There is a need for more experimental data in support of Freedman and his colleagues[5,55,77] in their preliminary work on measuring the spectral shape of the ejected orbital electrons.

As far as other experimental approaches are concerned, X/γ ratio measurement with semiconductor detectors is resulting in precise values whilst more measurements on some of the isotopes are needed to overcome

the considerable disparity among P_K values for the same isotope due to systematic errors.

The search for new elegant techniques is an advantage in this field. Van Eijk et al.[40,41] introduced a new experimental approach which is applicable to a special class of nuclides which disintegrate by two successive beta decays, where one of the decays involves only a negligible feeding of excited levels. K_{α_1} X-rays of nucleus Z due to autoionization are then compared with K_{α_1} X-rays of nucleus $Z \pm 1$; resulting from K conversion of γ-transitions in the other decay. Van Eijk and his colleagues applied their method to the two cases Pr^{143} and In^{114}, using a curved crystal spectrometer. Another recent technique was established independently by Bond et al.[47] and Thiband et al.[42], in the case of Hg^{203}, where Tl^{203} K X-rays resulting from K-conversion in 279 KeV gamma transition were recorded in single runs. Once again the K X-rays were measured in coincidence with unconverted 279 KeV gammas and these coincidences could be attributed only to autoionization. The ratio of coincidences and single K X-ray intensities then yields P_K. However, P_K estimated from this type of measurement would be of high uncertainty due to the large statistical errors.

So far, it seems there has been a reasonable amount of study of K-shell

autoionization in β^- decay but not as such for L-shell. Data regarding this shell is required as far as future experimental work is concerned in the field of autoionization in β^- decay.

Appendix A

TRIPLE SLOW COINCIDENCE UNIT

A.1 SUMMARY

A coincidence unit is described which will process up to three independent inputs.

It has been designed to operate with standard NIM signal levels. A limiter is incorporated which enables the unit to operate with Harwell-2000 standard signals as well.

Two standardized logic outputs are provided. The minimum resolving time is <100 n sec. The unit is a single-width Harwell module.

A.2 INTRODUCTION

A coincidence circuit resembles an AND gate in its basic form, since an output pulse occurs only when the activated inputs overlap in time.

A variety of these circuits has been published in recent years.[60-66]

In the present design, the input and output circuitry has been devised to operate with signals according to TTL specifications. This implies that signals from Harwell instruments must pass via an amplitude standardizer

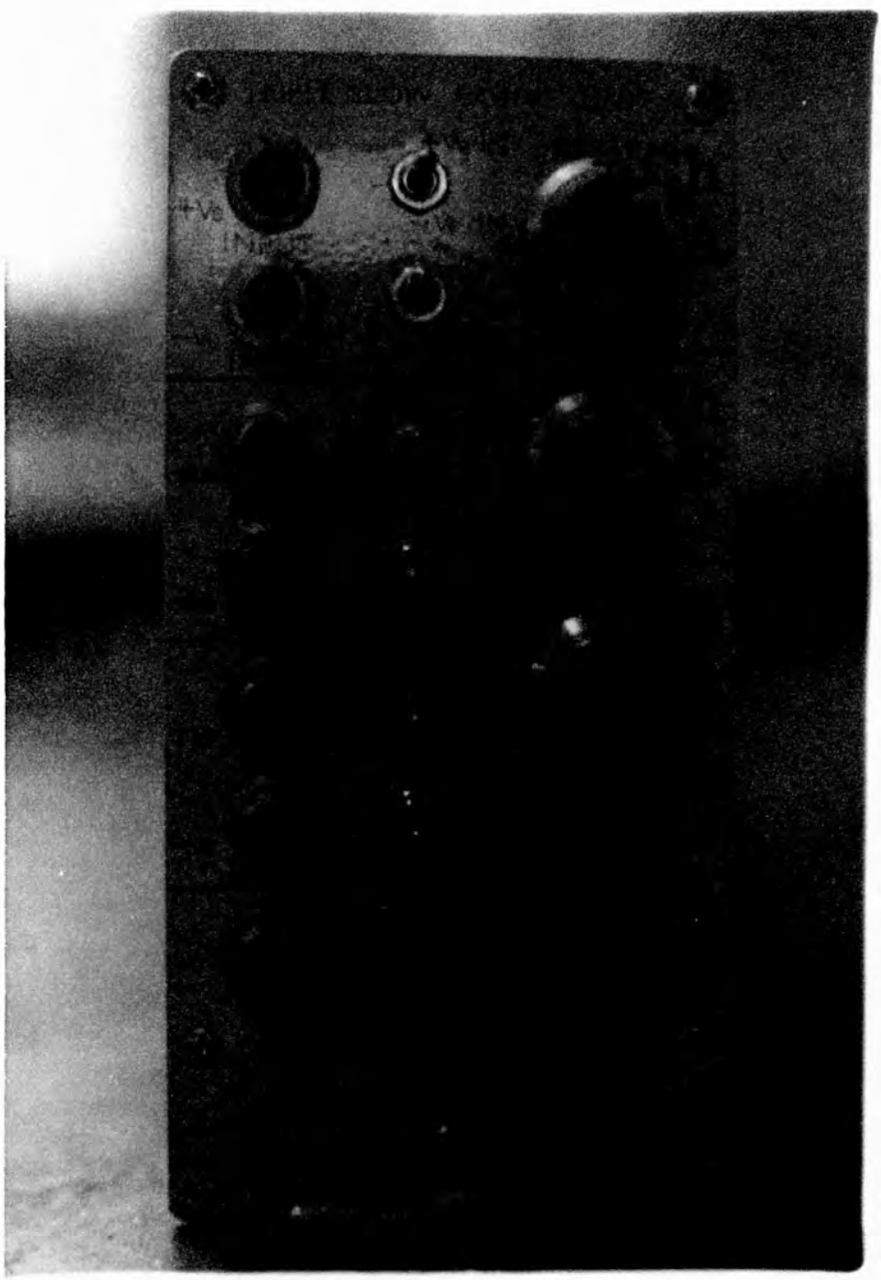

Fig A.1 Triple slow coincidence unit

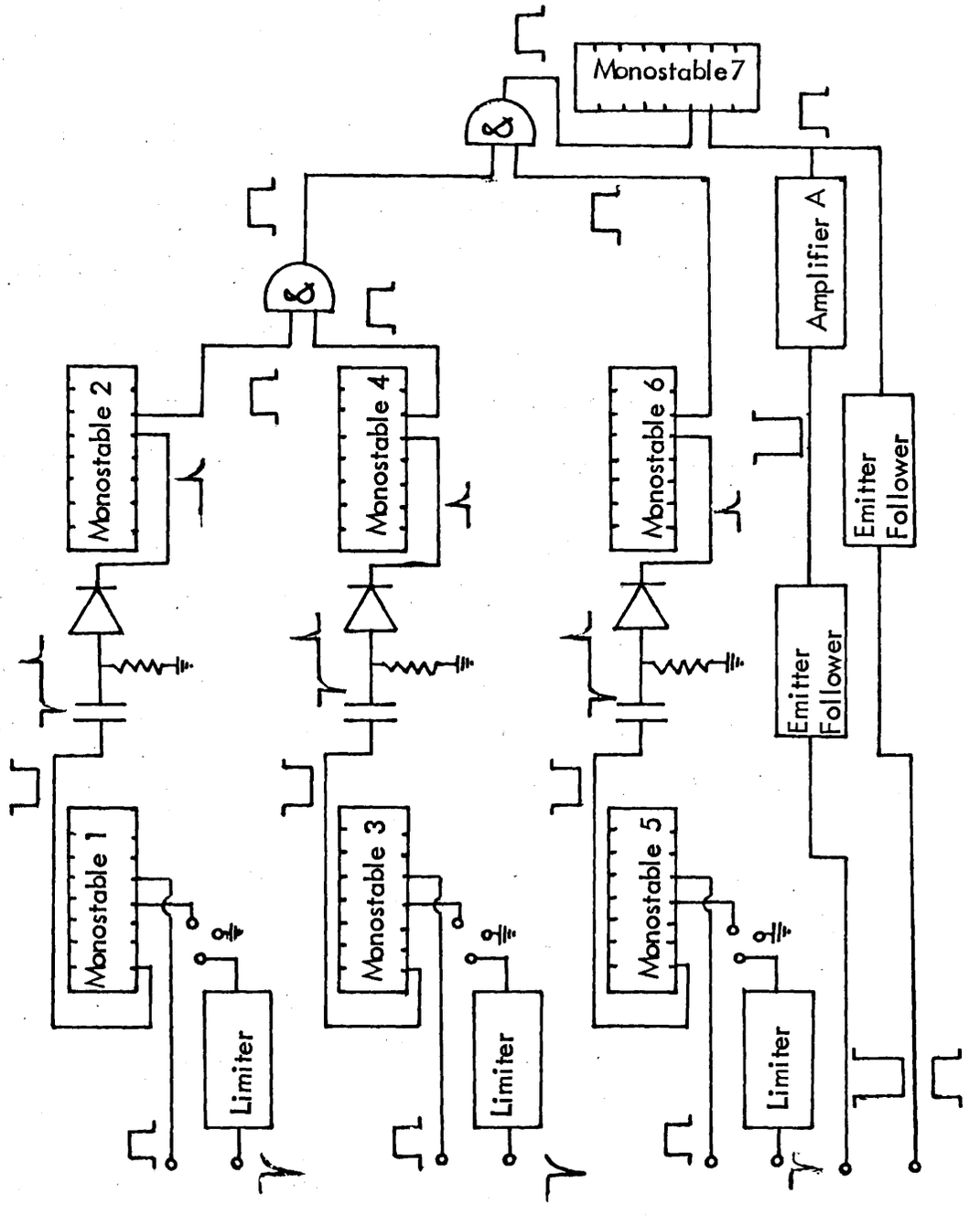

Fig A.2 Functional Block Diagram

(limiter, shaper, discriminator) before being connected to the unit. The unit incorporates an input limiter for this purpose.

The input AND-gate is d.c. coupled; therefore logic input pulses give coincidence operation and complementary logic input pulses gives anti-coincidence (inhibit or veto operation).

The unit will handle up to three inputs which can be switched "IN" or "OUT" independently from the front panel. Positive and negative inputs are accepted, and either polarity is selected through a switch marked "+Ve IN" or "- Ve IN" on the front panel.

A built-in delay is provided in each channel which could be varied independently from the front panel by a helipot marked "DELAY".

A close up of the unit is given in Fig. A.1 whilst a functional block diagram is shown in Fig. A.2

A.3 INPUT LIMITER

Input negative pulses are fed, via limiters (amplitude standardizer). The input signal drives the limiter transistor from zero bias to cut off

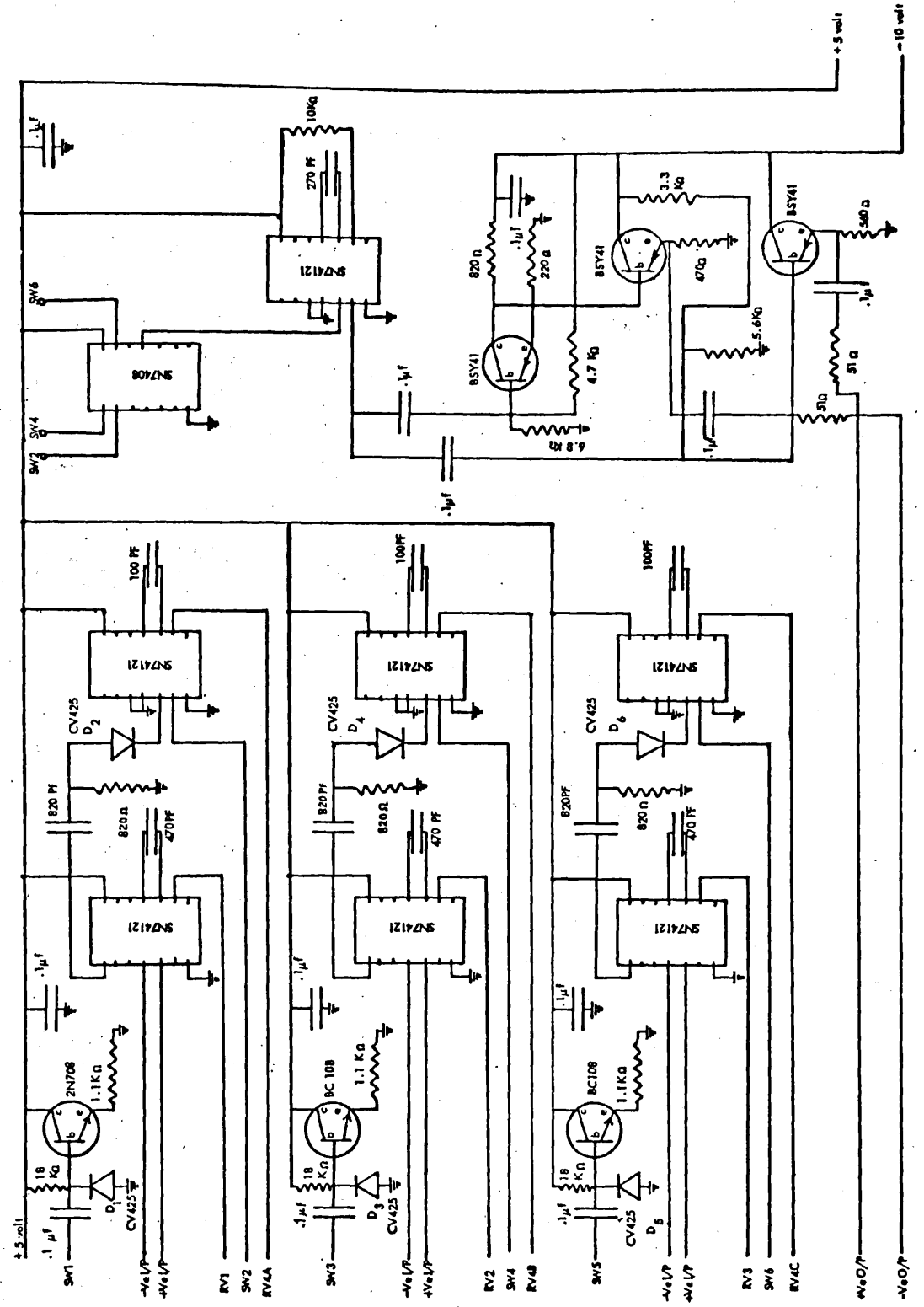

Fig A.3 Circuit diagram for triple slow coincidence unit

producing current pulses in the collector circuit that are standardized in amplitude and the resultant signal appears at the emitter. To inhibit recording any supurions pulses which might arise from positive overshoot triggering of input signals, diodes "D_1, D_3, and D_4" were placed in series with the limiters bases, oriented to pass negative signals and reject positive ones. Limiter circuit is shown (see circuit diagram Fig. A.3).

A.4 TIMING

Use was made of integrated circuits where two monostables type SN74121 provided the required timing (delay and resolving time). Information was obtained from ref. 67.

RV1, RV2 and RV3 controlled the complement pulse width out of monostables 1, 3, and 5, where the pulse was differentiated by CR circuits. Diodes D_2, D_4, and D_6 were incorporated to eliminate the negative side of the differentiated signals while the positive signals are fed to monostables 2, 4, and 6 with certain delay with respect to the input pulses. Any input could be linearly delayed in the range of 0.8 to 4 μsec., by means of a helical potentiometer.

Now monostables 2, 4, and 6 are triggered and an output pulse of variable duration of range, 100 .n sec, 500 n sec, 1 μsec, and 2 μ sec is obtained. This pulse width represents the resolving time of the coincidence unit which is accomplished through the rotary switches RV4A, RV4B, and RV4C.

A.5 INPUT AND-GATE

Quadruple 2-input positive AND-gates SN7408 have been used, where the inputs are coupled through switches SW2, SW4, and SW6. These are two way switches marked on the front panel as "IN" or "OUT'. At "IN" position the input to the AND-gate is connected to monostable 2 output. In the "OUT" position the AND-gate input is linked to + 5 volts supply, in order not to inhibit or veto the appearance of an output from the coincident pulses applied to the gate from any of the other two channels.

The output from the AND-gate triggers monostable 7 which presents an output pulse with selected width of $\sim$ 2μsec., to make it compatible with multichannel analyzer requirements for a gate pulse.

A.6 OUTPUTS

Two types of output have been processed. Positive Logic output and negative output (for use with scaler; Harwell type). To obtain the negative output; the positive signal from monostable 7 is fed to amplifier A (see Figs. A.2, and A.3). The amplification of A is $\sim$ 2X with inverted polarity.

Finally, both outputs are processed, via buffer emitter follower. The emitter follower is an impedance matching device with a very high input impedance and a very low output impedance, its voltage gain is less or close to unity.

A.7 POWER CONSUMPTION

+ 5 volts	350 mA	[+ 5 volts line supply was obtained using RS voltage regulator]
- 10 volts	10 mA	

Appendix B

VACUUM MONITOR

B.1 SUMMARY

A safety device has been constructed to switch off the bias voltage on the lithium drifted silicon detector in case of vacuum failure. A view of the unit is shown in Fig B.1.

B.2 INTRODUCTION

(i) Servos

It is often useful to control a mechanical motion of a device in accordance with an electric signal. To assure that the desired motion takes place, a voltage feedback signal corresponding to the motion is developed. This voltage is compared with the input signal. When the two signals are equal, mechanical motion is ceased. Feedback systems incorporating a mechanical link in the feedback network are called Servomechanisms, or servos. They are widely used in control application[68].

(ii) Thermistors

Thermistors, or thermally dependent resistors, are devices which make use of the large temperature coefficient of resistivity of semiconductors.

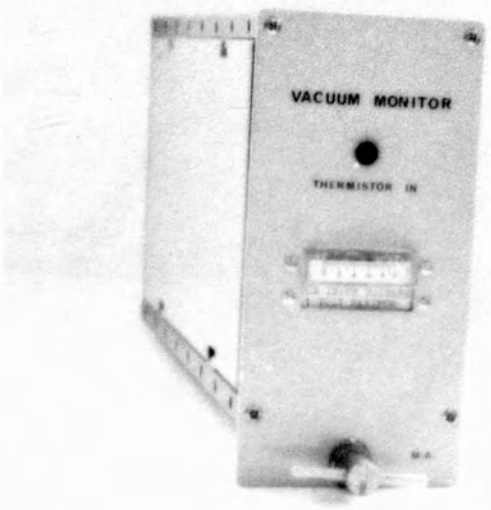

Fig B.1 Vacuum monitor

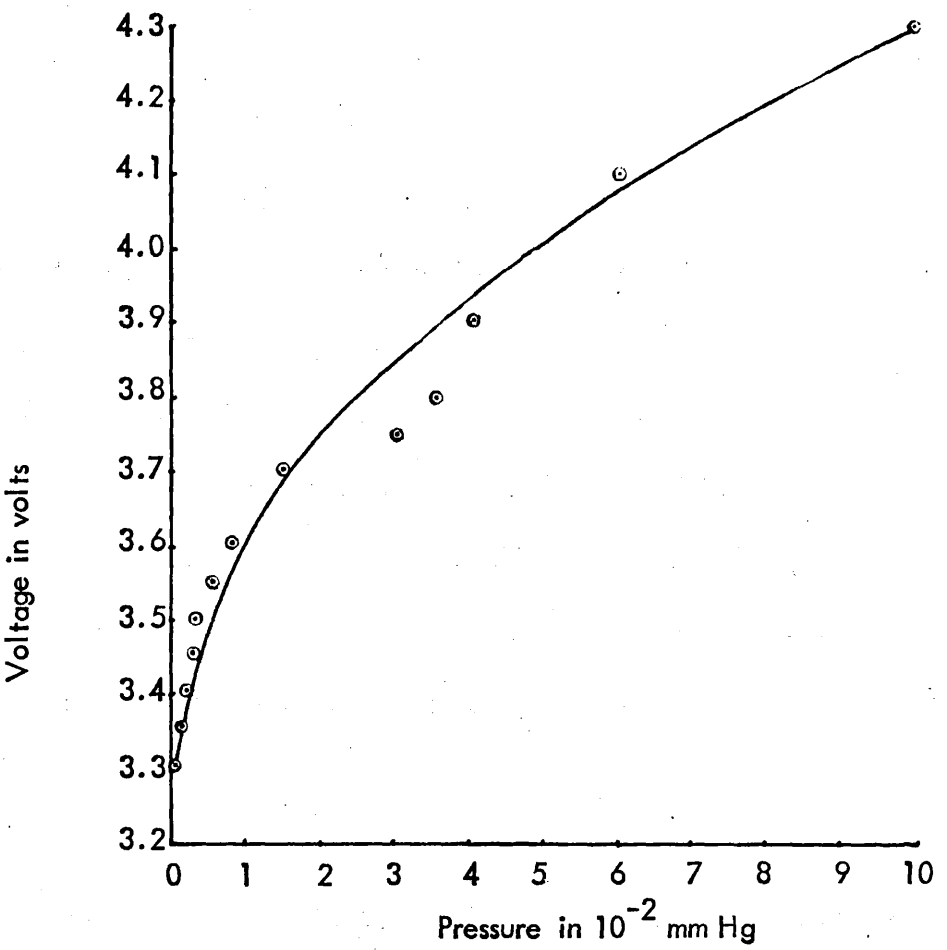

Fig B.2 Characteristic curve for TH-B12 Thermistor

Thermistor vacuum gauges for intermediate vacuum ranges are in common use[69].

The use of a thermistor element as a vacuum-gauge depends on the fact that the dissipation constant of a thermistor element suspended in air decreases as the air pressure is decreased.

Fig. B.2 shows characteristic curve obtained for TH-B12,2.5 mm diameter glass-encapsulated thermistor bead held in air at different pressures from atmospheric down to high vacuum. Such a curve is the basis for the use of the thermistor as a vacuum measure.

Any circuit in which the resistance of the thermistor could be measured at some known value of current would give an indication of the pressure of the air surrounding the thermistor.

The thermistor TH-B12 was selected since it is recommended for temperature measurement by the manufacturer[70].

The present vacuum monitor design made use of both servomechanisms and thermistors. The device acted as a control unit to switch off the detector bias in case of vacuum failure besides monitoring the pressure.

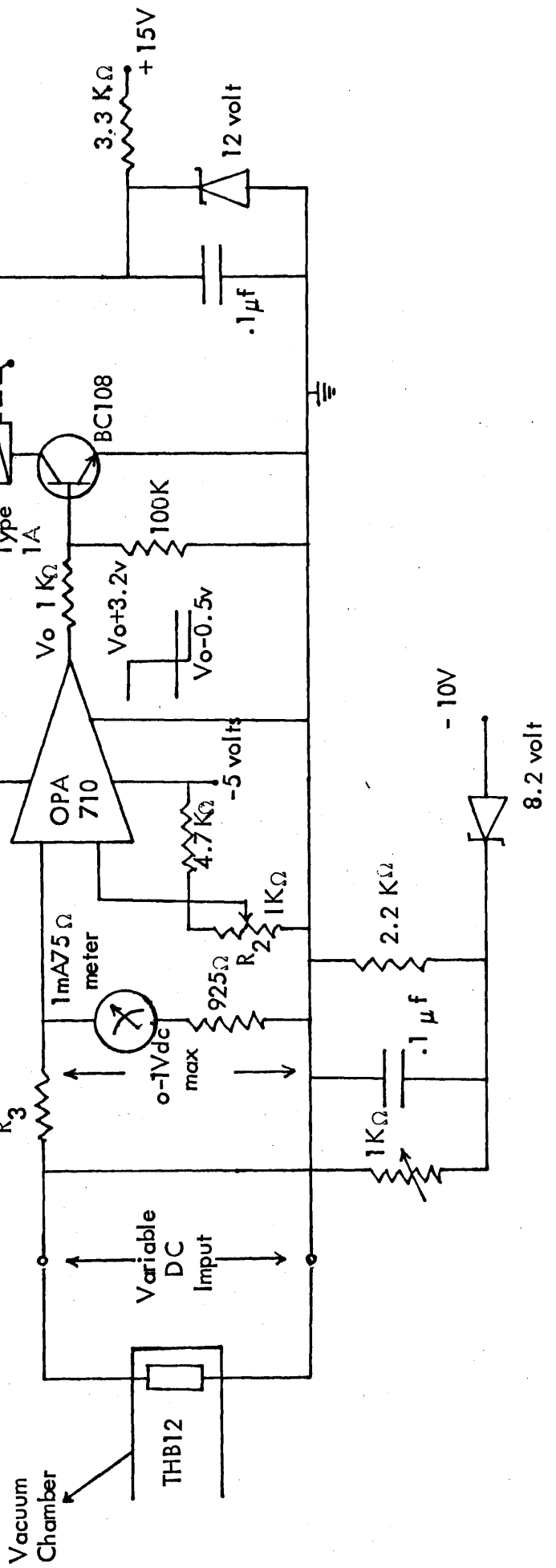

Fig B.3 Circuit diagram for vacuum monitor

B.3 CIRCUIT DESCRIPTION

Fig. B.3 shows the circuit diagram, the thermistor TH-B12 was housed by the detector cryostat. Physically it was close to the detector (to present more accurate measurement of the detector surroundings). The thermistor ends were fed outside the cryostat using feed through leads, and linked to the vacuum monitor through "THERMISTOR IN", as shown on the front panel Fig. B.1.

The reference voltage and the variable DC output from the thermistor acted as inputs for the 710 operational amplifier. Adjustment of R_2 will give the level of operation, whilst the output V_0 switches over from -0.5 V to + 3.2 V, or vice versa. The operating level can be noted on the meter (1 m A, 75Ω miniature edge meter). The resistor R_3 is incorporated to limit V to a maximum of 1 volt.

The output pulses from the voltage comparator 710 OPA are transmitted to a two pole change over solid silver contact 12 V d.c relay type 1A (RS components limited), through transistor BC 108 circuit which provides positive logic to operate the relay.

The circuit showed very good stability and reliable performances.

Appendix C

DETECTOR CRYOSTAT

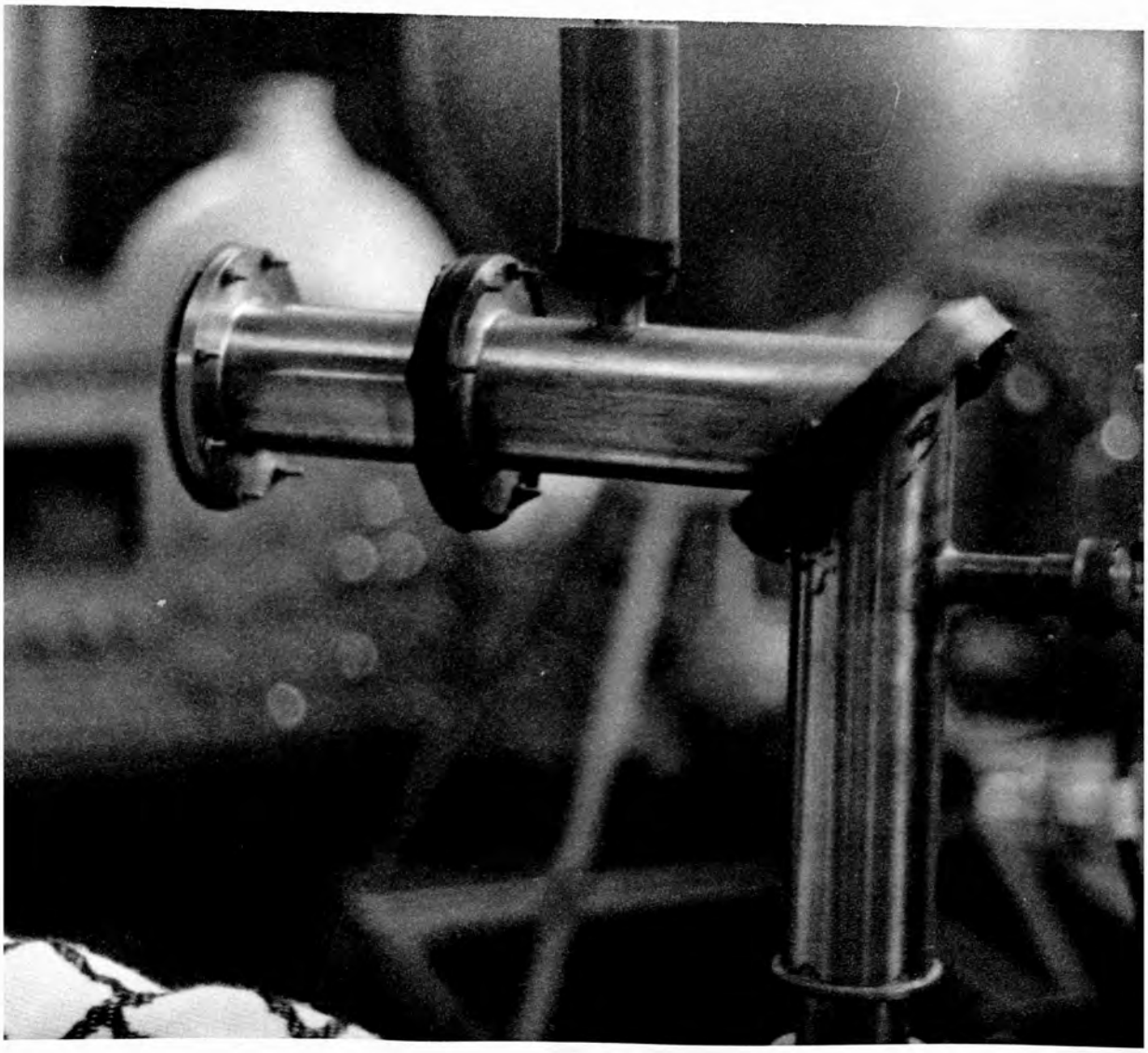

Fig C.3 Si(li) detector cryostat

Although the lithium in drifted silicon detectors is not mobile at room temperature, the thermally excited reverse bias current is high enough to make cooling an advantage. A number of cryostats have been proposed.[71.72,73]

There are two types of basic cryostat design available commercially: the dripfeed cryostat and the dipstick cryostat. The cryostat constructed here is of the second type. Figs. C.1 and C.2 show schematic diagrams of the cryostat design.

The design incorporates a solid cooling copper rod which has one end dipped into normal liquid nitrogen dewar, while the other end is soldered to a stainless steel vacuum chamber. The detector is clamped to the end of this rod. The thermal contact between the two is made by inter-position of aluminium discs.

Evacuation of the cryostat is done initially by rotary oil pump attached to the system to rough pump the cryostat chamber to 10^{-3} torr as measured on a pirani gauge. Then diffusion pump is turned on and vacuum maintained is $\sim 10^{-6}$ torr.

Electrical feed throughs are used to offer the necessary electrical connections.

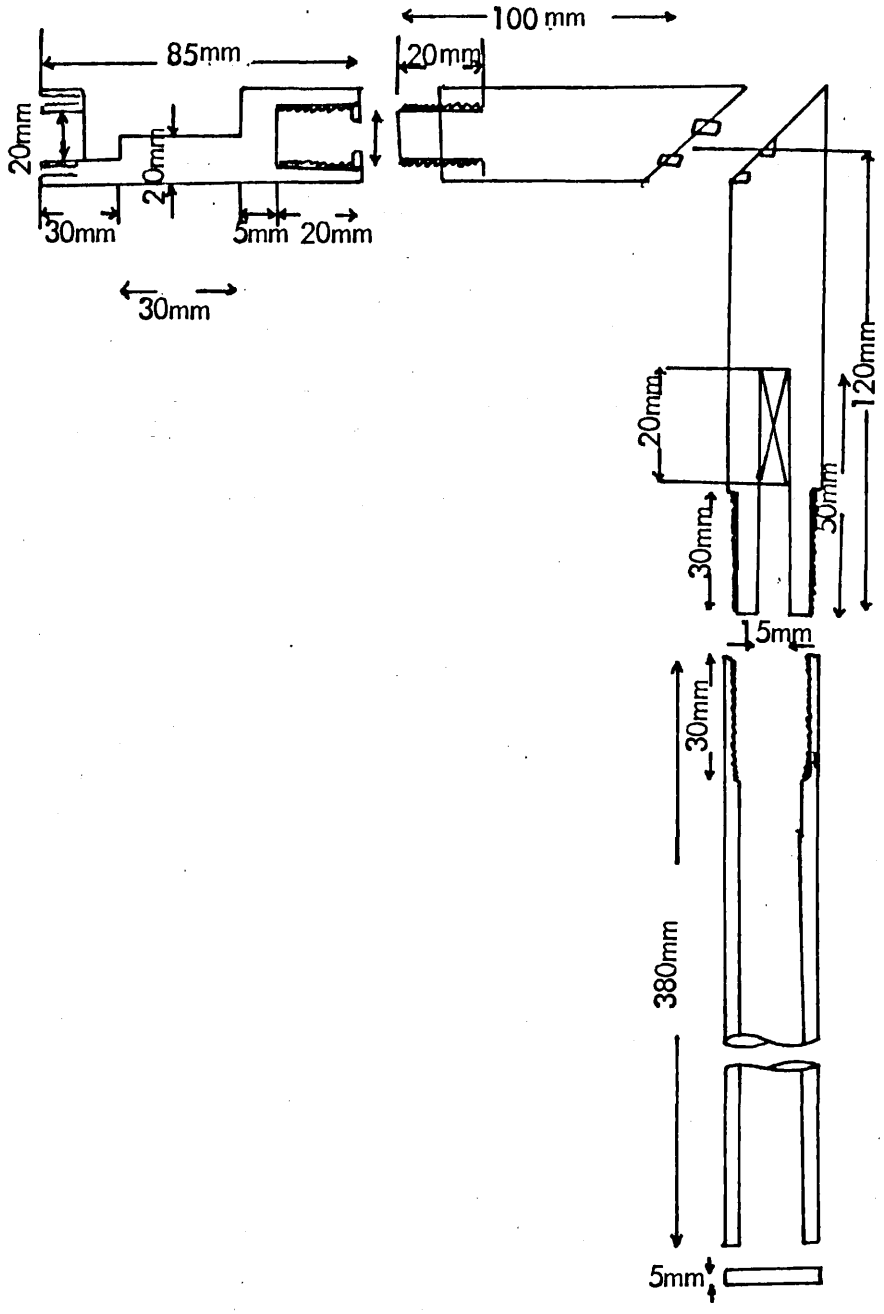

Fig C.1 Schematic diagram of the Cryostat

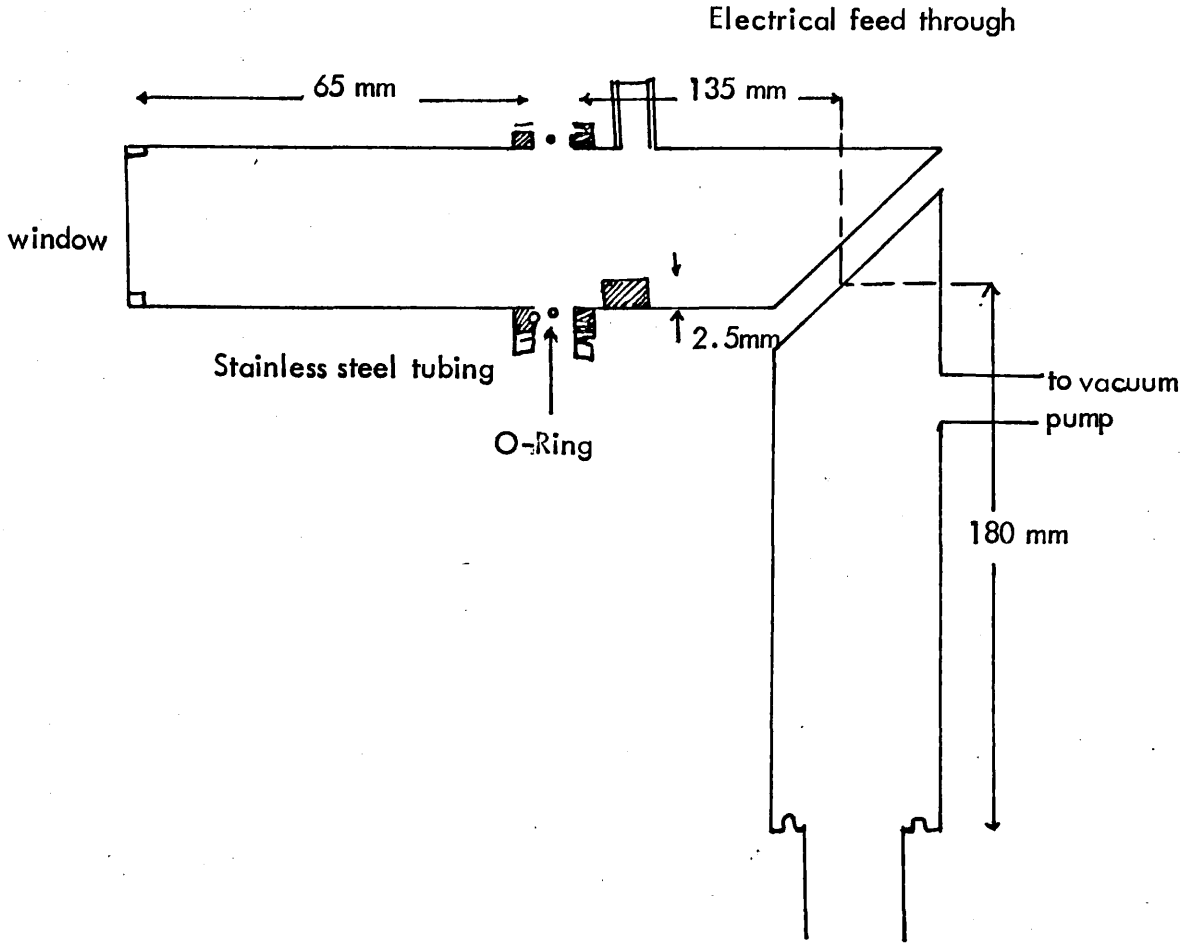

Fig C.2 Cross sectional view of the Cryostat

Sufficient space is provided to accommodate the required circuitry for use of a preamplifier with a cooled first stage interior to the vacuum chamber.

A view of the cryostat housing the detector is shown in Fig. C.3.

REFERENCES

(1) E.L. Feinberg, J.Nucl. Phys. (U.S.S.R.) 1, 612-620 (April, 1965) [Soviet journal of nuclear physics Vol. 1 No.4 (Oct. 1965) p.438]

(2) J. Law and J.L. Campbell, Nuclear Physics A 199 (1973) 481

(3) Paul Stephas, Phys. Rev. Vol. 186 (1969) 1013

(4) Kenneth D. Sevier, "Low Energy Electron Spectrometry", Wiley, 1972 p.165.

(5) T. Porter, M.S. Freedman, and F. Wagner, Phys. Rev. C3 (1971) 2246

(6) M.O. Krause, T.A. Carlson, and R.D. Dismukes, Phys. Rev. 170 (1968) 37.

(7) D. Bere'nyi Proc. International Conference on Inner Shell Ionization Phenomena Atlanta 1972 Vol. 4 p.2175.

(8) E.L. Feinberg, 1941, J. Phys. (U.S.S.R.) 4, 423.

(9) A. Migdal, 1941, J. Phys. (U.S.S.R.) 4, 449.

(10) J.S. Levinger, Phys. Rev. 90 (1953) 11.

(11) Thomas A. Carlson, C.W. Nestor, and Thomas C. Tucker and F.B. Malik Phys. Rev. 169 (1968) 27.

(12) Paul Stephas and Bernd Crasemann, Phys. Rev. 164 (1967) 1509.

(13) B. Crasemann and P. Stephas, Nucl. Phys. A134 (1969) 641.

(14) Paul Stephas and Bernd Crasemann, Phys. Rev. C3 (1971) 2495.

(15) J. Law and J.L. Campbell, Nucl. Phys. A185 (1972) 529.

(16) J. Law and J.L. Campbell, Ref. 7 Vol. 4, P. 2110.

(17) A.J. Mord, Nucl. Phys. A192 (1972) 305.

(18) A.J. Mord, Ref. 7, P.2079.

(19) J.L. Campbell and J. Law, Canadian J. Phys. 50 (1972) 2451.

(20) H. Boehm and C.S. Wu, Phys. Rev. 95 (1954) 518

(21) F. Suzor and G. Charpak, J. Phys. Rad. 20 (1959) 25

(22) G. Charpak and F. Suzor, Ref.21, P.31.

(23) H.J. Fishbeck, F. Wagner, F.T. Porter and M.S. Freedman, Phys. Rev. C3 (1971) 265.

(24) Peter Erman, Bertil Sigfridsson, Thomas A. Carlson and Kjell Fransson, Nucl. Phys. A112 (1968) 117

(25) A.J. Mord, 1971, Ph.D. Thesis, University of Oregon (U.S.A.) unpublished.

(26) Yasuhito Isozumi and Sakae Shimizu, Phys. Rev. C4 (1971) 522.

(27) T. Kitahara, Y. Isozumi and S. Shimizu, Phys. Rev. C5 (1972) 1810.

(28) M. Spighel and F. Suzor, Nucl. Phys. 32 (1962) 346 (in French)

(29) R.M. Weiner, Phys. Rev. 144 (1966) 127

(30) F. Suzor, Le Journal de Physique et le Radium, 21 (1960) 223 (in French)

(31) T.A. Carlson, F. Pleasanton and C.H. Johnson, Phys. Rev. 129, (1963) 2220

(32) G.A. Renard, J. Phys. Rad. 16 (1955) 575 (in French)

(33) W. Rubinson and J.J. Howland Jr., Phys. Rev. 96 (1954) 1610

(34) H.H. Hansen and K. Parthasaradhi, Phys. Rev. C9 (1974) 1143

(35) A. Michalowicz and R. Bouchez, Ref. 32 P.578.

(36) G.A. Renard, J. Phys. Rad. 18 (1957) 681.

(37) H. Langevin, joliot, Ann. de Phys. 2 (1957) 16 (in French)

(38) J.L. Campbell, L.A. McNelles and J.Law, Canadian J. Phys. 49 (1971) 3142.

(39) R.L. Watson, E.T. Chulick, and R.W. Howard, Phys. Rev. C6 (1972) 2189.

(40) C.W.E. Van Eijk, R.W. Kooy and M.J.C. Visscher, Phys. Rev. C9 (1974) 2074

(41) C.W.E. Van Eijk and R.W. Kooy, Phys. Lett. 46B (1973) 351

(42) J.P. Thiband, ch. Briancon et R.J. Walen, Le Journal de Physique - Lettres Vol 35 (1974) L-89 (in French)

(43) J.M. Howard, E.J. Seykora and A.W. Waltner, Phys. Rev. A4 (1971) 1740

(44) B.P. Pathak, Phys. Rev. C10 (1974) 1599

(45) A. Ljubicic, D. Martel, R.T. Jones, and B.A. Logan, Canadian J. Phys., 52 (1974) 1152.

(46) J.L. Campbell, Phys. Lett. 31B (1970) 563

(47) A. Bond, O.P. Gupta, and A. Zide, Phys. Rev. C9 (1974) 1529

(48) G. Bertolini and A . Coche (Semi-conductor Detectors) North-Holland Publishing Company, P.350.

(49) R.V. Thomas, 1973, Ph.D. Thesis, University of London (U.K.) unpublished.

(50) H.T. Easterday, A.J. Haverfield and J.M. Hollander, Nucl. Inst. Meth. 32 (1965) 333.

(51) J.T. Routti and S.G. Prussin, Nucl. Inst. Meth. 72 (1969) 125

(52) Y. Isozumi, T. Mukoyama and Shimizu, Lett. Nuovo Cimento, 10 (1974) 355

(53) J. Law and J.L. Campbell, Lett. Nuovo Cimento,11 (1974) 676

(54) J.L. Campbell and J. Law, 1975, Private Communication, unpublished review on the mechanisms contributing to K-electron ejection in nuclear β-decay.

(55) M.S. Freedman and D.A. Beery, Phys. Rev. Lett. 34 (1975) 406

(56) D. Bere'nyi et al., Nucl. Inst. Meth. 124, (1975) 505.

(57) M.S. Rapaport, F. Asaro and I. Perlman, Phys. Rev. C11 (1975) 1740

(58) M.S. Rapaport, F. Asaro and I. Perlman, Phys. Rev. C11 (1975) 1746

(59) H.H. Hansen, Physica Fennica (Finland) Vol. 9, Suppl. S1 (1974) 264.

(60) C. Wieg et al., Nucl. Inst. Meth. 20 (1963) 313

(61) A.F. Dunaitsev, Nucl. Inst. Meth. 28 (1964) 341

(62) J. Garvey, Nucl. Inst. Meth, 29 (1964) 137

(63) K.P.A. Porgess et al., Nucl. Inst. Meth. 29 (1964) 157

(64) M. Bertolaccini et al., Nucl. Inst. Meth. 37 (1965) 297

(65) G. Iaci and M. Losavio, Nucl. Inst. Meth. 65 (1968) 103

(66) F. Nanni and H. Verweij, CERN NP Internal Report 69-31 (1969)

(67) The TTL Data Book for Design Engineers, Texas Instruments Limited.

(68) P.L. Taylor, 1960, Servomechanisms, (Longmas, Green and Co. Ltd.)

(69) John N. Shive, The Properties, Physics and Design of Semi-Conductor Devices (D. Van Nostrand Company Inc.), 1959.

(70) R.S. Components Limited, Catalogue (1971)

(71) J. Lippert, Nuc. Inst. Meth. 32 (1965) 360

(72) C. Chasman and R.A. Ristinen, Nucl. Inst. Meth. 34 (1965) 250

(73) S. Buhler and L. Marcus, Nucl. Inst. Meth. 50 (1967) 170

(74) R. Serber and H.S. Snyder, Phys. Rev. 87 (1952) 152

(75) M.S. Freedman et al., Phys. Rev. 88 (1952) 1155

(76) A.E.S. Green, Phys. Rev. 107 (1957) 1646

(77) M.S. Freedman, Ann. Rev. Nucl. Sci. 24 (1974) 209.

(78) J. Law and J.L. Campbell, Nucl. Phys. A187 (1972) 525

(79) Kai Siegbahn, Alpha-, Beta- and Gamma-ray Spectroscopy, North-Holland Publishing Company, P.827, 1965.

(80) C.M. Lederer, J.M. Hollander, and I. Perlman, 1967, Table of Isotopes, 6th ed. (John Wiley & Sons, Inc., London).

(81) D.P. Donnelly and M.L. Wiedenbeck, Nucl. Inst. Meth. 64 (1968) 26

(82) J. Konijn and E.W.A. Lingeman, Nucl. Inst. Meth. 94 (1971) 389

(83) A. Notea and E. Elias, Nucl. Inst. Meth. 86 (1970) 269

(84) G. Wallace and G.E. Coote, Nucl. Inst. Meth. 74 (1969) 353

(85) The Radiochemical Centre (Amersham), Data Sheet 11166

(86) M.J. Martin and P.H. Blichert-Toft, Nucl. Data A8, (Nos. 1,2), (1970) 124

(87) A. Bond and H. Lancman, Phys. Rev. C6 (1972) 2231

(88) L. Yaffe, Ann. Rev. Nucl. Sci., 12 (1962) 153

(89) W. Bambynek et al., Rev. Mod. Phys., 44 (1972) 716

(90) R. Hager and E. Seltzer, Nucl. Data A,4,1 (1968)

(91) P.V. Rao et al., Phys. Rev. A5 (1972) 997

(92) McCrary et al., Phys. Rev. A4, (1971) 1745

(93) R.S. Mowatt and J.S. Merritt, Can. J. Phys. 48 (1970) 453

(94) I. Adam et al., Phys. Rev. 159 (1967) 985

(95) J.S. Merritt et al., Can. J. Chemistry, 37, (1959) 1109

(96) R.P. Sharma et al., Nucl. Phys. A152 (1970) 225